Available online at www.sciencedirect.com
SCIENCE DIRECT®
Annals of Physics 315 (2005) 352–418
ANNALS of PHYSICS
www.elsevier.com/locate/aop

A recursive transfer-matrix solution for a dipole radiating inside and outside a stratified sphere

Alexander Moroz

Wave-Scattering.com

Received 18 March 2004; accepted 9 July 2004
Available online 7 October 2004

Abstract

Fast and numerically stable transfer-matrix solution is presented for the classical electromagnetics problem of a dipole radiating inside and outside a stratified sphere consisting of concentric spherical shells. There is no limitation on the dipole position, the number of the concentric shells, the shell medium, or on the sphere radius. Electromagnetic fields are determined anywhere in the space, the time-averaged angular distribution of the radiated power, the total radiated power, Ohmic losses due to an absorbing shell, and Green's function are calculated. An absorbing, optically active, and ultrathin ($\lesssim$10 nm) metallic shell (core), characterized by a nonlocal dielectric function, are all allowed. The classical results are then applied to inelastic light scattering (fluorescence and Raman), the radiative and nonradiative normalized decay rates, and frequency shift. Using correspondence principle, the radiative decay rate is calculated from the Poynting vector, whereas the nonradiative decay rate is calculated from the Ohmic losses inside a sphere absorptive shell. Numerical stability of our method and limitations of classical description of decay rates are addressed. The importance of grouping various radiative and nonradiative decay mechanisms into local and nonlocal decay rates is emphasized. Further possible extensions of the theory presented here to the case of an arbitrary multilayered (axially symmetric) particle and to the classical problem of a radiating quadrupole in the presence of a multilayered particle are briefly outlined. Various applications

E-mail address: moroz@phys.uu.nl.
URL: http://www.wave-scattering.com.

0003-4916/$ - see front matter
doi:10.1016/j.aop.2004.07.002

for chemical speciation, LIDAR, fluorescent microscopy, engineering of decay rates, identification of biological particles, and monitoring specific cell functions are envisaged. Computer program is freely available at http://www.wave-scattering.com.

PACS: 78.67.Bf; 33.70.Ca; 33.50.Dq; 42.68.Wt; 41.20.−q
Keywords: Radiative decay rate; nonradiative decay rate; multilayered sphere; engineering of decay rates; optical properties of nanoparticles; inelastic scattering; Raman scattering; chiral spheres; ultrathin layers with a nonlocal dielectric function; LIDAR; fluorescent microscopy; spectroscopy; optical probes; near-field optical

1. Introduction

Pioneering work by Chew et al. [1,2] provided a complete description of the classical electromagnetic fields of an electric dipole radiating outside and inside a homogeneous and isotropic spherical particle. This solution found an immediate application in inelastic light-scattering (fluorescence or Raman) spectroscopy [1,3,4] and, in particular, in the surface enhanced Raman scattering (SERS) [1,4,5]. Raman spectroscopy had been developed into a sensitive tool for characterizing single micrometer sized particles of both inorganic and organic compounds [6]. Later on, Raman microprobe analysis of particulates was used for identification of biological particles in fluorescence-activated flow of cytomeres [7]. The inelastic scattering of species embedded within a spherical particle is also of considerable interest in studies employing light detecting and ranging (LIDAR) for remote sensing of both molecular and particulate constituents of atmosphere [6,8]. Indeed, atmospheric aerosols may fluoresce and that may be used to provide a means for chemical identification of ambient aerosols and to measure aerosol content in the atmosphere [8]. As another example, the particle may be a biological cell which has been tagged with fluorescent molecules that attach to the DNA, the cytoplasm, or to the cell membrane. The fluorescence can be used to monitor specific cell functions, or in the cell identification and sorting systems [9,10]. Chew et al. [1,2] solution found also application in the investigation thermal radiation from spherical microparticles [11].

Last but not the least, Chew et al. [1,2] solution was employed first by Ruppin [12] and then by Chew [13,14] for the description of spontaneous electric-dipole transition, or decay, rates of atoms and molecules adsorbed at or embedded in spherical particles. The applicability of purely classical theory for the description of the lifetime of an excited energy level of a quantum-mechanical system follows from the correspondence principle. According to the latter, the quantum theoretical expression for the power radiated by the spontaneous emission from an excited state in an electric (a magnetic) dipole transition is obtained from the classical expression for the power P radiated by an electric (a magnetic) dipole by replacement of the dipole moment $\mathbf{p}$ by the corresponding transition matrix element. The spontaneous emission rate W is then given by

$$W = \frac{P}{\hbar\omega}. \tag{1}$$

The basic assumption is, of course, that neither the transition matrix element nor the transition frequency are appreciably changed by the presence of the interface. An explicit verification of the equivalence of the classical and quantum-mechanical results for spherical geometry has been provided by Chew in Sec. IV of his article [13] (see also Appendix D for some intermediary steps of Chew's derivation). Chew has shown that the results for decay rates derived on the basis of classical electromagnetic theory agree with those computed quantum mechanically with the linear-response formalism [15] adapted to spherical geometry. Since then Chew's treatment of decay rates within the framework of classical electrodynamics has proved to be extremely successful and has been applied, among others, for the radiative decay engineering for biophysical and biomedical applications [16], in near-field optical microscopy for imaging of buried saturated fluorescent molecules [17] and of surfaces [18], and in the study of the effects of light absorption and amplification on the *stimulated* transition rates of the electric-dipole emission of atoms or molecules embedded in micrometer-sized dielectric spheres [19,20]. For a recent comparison of theory and experiment see [21] for the case of microspheres and [22] for nanospheres.

All the previous studies have been performed for the case of a homogeneous and isotropic spherical bead in a predetermined environment. However, particles found in nature are frequently not homogeneous and sometimes exhibit a layered or radially stratified structure. As an example, water-insoluble aerosols in atmosphere have often a thin liquid layer adsorbed on their surface. In addition to such a water-coated soot particles, the case of a sphere having two coatings is also important for modeling hydrological particles coated with biological material and micro-encapsulated material. In the case of a biological cell, the appropriate model consists of concentric three-layered sphere, corresponding to nucleus, cytoplasm, and membrane [5]. Furthermore, current experimental colloidal techniques allow one to design a variety of multi-structured beads having a plurality of concentric shells with the core radius from cca 1 nm till 1 μm and controlled shell thicknesses. For instance, a metal (Au, Ag, and Pt) or dielectric (ZnS) spherical core can be coated in a controlled way by a silica shell [23–27]. A reverse situation, in which a dielectric (silica, Au_2S) bead is coated by gold or some other noble metal, is also possible [28–32]. Having metal cores means that an active light-emitting dielectric material (semiconductor or polymer) is not isolated as in the case of metal shells. Hence, at first glance, metal-core dielectric-shell beads can perform more easily some useful optoelectronic functions. Nevertheless, dielectric-core metal-shell beads, also called metal nanoshells, consisting of a dielectric core with a metallic shell of nanometer thickness (cca 50 nm), made it possible to vary the optical resonances of such nanoparticles over hundreds of nanometers in wavelength by varying the relative dimensions of the core and shell [28,29]. For a comparison, the tunability of the single-sphere Mie resonances in the case of metal-core dielectric-shell beads is much smaller. However, experimentally available design options do not stop here. One can subsequently etched away silica core of a silica-core metal-shell bead and obtain a hollow metallic nanoshell. Either hollow metallic nanoshell or a dielectric-core metal-shell bead can be in turn coated in a controlled way by the second silica shell [31]. Note that such a dielectric

overcoat of either metallic shell or metallic core is advantageous as it prevents aggregation of the particles by reducing the Van der Waals forces between them. In the latter case, a dielectric coating of roughly 20 nm thickness is required. It is known that fluorescent organic groups can be placed with nm control over the radial position inside the silica core of a silica-core metal-shell bead, or in the silica shell of either a dielectric-core metal-shell silica shell bead or a metal-core silica shell bead [26,32]. Subsequently, there is a hope that such multi-structured spherical micro- and nanoparticles will provide a lot of freedom in engineering of inelastic light-scattering properties, such as SERS, and of atomic, molecular, and nanoprobe fluorescence properties, such as spontaneous and stimulated decay rates, according to one's need and a desired application. To treat the case of the spherical bead with several concentric shells it turns out necessary to extend the original work by Chew et al. [1,2,13,14] and Ruppin [12].

In what follows, a complete classical description of the electromagnetic fields of an electric-dipole radiating outside and inside such a multi-structured spherical particle is provided. After introducing our notation and definitions in Section 2, a recursive transfer-matrix solution is provided in Sections 3 and 4, which allows one to determine electromagnetic fields anywhere inside or outside the particle without any limitation on the number of concentric shells and on position of the radiating dipole. First forward and backward transfer matrices are introduced in Section 3, which enable one a complete description of the scattering off a multilayered sphere. Both penetrable and impenetrable (perfectly conducting sphere core) shells can be included into our formalism. The forward and backward transfer matrices are then used in Section 4 to provide a transfer-matrix solution for a multicoated sphere with a dipole source. The dipole position is neither limited to coincide with the center of the particle, nor is the number of concentric shells limited to two, as in a recent work by Klimov and Letokhova [33] and Enderlein [34]. Electromagnetic fields are determined everywhere inside and outside the multilayered sphere. Our recursive transfer-matrix solution can be viewed as an extension of Abelés work on multilayered thin films (stratified media) [35,36] (Abelés theory can also be found in Sec. 1.6 of Born and Wolf [37]) to the case of spherical geometry. The general formulas are then applied to calculate the time-averaged dipole radiated power from the Poynting vector in Section 5. Both the angular distribution of the radiated power, $\mathrm{d}P^{\mathrm{rad}}/\mathrm{d}\Omega$, (Section 5.1) and the total radiated power, P^{rad}, (Section 5.2) are obtained. In the case of P^{rad}, the resulting expressions are substantially simplified by performing sums over the magnetic angular number m. Energy dissipation in the case of an absorbing shell (either beads core or one of its shell) is discussed in Section 6. There the time-averaged nonradiative loss due to the Ohmic losses inside the sphere absorptive shell, P^{nrad}, is determined. It is worthwhile to remind that Chew, Kerker, and McNulty [5] provided a formal solution to the problem of a dipole radiating in the presence of a multilayered sphere. However, their solution for the sphere with N concentric shells (the sphere core counts as shell number one) is written in terms of a $2N \times 2N$ matrix and appears awkward and impractical for numerical calculations. Indeed, neither Chew nor anybody else have appeared to implement the Chew et al. [5] solution numerically. The main obstacles are that as N increases so do com-

puter memory requirements to store the matrix and the time to carry out the matrix calculations, which increases as N^3. These problems are overcome by our recursive solution which only employs 2×2 transfer matrices and their ordered products and provides a fast and reliable algorithm which can easily be implemented numerically. Moreover, sums over magnetic angular momentum number m are performed explicitly leading to further significant simplifications.

Beginning with Section 7, various applications of our classical solution for an electric-dipole radiating outside and inside a multilayered sphere are discussed. In Section 7, the results of Sections 4 and 5 are used to provide description of the intensity and angular distribution of an inelastically scattered light. In Section 8, correspondence principle (1) is used to relate the two mechanisms through which energy is dissipated, namely P^{rad} and P^{nrad}, to the corresponding *radiative*, W^{rad}, and *nonradiative*, W^{nrad}, decay rates. As in Chew et al. [1,2,13,14] treatment, any coherence between elementary emitters is neglected and only *coherence properties of the radiation field* are taken into account. When a radiating atom or molecule interacts with the electromagnetic fields perturbed by the presence of a multilayered spherical cavity, not only the spontaneous emission decay rate but also the transition frequency is modified [38,39]. This is discussed in Section 9, where the frequency shift is calculated from the knowledge of the scattering Green's function. Numerical simulations regarding the spontaneous emission decay rates are then presented in Section 10.

In principle, one can encounter situation when the theory outlined up to Section 10 has to be modified, even if one limits oneself to homogeneous and isotropic media. For instance, in the case of an ultra-thin metallic shell nonlocal effects due to excitation of longitudinal plasmon modes may come into play [40–43]. In Section 11 recipes are provided how to make necessary amendments for the ultra-thin metallic shell (Section 11.1) and the optically active shell [37,44,45] (Section 11.2). Afterward several specific subjects are discussed. The Ohmic loss is not the only mechanism which gives rise to a nonradiative decay rate [46,47]. Some other nonradiative processes, and the effect of concentration of elementary emitters on the nonradiative decay rate are discussed in Section 12.1. There it is suggested to organize different decay mechanism into nonlocal and local decay rates, according as to whether a particular decay mechanism depends on the geometry and material composition of the entire sphere and surrounding medium, or only on the immediate proximity of the radiating dipole. Limitations of the classical treatment of transition rates and the effect of concentration of elementary emitters on the radiative decay rate are discussed in Section 12.2. Numerical limitation on the size parameter and how to overcome them is the subject of Section 12.3. Further extensions and outlook can be found in Section 12.4. Eventually, in Section 13, we end up with summary and conclusions.

2. Notation and definitions

In what follows we shall consider a multilayered sphere with N concentric shells embedded in a host medium, which parameters are displayed on Fig. 1. In order to

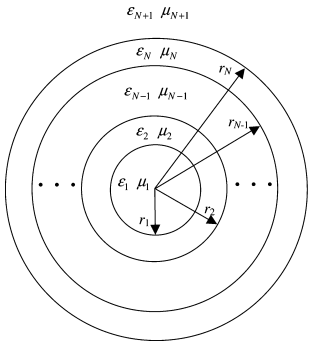

Fig. 1. Geometry and parameters of a multilayered sphere with N concentric shells embedded in a host medium.

keep recursive formulas compact, the sphere core counts as shell number one and the host medium is referred to as the $(N+1)$th shell. Any shell (host) will be assumed to be homogeneous and isotropic medium characterized by scalar permittivity ε_n ($\varepsilon_h \equiv \varepsilon_{N+1}$) and permeability μ_n ($\mu_h \equiv \mu_{N+1}$). k_n will denote the corresponding wave vector in the nth shell, $k_n = (\omega/c)\sqrt{\varepsilon_n\mu_n} = (2\pi/\lambda)\sqrt{\varepsilon_n\mu_n}$, λ and c being the wavelength and speed of light in vacuum, respectively. The nth shell radius will be denoted by r_n. Occasionally, the total sphere radius r_N will also be denoted by r_s (see Fig. 1). Spherical coordinates are centered at the sphere origin and $\mathbf{r}_d$ denotes the electric-dipole location.

Assuming for simplicity an isotropic homogeneous medium, electromagnetic fields in any shell are described by the stationary macroscopic Maxwell's equations (in Gaussian units, with time dependence $\mathrm{e}^{-\mathrm{i}\omega t}$ assumed),

$$\mathbf{E} = \frac{\mathrm{i}c}{\omega\varepsilon}(\boldsymbol{\nabla}\times\mathbf{H}), \quad \mathbf{H} = -\frac{\mathrm{i}c}{\omega\mu}(\nabla\times\mathbf{E}), \tag{2}$$

where the permittivity, ε, and permeability, μ, are scalars. (A generalization to tensor permittivities and permeabilities is straightforward although a bit tedious.) Using spherical symmetry of the problem, the fields within a given nth shell, $1 \leqslant n \leqslant N+1$, are expanded in the basis of normalized transverse vector multipoles,

$$\begin{aligned}
&\mathbf{F}_{ML}(k_n,\mathbf{r}) = f_{Ml}(k_n r)\mathbf{Y}_L^{(m)}(\mathbf{r}),\\
&\mathbf{F}_{EL}(k_n,\mathbf{r}) = \frac{1}{k_n r}\left\{\sqrt{l(l+1)}f_{El}(k_n r)\mathbf{Y}_L^{(o)}(\mathbf{r}) + (rf_{El})'(k_n r)\,\mathbf{Y}_L^{(e)}(\mathbf{r})\right\},
\end{aligned} \tag{3}$$

where $f_{\gamma l}$ is an arbitrary linear combination of spherical Bessel functions, $\mathbf{Y}_L^{(a)}$ are vector spherical harmonics, L is a composite angular momentum index, $L = lm$, where the respective l and m label the orbital and magnetic angular numbers, the respective indices M and E denote the TM and TE polarizations, and prime denotes the derivative $\mathrm{d}/\mathrm{d}r$. In the respective cases that $f_{\gamma l} = j_l$ and $f_{\gamma l} = h_l^{(1)}$, j_l and $h_l^{(1)}$ being the standard spherical Bessel functions of the first and third kind (see Chapter 10 of [48]), the multipoles $\mathbf{F}_{\gamma L}$ will be denoted as $\mathbf{J}_{\gamma L}$ and $\mathbf{H}_{\gamma L}$. For the sake of notation and transparency, in some formulas $h_l^{(1)}$ will be written as h_l.

Vector spherical harmonics $\mathbf{Y}_L^{(a)}$ in Eq. (3) are defined as

$$\begin{aligned}\mathbf{Y}_L^{(m)} &= \frac{1}{\sqrt{l(l+1)}}\mathbf{L}\,Y_L = -(\mathbf{r}_0 \times \mathbf{Y}_L^{(e)}) = r(\boldsymbol{\nabla} \times \mathbf{Y}_L^{(e)}),\\ \mathbf{Y}_L^{(e)} &= \frac{\mathrm{i}}{\sqrt{l(l+1)}}\, r\boldsymbol{\nabla} Y_L,\\ \mathbf{Y}_L^{(o)} &= \mathrm{i}Y_L\mathbf{r}_0 = \frac{\mathrm{i}r^2}{\sqrt{l(l+1)}}\,\boldsymbol{\nabla} \times (\boldsymbol{\nabla} \times Y_L^{(e)}),\end{aligned} \tag{4}$$

where $\mathbf{L} = -\mathrm{i}(\mathbf{r} \times \boldsymbol{\nabla})$ is the orbital angular momentum operator, $\mathbf{r}_0$ is the unit radius vector, and Y_L are the orthonormal scalar spherical harmonics in the Condon–Shortley convention as defined, for instance, by Jackson [49]. According to their definition, $\mathbf{Y}_L^{(m)}$ (also called $\mathbf{X}_L$ by Jackson [49]) and $\mathbf{Y}_L^{(e)}$ are *transverse*, whereas $\mathbf{Y}_L^{(o)}$ is *longitudinal*. The harmonic $\mathbf{Y}_L^{(m)}$ is identical to $\mathbf{Y}_{llm}$ as used by Chew et al. [1,5,4,13,14], whereas $\mathbf{Y}_L^{(e)} = -\mathbf{r}_0 \times \mathbf{Y}_{llm}$. The transverse and longitudinal vector spherical harmonics coincide up to an additional factor i with those defined in Chapter 2.1.5 of Newton [50]. The respective $\mathbf{Y}_L^{(m)}$, $\mathbf{Y}_L^{(e)}$, and $\mathbf{Y}_L^{(o)}$ are also called *magnetic*, *electric*, and *longitudinal* vector spherical harmonics. They can be shown to be proportional to the vector spherical harmonics $\mathbf{C}_L$, $\mathbf{B}_L$, $\mathbf{P}_L$ as used by Tsang, Kong, and Shin [51] and Mishchenko [52], respectively. For their additional properties and the proportionality factors see Appendix A.

In the special case where $f_{Ml} = f_{El}$, the normalized vector multipoles $\mathbf{F}_{\gamma L}$ satisfy the following relations:

$$\begin{aligned}&\mathbf{F}_{EL}(k,\mathbf{r}) = \frac{1}{k}\boldsymbol{\nabla} \times \mathbf{F}_{ML}(k,\mathbf{r}), \quad \mathbf{F}_{ML}(k,\mathbf{r}) = \frac{1}{k}\boldsymbol{\nabla} \times \mathbf{F}_{EL}(k,\mathbf{r}),\\ &\boldsymbol{\nabla} \times [\boldsymbol{\nabla} \times \mathbf{F}_{ML}(k,\mathbf{r})] = k^2\mathbf{F}_{ML}(k,\mathbf{r}), \quad \boldsymbol{\nabla} \times [\boldsymbol{\nabla} \times \mathbf{F}_{EL}(k,\mathbf{r})] = k^2\mathbf{F}_{EL}(k,\mathbf{r}).\end{aligned} \tag{5}$$

The respective vector multipoles $\mathbf{F}_{ML}$ and $\mathbf{F}_{EL}$ are both transverse,

$$\boldsymbol{\nabla} \cdot \mathbf{F}_{\gamma L} \equiv 0. \tag{6}$$

Therefore, the second line of Eq. (5) reduces to the Helmholtz equation, which is satisfied by each vector component of $\mathbf{F}_{\gamma L}$ independently,

$$\boldsymbol{\nabla}^2\mathbf{F}_{\gamma L} + k^2\mathbf{F}_{\gamma L} = 0. \tag{7}$$

The respective vector multipoles $\mathbf{F}_{ML}$ and $\mathbf{F}_{EL}$ are identical to Stratton's vector multipoles $\mathbf{M}$ and $\mathbf{N}$ [53], which are orthogonal and complete for transverse waves (see Appendix B for their additional properties). The reason for a different notation adopted here is that in our case one will encounter a variety of specific linear combinations of spherical Bessel function, such as $f_{\gamma l}$ in the case of $\mathbf{F}_{\gamma L}$. Therefore, the Bessel function aspect will come to forefront also in the notation, whereas polarization label is reduced to a mere subscript γ. Additional, reasons are that the respective linear combinations of spherical Bessel functions f_{Ml} and f_{El} will often turn out to be different, $f_{Ml} \neq f_{El}$, and that the upper case M is reserved to label the TM polarization, whereas the lower case m labels magnetic angular number.

General solution for the electric field in the nth shell, $1 \leqslant n \leqslant N+1$, is written as

$$\mathbf{E}_\gamma(\mathbf{r}) = \sum_L [A_{\gamma L}(n)\mathbf{J}_{\gamma L}(k_n,\mathbf{r}) + B_{\gamma L}(n)\mathbf{H}_{\gamma L}(k_n,\mathbf{r})]. \tag{8}$$

The corresponding magnetic field solution is then obtained from the second Maxwell's equation (2). For the transverse magnetic (TM) mode ($\gamma \equiv M$) one finds

$$\mathbf{H}_M(\mathbf{r}) = -\mathrm{i}\sqrt{\frac{\varepsilon_n}{\mu_n}} \sum_L [A_{ML}(n)\mathbf{J}_{EL}(k_n,\mathbf{r}) + B_{ML}(n)\mathbf{H}_{EL}(k_n,\mathbf{r})], \tag{9}$$

whereas for the transverse electric (TE) mode ($\gamma \equiv E$) the corresponding magnetic field is

$$\mathbf{H}_E(\mathbf{r}) = -\mathrm{i}\sqrt{\frac{\varepsilon_n}{\mu_n}} \sum_L [A_{EL}(n)\mathbf{J}_{ML}(k_n,\mathbf{r}) + B_{EL}(n)\mathbf{H}_{ML}(k_n,\mathbf{r})]. \tag{10}$$

The expansion coefficients in the $N+1$th shell, i.e., in the surrounding sphere host medium will occasionally be written as $C_{\gamma L} \equiv A_{\gamma L}(N+1)$ and $D_{\gamma L} \equiv B_{\gamma L}(N+1)$ with $k_{N+1} = k_h$. Because of the spherical symmetry of the problem, one can set in advance, or verify a posteriori, that the coefficients $A_{\gamma L}(n)$ and $B_{\gamma L}(n)$ ($C_{\gamma L}$ and $D_{\gamma L}$) do not depend on the magnetic angular number m. Expansion coefficients $A_{\gamma L}(n)$, $B_{\gamma L}(n)$ are determined by matching fields across the shell interfaces by imposing appropriate boundary conditions. In the case of electromagnetic waves it means that the tangential components of $\mathbf{E}$ and $\mathbf{H}$ are continuous. (In the case of ultrathin metallic shells (cca 30 nm and less) nonlocal effects can take place which manifest themselves by the existence of *longitudinal waves*. In the latter case, as discussed in Section 11.1, there is an additional boundary condition of the continuity of the normal electric intensity components across an interface [40].)

To compare the tangential components on both sides of the boundary, let us recall that $\mathbf{J}_{ML}$ has only tangential components,

$$\mathbf{J}_{ML}(k,\mathbf{r}) = j_l(kr)\mathbf{Y}_L^{(m)}(\mathbf{r}) = \frac{1}{r}\,u_l(kr)\mathbf{Y}_L^{(m)}(\mathbf{r}), \tag{11}$$

where $u_l(kr) \equiv rj_l(kr)$ is the Riccati–Bessel function [48,50]. In the case of $\mathbf{J}_{EL}(k,\mathbf{r})$,

$$\mathbf{J}_{EL}(k,\mathbf{r}) = \frac{1}{kr}\left\{\sqrt{l(l+1)}\,j_l(kr)\mathbf{Y}_L^{(o)}(\mathbf{r}) + (rj_l)'(kr)\,\mathbf{Y}_L^{(e)}(\mathbf{r})\right\}, \tag{12}$$

the tangential component is obviously given by the term proportional to $\mathbf{Y}_L^{(e)}$, whereas the longitudinal component is given by the term proportional to $\mathbf{Y}_L^{(o)}$,

$$[\mathbf{J}_{EL}]_\parallel(k,\mathbf{r}) = \frac{1}{\sqrt{\mu\varepsilon}r}(rj_l)'(kr)\,\mathbf{Y}_L^{(e)}(\mathbf{r}), \quad [\mathbf{J}_{EL}]_\perp(k,\mathbf{r}) = \frac{1}{\sqrt{\mu\varepsilon}r}\sqrt{l(l+1)}\,j_l(kr)\mathbf{Y}_L^{(o)}(\mathbf{r}). \tag{13}$$

Similarly for $\mathbf{H}_{ML}$ and $\mathbf{H}_{EL}$ with j_l replaced by $h_l^{(1)}$. Here, as usual, prime means derivative d/dr, i.e., $' = \mathrm{d}/\mathrm{d}r$.

Last remark concerns the inverse of a matrix element $\mathscr{M}_{ik}$ of matrix $\mathscr{M}$. Throughout the text, the inverse is denoted by $\mathscr{M}_{ik}^{-1}$, which thus should not be confused with the (ik)th matrix element of the inverse matrix $\mathscr{M}^{-1}$.

3. Forward and backward transfer matrices

Let us first consider the simplest case of two shells, i.e., that of a *homogeneous* sphere embedded in a homogeneous host, in the absence of any dipole source. The boundary condition of the continuity of the tangential components of *magnetic* modes implies for each l two equations, one for $\mathbf{E}_M$ and the second for $\mathbf{H}_M$,

$$\begin{aligned} &u_l(k_1r_1)A_{ML}(1)+w_l(k_1r_1)B_{ML}(1)=u_l(k_2r_1)A_{ML}(2)+w_l(k_2r_1)B_{ML}(2),\\ &u_l'(k_1r_1)A_{ML}(1)/\mu_1+w_l'(k_1r_1)B_{ML}(1)/\mu_1=u_l'(k_2r_1)A_{ML}(2)/\mu_2+w_l'(k_2r_1)B_{ML}(2)/\mu_2, \end{aligned} \tag{14}$$

where $u_l(kr)=rj_l(kr)$ and we have introduced yet another Riccati–Bessel function, $w_l\equiv rh_l^{(1)}$ [48,50]. In arriving to the equations, note that the respective prefactors $\sqrt{\varepsilon_1/\mu_1}$ and $\sqrt{\varepsilon_2/\mu_2}$ of the total magnetic field $\mathbf{H}_M$ at the inner and outer sides of the shell boundary combine with the medium-dependent prefactors of the tangential components of multipoles $\mathbf{J}_{EL}$ and $\mathbf{H}_{EL}$ (cf. Eq. (13)). For the computational convenience, for each given l the two Eqs. (14) are assembled into the following matrix equation:

$$\begin{pmatrix} u_l(k_1r_1), & w_l(k_1r_1)\\ u_l'(k_1r_1)/\mu_1, & w_l'(k_1r_1)/\mu_1 \end{pmatrix}\begin{pmatrix} A_{ML}(1)\\ B_{ML}(1)\end{pmatrix}=\begin{pmatrix} u_l(k_2r_1), & w_l(k_2r_1)\\ u_l'(k_2r_1)/\mu_2, & w_l'(k_2r_1)/\mu_2 \end{pmatrix}\begin{pmatrix} A_{ML}(2)\\ B_{ML}(2)\end{pmatrix}. \tag{15}$$

Therefore,

$$\begin{aligned} \begin{pmatrix} A_{ML}(1)\\ B_{ML}(1)\end{pmatrix}&=\begin{pmatrix} u_l(k_1r_1), & w_l(k_1r_1)\\ u_l'(k_1r_1)/\mu_1, & w_l'(k_1r_1)/\mu_1 \end{pmatrix}^{-1}\begin{pmatrix} u_l(k_2r_1), & w_l(k_2r_1)\\ u_l'(k_2r_1)/\mu_2, & w_l'(k_2r_1)/\mu_2 \end{pmatrix}\begin{pmatrix} A_{ML}(2)\\ B_{ML}(2)\end{pmatrix}\\ &=\frac{\mu_1}{W_r[u_l(k_1r_1),w_l(k_1r_1)]}\\ &\quad\times\begin{pmatrix} w_l'(k_1r_1)/\mu_1, & -w_l(k_1r_1)\\ -u_l'(k_1r_1)/\mu_1, & u_l(k_1r_1)\end{pmatrix}\begin{pmatrix} u_l(k_2r_1), & w_l(k_2r_1)\\ u_l'(k_2r_1)/\mu_2, & w_l'(k_2r_1)/\mu_2 \end{pmatrix}\begin{pmatrix} A_{ML}(2)\\ B_{ML}(2)\end{pmatrix}\\ &=T_{Ml}^{-}(1)\begin{pmatrix} A_{ML}(2)\\ B_{ML}(2)\end{pmatrix}, \end{aligned} \tag{16}$$

where

$$\begin{aligned} T_{Ml}^{-}(1)&=-\mathrm{i}k_1\mu_1\\ &\quad\times\begin{pmatrix} w_l'(k_1r_1)u_l(k_2r_1)/\mu_1-w_l(k_1r_1)u_l'(k_2r_1)/\mu_2, & w_l'(k_1r_1)w_l(k_2r_1)/\mu_1-w_l(k_1r_1)w_l'(k_2r_1)/\mu_2\\ -u_l'(k_1r_1)u_l(k_2r_1)/\mu_1+u_l(k_1r_1)u_l'(k_2r_1)/\mu_2, & -u_l'(k_1r_1)w_l(k_2r_1)/\mu_1+u_l(k_1r_1)w_l'(k_2r_1)/\mu_2\end{pmatrix} \end{aligned} \tag{17}$$

is a *backward* transfer matrix. Given the expansion coefficients in the outer shell, the backward transfer matrix yields the expansion coefficients in the inner shell. In arriving to the result, two elementary relations were used. First the Cramers rule of linear algebra, when applied to 2×2 matrices,

$$\begin{pmatrix} a & b \\ c & d \end{pmatrix}^{-1} = \frac{1}{ad-bc}\begin{pmatrix} d & -b \\ -c & a \end{pmatrix}. \tag{18}$$

Second, the term $ad-bc$ in Eq. (18) reduces to the Wronskian of the spherical Riccati–Bessel functions for which the following relation holds:

$$W_r[u_l(k_1r), w_l(k_1r)] = \mathrm{i}/k_1. \tag{19}$$

Here the Wronskian $W_x[f(ax), g(ax)] \equiv f(ax)g'(ax) - f'(ax)g(ax)$ and prime denotes the derivative with respect to x, the subscript of W. The Wronskian relation is established by applying Eq. (10.1.6) of [48], according to which $W_z[j_l(z), n_l(z)] = 1/z^2$, n_l being the spherical Bessel function of the second kind [48]. In order to apply Eq. (10.1.6) of [48], the sequence of elementary identities was used:

$$W_r[u_l(k_1r), w_l(k_1r)] = k_1r^2 W_{k_1r}[j_l(k_1r), h_l^+(k_1r)] = \mathrm{i}k_1r^2 W_{k_1r}[j_l(k_1r), n_l(k_1r)].$$

Note in passing that

$$u_l' \equiv \frac{\mathrm{d}u_l(kr)}{\mathrm{d}r} = \frac{\mathrm{d}[rj_l(kr)]}{\mathrm{d}r} = \frac{\mathrm{d}[krj_l(kr)]}{\mathrm{d}(kr)}, \tag{20}$$

i.e., $u_l' = \mathrm{d}[u_l(kr)]/\mathrm{d}r$ (and similarly w_l') can be replaced throughout the formulas by $\mathrm{d}[krj_l(kr)]/\mathrm{d}(kr)$ $[\mathrm{d}[krh_l^{(1)}(kr)]/\mathrm{d}(kr)]$, as used for instance by Chew [13,14] and some other authors [51,52]. We have used the more compact form of writing to more easily identify all the medium-dependent factors. Upon the substitution $k_1 \to k_2$, $k_2 \to k_1$, and $\mu_1 \to \mu_2$, $\mu_2 \to \mu_1$, one finds

$$\begin{pmatrix} A_{ML}(2) \\ B_{ML}(2) \end{pmatrix} = T_{Ml}^+(1)\begin{pmatrix} A_{ML}(1) \\ B_{ML}(1) \end{pmatrix}, \tag{21}$$

where

$$\begin{aligned} T_{Ml}^+(1) = {} & -\mathrm{i}k_2\mu_2 \\ & \times \begin{pmatrix} w_l'(k_2r_1)u_l(k_1r_1)/\mu_2 - w_l(k_2r_1)u_l'(k_1r_1)/\mu_1, & w_l'(k_2r_1)w_l(k_1r_1)/\mu_2 - w_l(k_2r_1)w_l'(k_1r_1)/\mu_1 \\ -u_l'(k_2r_1)u_l(k_1r_1)/\mu_2 + u_l(k_2r_1)u_l'(k_1r_1)/\mu_1, & -u_l'(k_2r_1)w_l(k_1r_1)/\mu_2 + u_l(k_2r_1)w_l'(k_1r_1)/\mu_1 \end{pmatrix} \end{aligned} \tag{22}$$

is a *forward* transfer matrix. Given the expansion coefficients in the inner shell, the forward transfer matrix yields the expansion coefficients in the outer shell.

For *electric*, TE modes one proceeds in entirely analogous way. After matching first the tangential components of magnetic field and then the tangential components of electric field (note the medium-dependent prefactors of the tangential components of $\mathbf{J}_{EL}$ and $\mathbf{H}_{EL}$ [cf. Eq. (13)]), the resulting equations are,

$$\sqrt{\frac{\varepsilon_1}{\mu_1}}\begin{pmatrix} u_l(k_1r_1), & w_l(k_1r_1) \\ u_l'(k_1r_1)/\varepsilon_1, & w_l'(k_1r_1)/\varepsilon_1 \end{pmatrix}\begin{pmatrix} A_{EL}(1) \\ B_{EL}(1) \end{pmatrix} = \sqrt{\frac{\varepsilon_2}{\mu_2}}\begin{pmatrix} u_l(k_2r_1), & w_l(k_2r_1) \\ u_l'(k_2r_1)/\varepsilon_2, & w_l'(k_2r_1)/\varepsilon_2 \end{pmatrix}\begin{pmatrix} A_{EL}(2) \\ B_{EL}(2) \end{pmatrix}. \tag{23}$$

Hence

$$\begin{pmatrix} A_{EL}(1) \\ B_{EL}(1) \end{pmatrix} = T_{El}^{-}(1)\begin{pmatrix} A_{EL}(2) \\ B_{EL}(2) \end{pmatrix}, \quad \begin{pmatrix} A_{EL}(2) \\ B_{EL}(2) \end{pmatrix} = T_{El}^{+}(1)\begin{pmatrix} A_{EL}(1) \\ B_{EL}(1) \end{pmatrix}, \tag{24}$$

where

$$T_{El}^{-}(1) = -\mathrm{i}k_1n_1 \times \sqrt{\frac{\varepsilon_2}{\mu_2}}\begin{pmatrix} w_l'(k_1r_1)u_l(k_2r_1)/\varepsilon_1 - w_l(k_1r_1)u_l'(k_2r_1)/\varepsilon_2, & w_l'(k_1r_1)w_l(k_2r_1)/\varepsilon_1 - w_l(k_1r_1)w_l'(k_2r_1)/\varepsilon_2 \\ -u_l'(k_1r_1)u_l(k_2r_1)/\varepsilon_1 + u_l(k_1r_1)u_l'(k_2r_1)/\varepsilon_2, & -u_l'(k_1r_1)w_l(k_2r_1)/\varepsilon_1 + u_l(k_1r_1)w_l'(k_2r_1)/\varepsilon_2 \end{pmatrix} \tag{25}$$

and

$$T_{El}^{+}(1) = -\mathrm{i}k_2n_2 \times \sqrt{\frac{\varepsilon_1}{\mu_1}}\begin{pmatrix} w_l'(k_2r_1)u_l(k_1r_1)/\varepsilon_2 - w_l(k_2r_1)u_l'(k_1r_1)/\varepsilon_1, & w_l'(k_2r_1)w_l(k_1r_1)/\varepsilon_2 - w_l(k_2r_1)w_l'(k_1r_1)/\varepsilon_1 \\ -u_l'(k_2r_1)u_l(k_1r_1)/\varepsilon_2 + u_l(k_2r_1)u_l'(k_1r_1)/\varepsilon_1, & -u_l'(k_2r_1)w_l(k_1r_1)/\varepsilon_2 + u_l(k_2r_1)w_l'(k_1r_1)/\varepsilon_1 \end{pmatrix} \tag{26}$$

are the respective *backward* and *forward* transfer matrices for the *electric*, TE modes. Here $n_j = \sqrt{\varepsilon_j\mu_j}$, $j = 1, 2$ is the refractive index of the jth shell. Again, at arriving at the results (25) and (26), the Cramers rule (18) and the Wronskian identity (19) have been used.

Given the respective forward and backward transfer matrices, the case of a multicoated sphere with an arbitrary number of shells then follows straightforwardly from the two-shell case of the homogeneous sphere. The respective backward $T^{-}(n)$ and forward $T^{+}(n)$ transfer 2×2 matrices,

$$\begin{pmatrix} A(n+1) \\ B(n+1) \end{pmatrix} = T^{+}(n)\begin{pmatrix} A(n) \\ B(n) \end{pmatrix}, \tag{27}$$

$$\begin{pmatrix} A(n) \\ B(n) \end{pmatrix} = T^{-}(n)\begin{pmatrix} A(n+1) \\ B(n+1) \end{pmatrix}, \tag{28}$$

which translate the expansion coefficients $A(n)$ and $B(n)$ from the nth shell into the coefficients $A(n+1)$ and $B(n+1)$ in the $(n+1)$th shell, and vice versa, are obtained from Eqs. (17), (22), (25), and (26) by a simple substitution of the medium-dependent parameters labeled by the subscript 1 (2) with those of the nth ($n+1$th) shell.

Provided that the respective coefficients $A_{\gamma L}(n-1)$ and $B_{\gamma L}(n-1)$ are known, the coefficients $A_{\gamma L}(n)$ and $B_{\gamma L}(n)$ can be unambiguously determined, and vice versa. In the case that the shell is the sphere shell different from the sphere core, one has for each given γ and l and at a given spherical interface of two shells 2 equations for 4

sets of expansion coefficients $A_{\gamma L}(j)$ and $B_{\gamma L}(j)$, where $j = n$ and either $n-1$ or $n+1$. Hence, the total number of different sets of expansion coefficients comprising all j's from the interval $1 \leqslant j \leqslant N+1$ is larger by two than the number of corresponding equations. Therefore, in order to unambiguously determine the expansion coefficients at any shell, boundary conditions have to be imposed which unambiguously fix *two* of the coefficients $A_{\gamma L}(j)$ and $B_{\gamma L}(j')$ for each given γ and L, where in general $j \neq j'$. First is the *regularity* condition of the physical solution at the sphere origin,

$$B_{EL}(1) = B_{ML}(1) \equiv 0. \tag{29}$$

Before we proceed further, it turns out convenient to introduce the following ordered products of the respective forward and backward 2×2 matrices,

$$\mathscr{T}_{\gamma l}(n) = \prod_{j=1}^{n-1} T^{+}_{\gamma l}(j), \quad \mathscr{M}_{\gamma l}(n) = \prod_{j=n}^{N} T^{-}_{\gamma l}(j). \tag{30}$$

The ordered products $\mathscr{T}_{\gamma l}(n)$ are defined for $2 \leqslant n \leqslant N+1$, whereas $\mathscr{M}_{\gamma l}(n)$ are defined for $1 \leqslant n \leqslant N$. Note that according to the definition, $\mathscr{T}_{\gamma}(2) = T^{+}_{\gamma}(1)$. $\mathscr{T}_{\gamma}(n)$ ($\mathscr{M}_{\gamma}(n)$, $1 \leqslant n \leqslant N$) transfers expansion coefficients from the sphere core (surrounding medium) to the nth shell. In the following, $\mathscr{T}_{\gamma}(n)$ and $\mathscr{M}_{\gamma}(n)$ will also be referred to as transfer matrices. In terms of transfer matrices $\mathscr{T}_{\gamma}(n)$ and $\mathscr{M}_{\gamma}(n)$, the regularity boundary condition (29) implies the following matrix equation for the unknown coefficients $A_{\gamma L}(N+1) = C_{\gamma L}$ and $B_{\gamma L}(N+1) = D_{\gamma L}$,

$$\begin{pmatrix} A_{\gamma L}(N+1) \\ B_{\gamma L}(N+1) \end{pmatrix} = \begin{pmatrix} C_{\gamma L} \\ D_{\gamma L} \end{pmatrix} = \mathscr{T}_{\gamma l}(N+1) \begin{pmatrix} A_{\gamma L}(1) \\ 0 \end{pmatrix}. \tag{31}$$

Hence, the *regularity* condition unambiguously determines the m-independent ratio $D_{\gamma L}/C_{\gamma L}$ (denoted by $\alpha/2$ and $\beta/2$ for the respective TM and TE modes by Jackson [49]),

$$D_{\gamma L}/C_{\gamma L} = \mathscr{T}_{21;\gamma l}(N+1)/\mathscr{T}_{11;\gamma l}(N+1). \tag{32}$$

Note that for the case of a homogeneous sphere $\mathscr{T} \equiv T^{+}$, $r_1 \equiv r_s$, and hence

$$\begin{aligned} D_{ML}/C_{ML} &= -\frac{u_l'(k_2 r_s)u_l(k_1 r_s)/\mu_2 - u_l(k_2 r_s)u_l'(k_1 r_s)/\mu_1}{w_l'(k_2 r_s)u_l(k_1 r_s)/\mu_2 - w_l(k_2 r_s)u_l'(k_1 r_s)/\mu_1}, \\ D_{EL}/C_{EL} &= -\frac{u_l'(k_2 r_s)u_l(k_1 r_s)/\varepsilon_2 - u_l(k_2 r_s)u_l'(k_1 r_s)/\varepsilon_1}{w_l'(k_2 r_s)u_l(k_1 r_s)/\varepsilon_2 - w_l(k_2 r_s)u_l'(k_1 r_s)/\varepsilon_1}. \end{aligned} \tag{33}$$

Upon taking into account our definition of Riccati–Bessel functions u_l and w_l and the identity (20), one can easily verify that, in the case of a homogeneous sphere, the ratios D/C for the respective TM and TE modes correspond to the Mie expansion coefficients a and b (see Eqs. (2.127) of [50]),

$$\begin{aligned} D_{ML}/C_{ML} &= a_l = -\frac{m\psi_l'(k_2 r_s)\psi_l(k_1 r_s) - q\psi_l(k_2 r_s)\psi_l'(k_1 r_s)}{m\zeta_l'(k_2 r_s)\psi_l(k_1 r_s) - q\zeta_l(k_2 r_s)\psi_l'(k_1 r_s)}, \\ D_{EL}/C_{EL} &= b_l = -\frac{q\psi_l'(k_2 r_s)\psi_l(k_1 r_s) - m\psi_l(k_2 r_s)\psi_l'(k_1 r_s)}{q\zeta_l'(k_2 r_s)\psi_l(k_1 r_s) - m\zeta_l(k_2 r_s)\psi_l'(k_1 r_s)}, \end{aligned} \tag{34}$$

where, in the notation of Mie scattering community [54–57], here and only here $m = \sqrt{\varepsilon_2/\varepsilon_1}$, $q = \sqrt{\mu_2/\mu_1}$, and a more common form of the Riccati–Bessel functions is used, namely $\psi_l(x) = xj_l(x) = ku_l$ and $\zeta_l(x) = xh_l^{(1)}(x) = kw_l$. Note that the Mie expansion coefficients a and b determine all the (extinction, scattering, absorption) cross sections [50]. In the present case, by unambiguously specifying the m-independent ratio $D_{\gamma L}/C_{\gamma L}$ the regularity boundary condition (29) turns out sufficient to determine all the (extinction, scattering, and absorption) cross sections of a multicoated sphere. One can show that the m-independent ratio $D_{\gamma L}/C_{\gamma L}$ is, up to a proportionality factor, nothing but the transition, or T-matrix [51,52] of a multicoated sphere

$$-\mathrm{i}k_h t_{\gamma l}(k_h) = \frac{D_{\gamma L}}{C_{\gamma L}} = \frac{1}{2}\left(\mathrm{e}^{2\mathrm{i}\eta_{\gamma l}} - 1\right) = \mathrm{i}\sin\eta_{\gamma l}\mathrm{e}^{\mathrm{i}\eta_{\gamma l}}, \tag{35}$$

where $\eta_{\gamma l}$ are the scattering phase shifts. According to Eq. (32), the resonances of a multicoated sphere are determined as zeroes of $\mathscr{T}_{11;\gamma l}(N+1)$. The above discussion can be summarized by the statement that the 2×2 matrix $\mathscr{T}_{\gamma l}(N+1)$ provides a complete description of the scattering properties of a multicoated sphere with an arbitrary number of shells.

Although the single interior boundary condition (29) is sufficient to determine all the (extinction, scattering, and absorption) cross sections, it determines the fields inside and outside the multicoated sphere only up to an overall proportionality factor. This proportionality factor can be fixed by requiring that, for a given frequency ω, the $C_{\gamma L}$ coefficients be equal to the expansion coefficients of an incident electromagnetic field in spherical coordinates. For the corresponding second (exterior) boundary condition in the case of a dipole source, see Section 4. The second boundary condition is only necessary if one wants to determine the field intensities within a multicoated sphere, as in the case of thermal radiation from spherical microparticles [11] and the stimulated Raman scattering [58,59].

The recursive transfer algorithm for the description of the scattering of a multicoated sphere has been successfully employed in our earlier studies [27,60,61] and a comparison with experiment was performed [27,31]. For completeness, a different matrix formulation has recently been initiated by Burlak et al. [62,63]. Some other approaches are discussed by Fuller and Mackowski [64].

3.1. Perfectly conducting sphere core

The approximation of a perfect conductor is often used in model calculations involving metals. Therefore, it is also included in our transfer-matrix treatment. The approximation is an idealization of the metallic case which yields a reasonable approximation in the far-infrared and microwave frequency ranges. Since a perfectly conducting shell of radius $\mathbf{r}_n$ effectively shields all its interior, the case a perfectly conducting shell of radius $\mathbf{r}_n$ is entirely equivalent to that of a perfectly conducting core of radius $\mathbf{r}_n$. Hence, only the latter case is considered.

In the case of a perfectly conducting core, the regularity boundary condition (29) is replaced by the conditions of vanishing of the *tangential* component of the electric field and the *radial* component of the magnetic field [49],

$$\mathbf{E}_{\|} = 0, \quad \mathbf{B}_{\perp} = 0. \tag{36}$$

In the preceding section, the interior (regularity) boundary condition (29) specified (up to a proportionality factor) the following initial vector for a forward recurrence,

$$\begin{pmatrix} A_{\gamma L}(1) \\ B_{\gamma L}(1) \end{pmatrix} = \begin{pmatrix} 1 \\ 0 \end{pmatrix}. \tag{37}$$

We will show here that the case of the perfectly conducting boundary conditions (36) at the sphere core differs from the case treated in Section 3 merely in the choice of the recurrence initial vector. Indeed, outside the core, the electric and magnetic fields are as usual expanded into series (8)–(10). For a given mode, the two boundary conditions in Eq. (36) yield an identical constraint on the expansion coefficients $A_{\gamma L}(2)$ and $B_{\gamma L}(2)$. For the magnetic mode, the constraint is

$$u_l(k_2 r_1) A_{ML}(2) + w_l(k_2 r_1) B_{ML}(2) = 0, \tag{38}$$

whereas for the electric mode the constraint is

$$u_l'(k_2 r_1) A_{EL}(2) + w_l'(k_2 r_1) B_{EL}(2) = 0. \tag{39}$$

The respective constraints are solved by taking

$$A_{ML}(2) = \xi_1 w_l(k_2 r_1), \quad B_{ML}(2) = -\xi_1 u_l(k_2 r_1), \tag{40}$$

$$A_{EL}(2) = \xi_2 w_l'(k_2 r_1), \quad B_{EL}(2) = -\xi_2 u_l'(k_2 r_1), \tag{41}$$

where ξ_j, $j = 1, 2$ are some ambiguous, in general complex proportionality factors, which may depend on the magnetic angular number m. Therefore, the corresponding initial vectors for the forward recurrence become

$$\begin{pmatrix} A_{ML}(2) \\ B_{ML}(2) \end{pmatrix} = \xi_1 \begin{pmatrix} w_l(k_2 r_1) \\ u_l(k_2 r_1) \end{pmatrix}, \quad \begin{pmatrix} A_{EL}(2) \\ B_{EL}(2) \end{pmatrix} = \xi_2 \begin{pmatrix} w_l'(k_2 r_1) \\ u_l'(k_2 r_1) \end{pmatrix}. \tag{42}$$

Since the perfectly conducting boundary conditions (36) imply that no electromagnetic field penetrates the core, it turns out convenient to relabel the shells according to $n \to n - 1$, by which the sphere core formally disappears from the formalism. The only remnant of the perfectly conducting core is the said change in the initial vector for a forward recurrence [Eq. (37) vs Eq. (42)].

Once the initial vectors for a forward recurrence are (up to proportionality factors) determined, the rest of the procedure is exactly the same as in the preceding section and the case of a multilayered sphere with a perfectly conducting core becomes formally the same as that of a penetrable core of Section 3. Again, as in the previous section, the proportionality factors ξ_1 and ξ_2 are, if necessary, fixed by imposing an appropriate second boundary condition. However (see Section 3), the latter is not required if only cross sections are to be calculated.

4. Transfer-matrix solution for a multicoated sphere with a source

In this section, the forward $T^{+}(n)$ and backward $T^{-}(n)$ transfer matrices (17), (22), (25), and (26), and their ordered products $\mathscr{T}(n)$ and $\mathscr{M}(n)$, as introduced by Eqs.

(30) in the preceding section, will be employed for the description of electromagnetic fields of a multicoated sphere with an electric-dipole source. In the case of a multilayered sphere with a perfectly conducting core it will be assumed that, as described in Section 3.1, the shells have been relabeled according to $n \to n-1$.

The electric field at $\mathbf{r}$ due to an electric-dipole $\mathbf{p}$ at $\mathbf{r}_d$ radiating at frequency ω in a medium with ε, μ is given for $r > r_d$ by [13]

$$\begin{aligned}\mathbf{E}_d(\mathbf{r}) &= \sum_L \left[a^d_{ML}\mathbf{H}_{ML}(k,\mathbf{r}) + a^d_{EL}\mathbf{H}_{EL}(k,\mathbf{r})\right],\\ \mathbf{H}_d(\mathbf{r}) &= -\mathrm{i}\sqrt{\frac{\varepsilon}{\mu}}\sum_L \left[a^d_{ML}\mathbf{H}_{EL}(k,\mathbf{r}) + a^d_{EL}\mathbf{H}_{ML}(k,\mathbf{r})\right],\end{aligned} \tag{43}$$

where

$$\begin{aligned}a^d_{ML} &= 4\pi\mathrm{i}(k^3/\varepsilon)\,\mathbf{p}\cdot\mathbf{J}^*_{ML}(k,\mathbf{r}_d),\\ a^d_{EL} &= 4\pi\mathrm{i}(k^3/n)\sqrt{\frac{\mu}{\varepsilon}}\mathbf{p}\cdot\mathbf{J}^*_{EL}(k,\mathbf{r}_d) = 4\pi\mathrm{i}(k^3/\varepsilon)\,\mathbf{p}\cdot\mathbf{J}^*_{EL}(k,\mathbf{r}_d),\end{aligned} \tag{44}$$

k being the wave vector in the medium where the dipole is embedded. For $r < r_d$, one interchanges j_l and $h^{(1)}_l$ and one has

$$\begin{aligned}\mathbf{E}_d(\mathbf{r}) &= \sum_L \left[\alpha^d_{ML}\mathbf{J}_{ML}(k,\mathbf{r}) + \alpha^d_{EL}\mathbf{J}_{EL}(k,\mathbf{r})\right],\\ \mathbf{H}_d(\mathbf{r}) &= -\mathrm{i}\sqrt{\frac{\varepsilon}{\mu}}\sum_L \left[\alpha^d_{ML}\mathbf{J}_{EL}(k,\mathbf{r}) + \alpha^d_{EL}\mathbf{J}_{ML}(k,\mathbf{r})\right],\end{aligned} \tag{45}$$

where

$$\begin{aligned}\alpha^d_{ML} &= 4\pi\mathrm{i}(k^3/\varepsilon)\,\mathbf{p}\cdot\mathbf{H}^*_{ML}(k,\mathbf{r}_d),\\ \alpha^d_{EL} &= 4\pi\mathrm{i}(k^3/n)\sqrt{\frac{\mu}{\varepsilon}}\mathbf{p}\cdot\mathbf{H}^*_{EL}(k,\mathbf{r}_d) = 4\pi\mathrm{i}(k^3/\varepsilon)\,\mathbf{p}\cdot\mathbf{H}^*_{EL}(k,\mathbf{r}_d).\end{aligned} \tag{46}$$

To avoid confusion, asterisk here and in Eq. (44) above denotes the complex conjugation which only applies to the vector spherical harmonics and not to the spherical Bessel functions [13,14].

Let the dipole be radiating in the nth shell. Then the combined field in the nth shell is characterized by two sets of the expansion coefficients, one at the *lower* shell boundary and the other at the *upper* shell boundary (unless the shell is the $(N+1)$th shell, i.e., the ambient host medium). Hence, the electromagnetic fields within a generic shell, where the dipole is located, are given for $r < r_d$ as

$$\begin{aligned}\mathbf{E}_<(\mathbf{r}) &= \sum_{\gamma L}[(A_{\gamma L} + \alpha^d_{\gamma L})\mathbf{J}_{\gamma L}(k_n,\mathbf{r}) + B_{\gamma L}\mathbf{H}_{\gamma L}(k_n,\mathbf{r})],\\ \mathbf{H}_<(\mathbf{r}) &= -\mathrm{i}\sqrt{\frac{\varepsilon_h}{\mu_h}}\sum_{\gamma L}[(A_{\gamma L} + \alpha^d_{\gamma L})\mathbf{J}_{EL}(k_n,\mathbf{r}) + B_{\gamma L}\mathbf{H}_{\gamma L}(k_n,\mathbf{r})],\end{aligned} \tag{47}$$

and, for $r > r_d$, as

$$\begin{aligned}\mathbf{E}_{>}(\mathbf{r}) &= \sum_{\gamma L}[A_{\gamma L}\mathbf{J}_{\gamma L}(k_n,\mathbf{r}) + (B_{\gamma L} + a^d_{\gamma L})\mathbf{H}_{\gamma L}(k_n,\mathbf{r})],\\ \mathbf{H}_{>}(\mathbf{r}) &= -\mathrm{i}\sqrt{\frac{\varepsilon_h}{\mu_h}}\sum_{\gamma L}[A_{\gamma L}\mathbf{J}_{EL}(k_n,\mathbf{r}) + (B_{\gamma L} + a^d_{\gamma L})\mathbf{H}_{\gamma L}(k_n,\mathbf{r})]\end{aligned} \tag{48}$$

[see also Eq. (52) below]. Within any other shell, electromagnetic fields are expanded into series (8)–(10) as in Section 3.

By imposing two boundary conditions, an *interior* boundary condition (either *regularity* condition (29) at the sphere center, or a *perfectly conducting* boundary condition (36) at the sphere core boundary) and an *exterior* boundary condition at the sphere outer boundary, it will be shown that the expansion coefficients $A_{\gamma L}$ and $B_{\gamma L}$ at any shell are unambiguously determined as m-independent linear combinations of the dipole expansion coefficients $a^d_{\gamma L}$ and $\alpha^d_{\gamma L}$. The interior boundary condition does not depend on the dipole position, i.e., whether the dipole is inside or outside the sphere. The condition is the same as in the absence of the dipole source. We have seen in Section 3 that imposing an interior boundary condition is tantamount to the choice of an appropriate initial vector for the forward recurrence, i.e., either (37) or (42). On the other hand, the exterior boundary condition at the sphere outer boundary does depend on the dipole position. One has to strictly distinguish whether the dipole is inside or outside the sphere. The reason is that there is an incident dipole field on the sphere in the latter case, whereas the incident dipole field is absent in the former case. Hence, iff the dipole is *within* the sphere, the resulting solution is required to satisfy the *outgoing boundary conditions* outside the sphere, i.e., $A_{EL}(N+1) = A_{ML}(N+1) \equiv 0$, or

$$C_{EL} = C_{ML} = 0. \tag{49}$$

On the other hand, if the dipole is *outside* the sphere, one imposes at the sphere outer boundary $A_{\gamma L}(N+1) = \alpha^d_{\gamma L}$, or

$$C_{\gamma L} = \alpha^d_{\gamma L}. \tag{50}$$

In the following, the focus will be mainly on the case of the interior regularity boundary condition (29), and hence of the initial vector (37) for the forward recurrence. The necessary modification to be made for the case of a perfectly conducting core specified by the perfectly conducting boundary conditions (36) are briefly summarized in Section 4.3.

4.1. Electromagnetic fields outside the multilayered sphere

The goal is to determine the $D_{\gamma L}$ coefficients. Three separate cases are distinguished: (i) dipole in a generic sphere shell different from the core and ambient (ii) dipole in the sphere core, and (iii) dipole outside the sphere. In all these case it will be shown that the $D_{\gamma L}$ coefficient is an m-independent linear combination of the dipole field expansion coefficients $a^d_{\gamma L}$ and $\alpha^d_{\gamma L}$. We shall begin with the case of an electric dipole in a generic sphere shell different from the core.

4.1.1. Dipole source within a generic shell

According to expansions (47) and (48), combined field in the nth shell, which is different from the core and from the ambient, is characterized by two sets of the expansion coefficients, one at the *lower* shell boundary [with the $(n-1)$th shell],

$$A_{\gamma L}(n)+\alpha^d_{\gamma L},\quad B_{\gamma L}(n), \tag{51}$$

and the other at the *upper* shell boundary [with the $(n+1)$th shell],

$$A_{\gamma L}(n),\quad B_{\gamma L}(n)+a^d_{\gamma L}. \tag{52}$$

Using ordered products of the forward (backward) transfer matrices one can translate the expansion coefficients $A_{\gamma L}$ and $B_{\gamma L}$ between the sphere core (sphere exterior) and any given interior shell. Indeed, upon imposing the boundary conditions (49), or, equivalently, using the initial vector (37), one finds,

$$\begin{pmatrix} A(n)+\alpha^d \\ B(n)\end{pmatrix}=\mathscr{T}(n)\begin{pmatrix} A(1)\\ 0\end{pmatrix}, \tag{53}$$

$$\begin{pmatrix} A(n) \\ B(n)+a^d\end{pmatrix}=\mathscr{M}(n)\begin{pmatrix} 0\\ D\end{pmatrix}, \tag{54}$$

where $\mathscr{T}(n)=\prod_{j=1}^{n-1}T^+(j)$ and $\mathscr{M}(n)=\prod_{j=n}^{N}T^-(j)$ are the ordered products of transfer matrices introduced by Eq. (30). In what follows, only the relations between expansion coefficients $A_{\gamma L}$ and $B_{\gamma L}$ for a given polarization γ and angular momentum L in different shells mediated by ordered products $\mathscr{T}$ and $\mathscr{M}$ of transfer matrices are of any relevance. Therefore, for the sake of clarity, the γ and L subscripts of the expansion coefficients and of ordered products will be temporarily suspended here and hereafter, except for the resulting formulas. Eqs. (53) and (54) imply

$$B(n)=\mathscr{T}_{21}(n)A(1),\quad A(n)=\mathscr{M}_{12}(n)D, \tag{55}$$

and

$$A(n)+\alpha^d=\mathscr{T}_{11}(n)A(1),\quad B(n)+a^d=\mathscr{M}_{22}(n)D. \tag{56}$$

We remind that the goal is to determine D in terms of the dipole field expansion coefficients α^d and a^d. Upon inverting the second equation in (56),

$$D=\mathscr{M}^{-1}_{22}B(n)+\mathscr{M}^{-1}_{22}a^d=[\mathscr{M}_{22}]^{-1}\mathscr{T}_{21}A(1)+\mathscr{M}^{-1}_{22}a^d, \tag{57}$$

where, in the last equation, we have substituted for $B(n)$ according to the first equation in (55). We remind here that $\mathscr{M}^{-1}_{ik}$ denotes the inverse of the matrix element $\mathscr{M}_{ik}$ and should not be confused with the (ik)th matrix element of the inverse matrix $\mathscr{M}^{-1}$. Similarly for $\mathscr{T}^{-1}_{ik}$. For the sake of clarity, the argument n of $\mathscr{M}$ and $\mathscr{T}$ will be disregarded for the rest of the section. According to the first equation in (56),

$$A(1)=\mathscr{T}^{-1}_{11}A(n)+\mathscr{T}^{-1}_{11}\alpha^d=\mathscr{T}^{-1}_{11}\mathscr{M}_{12}D+\mathscr{T}^{-1}_{11}\alpha^d. \tag{58}$$

Therefore,

$$D=\mathscr{M}^{-1}_{22}\mathscr{T}_{21}A(1)+\mathscr{M}^{-1}_{22}a^d=\mathscr{M}^{-1}_{22}\mathscr{T}_{21}\mathscr{T}^{-1}_{11}(\mathscr{M}_{12}D+\alpha^d)+\mathscr{M}^{-1}_{22}a^d. \tag{59}$$

Hence, after inverting the second equation in (56), substituting for $B(n)$ from the first equation in (55), substituting for $A(1)$ from the first equation in (56), and for $A(n)$ from the second equation in (55),

$$D_{\gamma L} = \frac{\mathscr{M}^{-1}_{22;\gamma l}\left(\mathscr{T}_{21;\gamma l}\mathscr{T}^{-1}_{11;\gamma l}\alpha^d_{\gamma L} + a^d_{\gamma L}\right)}{1 - \mathscr{M}^{-1}_{22;\gamma l}\mathscr{T}_{21;\gamma l}\mathscr{T}^{-1}_{11;\gamma l}\mathscr{M}_{12;\gamma l}} = \frac{\mathscr{T}_{21;\gamma l}\mathscr{T}^{-1}_{11;\gamma l}\alpha^d_{\gamma L} + a^d_{\gamma L}}{\mathscr{M}_{22;\gamma l} - \mathscr{T}_{21;\gamma l}\mathscr{T}^{-1}_{11;\gamma l}\mathscr{M}_{12;\gamma l}}$$
$$= \frac{\mathscr{T}_{11;\gamma l}a^d_{\gamma L} + \mathscr{T}_{21;\gamma l}\alpha^d_{\gamma L}}{\mathscr{M}_{22;\gamma l}\mathscr{T}_{11;\gamma l} - \mathscr{M}_{12;\gamma l}\mathscr{T}_{21;\gamma l}}, \tag{60}$$

where the polarization and angular momentum subscripts are showed again. Similarly, after inverting the second equation in (55), substituting for $A(n)$ from the first equation in (56), substituting for $A(1)$ from the first equation in (55), and for $B(n)$ from the second equation in (56),

$$D_{\gamma L} = -\frac{\mathscr{M}^{-1}_{12;\gamma l}\left(\mathscr{T}_{11;\gamma l}\mathscr{T}^{-1}_{21;\gamma l}a^d_{\gamma L} + \alpha^d_{\gamma L}\right)}{1 - \mathscr{M}^{-1}_{12;\gamma l}\mathscr{T}_{11;\gamma l}\mathscr{T}^{-1}_{21;\gamma l}\mathscr{M}_{22;\gamma l}} = -\frac{\mathscr{T}_{11;\gamma l}a^d_{\gamma L} + \mathscr{T}_{21;\gamma l}\alpha^d_{\gamma L}}{\mathscr{M}_{12;\gamma l}\mathscr{T}_{21;\gamma l} - \mathscr{M}_{22;\gamma l}\mathscr{T}_{11;\gamma l}}. \tag{61}$$

As expected, the expressions (60) and (61) yield identical results.

4.1.2. Dipole source within the sphere core

In the case of a homogeneous sphere, or, in the case when the dipole source is located in the sphere core, one solves for

$$\begin{pmatrix} A(1) \\ a^d \end{pmatrix} = \mathscr{M}(1)\begin{pmatrix} 0 \\ D \end{pmatrix}, \tag{62}$$

which yields

$$D_{\gamma L} = a^d_{\gamma L}/\mathscr{M}_{22;\gamma l}(1). \tag{63}$$

Note in passing that the formula also follows from Eq. (60) by setting $\mathscr{T}_{21} = 0$ and $\mathscr{T}_{11}$ to an arbitrary *nonzero* number.

4.1.3. Dipole source outside the sphere

In the case of a dipole source located outside the sphere, the second boundary condition in Eq. (49) is to be replaced by the boundary condition (50). Hence one solves for

$$\begin{pmatrix} \alpha^d \\ D \end{pmatrix} = \mathscr{T}(N+1)\begin{pmatrix} A(1) \\ 0 \end{pmatrix}, \tag{64}$$

which yields

$$D_{\gamma L} = \left[\mathscr{T}_{21;\gamma l}(N+1)/\mathscr{T}_{11;\gamma l}(N+1)\right]\alpha^d_{\gamma L}. \tag{65}$$

Note in passing that the formula also follows from Eq. (60) by setting $\mathscr{M}_{12} = 0$, $\mathscr{M}_{22} = 1$, and $a^d_\gamma = 0$. It should be emphasized that Eq. (65) is only valid when the observation point $\mathbf{r}$ satisfies $r < r_d$. In view of the dipole field expansions (43) and (45), for $r > r_d$ the coefficient $C_{\gamma L}$ vanishes and $D_{\gamma L}$ changes into

$$D_{\gamma L} = a^d_{\gamma L} + [\mathscr{T}_{21;\gamma l}(N+1)/\mathscr{T}_{11;\gamma l}(N+1)]\alpha^d_{\gamma L}. \tag{66}$$

Note that the ratio $\mathscr{T}_{21}/\mathscr{T}_{11}$ has been related to the Mie coefficients a and b [see Eqs. (32)–(34)].

4.1.4. Compact form of the $D_{\gamma L}$ expansion coefficient

Results of preceding subsections prove that irrespective of the dipole position, the expansion coefficient $D_{\gamma L}$ is an m-independent linear combination of the dipole field expansion coefficients $a^d_{\gamma L}$ and $\alpha^d_{\gamma L}$, which have been defined by Eqs. (44) and (46). Schematically,

$$D_{\gamma L} = P_{\gamma l} a^d_{\gamma L} + Q_{\gamma l}\alpha^d_{\gamma L}, \tag{67}$$

where the coefficients $P_{\gamma l}$ and $Q_{\gamma l}$ do not depend on m. Consequently, each expansion coefficient $D_{\gamma L}$ can be written in terms of a general vector multipole $\mathbf{F}_{\gamma L}$ defined by Eq. (3) as follows:

$$D_{\gamma L} = 4\pi \mathrm{i}(k^3/\varepsilon)\,\mathbf{p}\cdot\mathbf{F}^*_{\gamma L}(k,\mathbf{r}_d), \tag{68}$$

where k and ε are the wave vector and dielectric constant in the dipole medium and [compare Eqs. (67) and (68)]

$$f_{\gamma l} = P_{\gamma l} j_l + Q_{\gamma l} h^{(1)}_l. \tag{69}$$

As a consequence of Eqs. (44) and (46), the complex conjugation in Eq. (68) only applies to the vector spherical harmonics and not to the spherical Bessel functions. Note that, in contrast to Eq. (3), the linear combinations $f_{\gamma l}$ for the electric and magnetic polarization are *different*. Therefore, the first line of Eq. (5) does not apply in the present case.

According to Eqs. (60) and (69), for the *dipole within a shell* different from the core,

$$\begin{aligned} P_{\gamma l} &= \frac{\mathscr{T}_{11;\gamma l}}{\mathscr{M}_{22;\gamma l}\mathscr{T}_{11;\gamma l} - \mathscr{T}_{21;\gamma l}\mathscr{M}_{12;\gamma l}}, \\ Q_{\gamma l} &= \frac{\mathscr{T}_{21;\gamma l}}{\mathscr{M}_{22;\gamma l}\mathscr{T}_{11;\gamma l} - \mathscr{T}_{21;\gamma l}\mathscr{M}_{12;\gamma l}}. \end{aligned} \tag{70}$$

For the *dipole source within the sphere core*, Eq. (63) implies that

$$P_{\gamma l} = \mathscr{M}^{-1}_{22;\gamma l}, \quad Q_{\gamma l} = 0. \tag{71}$$

For the *dipole source outside the sphere*, Eqs. (65) and (92) imply that

$$P_{\gamma l} = 1, \quad Q_{\gamma l} = \mathscr{T}_{21;\gamma l}/\mathscr{T}_{11;\gamma l}. \tag{72}$$

According to Eqs. (70)–(72) one can easily verify that the coefficients $P_{\gamma l}$ and $Q_{\gamma l}$ do not depend on m. The fact follows from the spherical symmetry of the problem, which implies that neither forward nor backward scattering matrix depends on m.

Therefore, as already indicated, the only dependence of $D_{\gamma L}$ on m is via the vector spherical harmonics of the general vector multipole $\mathbf{F}_{\gamma L}$ [see Eq. (3)].

4.2. Electromagnetic fields inside the multilayered sphere

Results of Section 4 provided compact formulas which allow one to determine electromagnetic fields *outside* the sphere, irrespective of the dipole position. However, for instance if energy dissipation is to be calculated, it is also important to determine electromagnetic fields *inside* the sphere. Provided the nth shell is between the dipole shell and the $(N+1)$th shell (see Section 4.2.1), the expansion coefficients $A_{\gamma L}(n)$ and $B_{\gamma L}(n)$ in the nth shell can be obtained as m-independent linear combinations of the expansion coefficients $C_{\gamma L}$ and $D_{\gamma L}$ on the outside sphere boundary by applying the backward transfer matrix $\mathscr{M}(n)=\prod_{j=n}^{N}T^{-}(j)$. Electromagnetic fields at $\mathbf{r}$ within the nth shell are then straightforwardly obtained using Eqs. (8)–(10). However, this formal approach would have overlooked that the linear combinations $A_{\gamma L}(n)\mathbf{J}_{\gamma L}(k_n,\mathbf{r})+B_{\gamma L}(n)\mathbf{H}_{\gamma L}(k_n,\mathbf{r})$ for a given γ and L often factorize into the product of two terms, one dependent of the dipole location $\mathbf{r}_d$ and the other dependent of $\mathbf{r}$ [see Eq. (75) below]. The latter will have important consequences for speeding up numerical calculations.

The goal of this section is to have closer look at the expansion coefficients $A_{\gamma L}(n)$ and $B_{\gamma L}(n)$ in the nth shell and to simplify the expression resulting by applying the backward and forward transfer matrices $\mathscr{M}(n)$ and $\mathscr{T}(n)$. Without any loss of generality, let n be the number of shell under consideration and n_d be the shell number, where dipole is radiating. We will distinguish the following three different cases: (i) $n_d<n$ or $n_d=N+1$, (ii) $n_d=n$, and (iii) $n<n_d<N+1$.

4.2.1. The case when either $n_d < n$ or $n < n_d = N + 1$

Using the backward transfer matrix $\mathscr{M}(n)$, the expansion coefficients $A_{\gamma L}(n)$ and $B_{\gamma L}(n)$ in the nth shell are obtained as linear combinations of $C_{\gamma L}(n)$ and $D_{\gamma L}(n)$,

$$\begin{aligned} A_{\gamma L}(n) &= \mathscr{M}_{11;\gamma l}(n)C_{\gamma L}+\mathscr{M}_{12;\gamma l}(n)D_{\gamma L},\\ B_{\gamma L}(n) &= \mathscr{M}_{21;\gamma l}(n)C_{\gamma L}+\mathscr{M}_{22;\gamma l}(n)D_{\gamma L}, \end{aligned} \tag{73}$$

where, in the sphere core, either the regular boundary condition, $B_{\gamma L}(1)\equiv 0$ [see Eq. (29)], or the perfectly conducting boundary condition (36) is applied. The $C_{\gamma L}$ coefficient is *zero* except for the case of a dipole outside the sphere. Therefore, for the dipole radiating *inside* the sphere, Eq. (73) for the expansion coefficients within the nth shell reduce to

$$A_{\gamma L}(n)=\mathscr{M}_{12;\gamma l}(n)D_{\gamma L},\quad B_{\gamma L}(n)=\mathscr{M}_{22;\gamma l}(n)D_{\gamma L}. \tag{74}$$

Eq. (73) then only apply if the dipole is radiating *outside* the sphere. Now, for the dipole radiating outside the sphere, one has $D_{\gamma L}=[\mathscr{T}_{21;\gamma l}(N+1)/\mathscr{T}_{11;\gamma l}(N+1)]\alpha^{d}_{\gamma L}$ [see Eq. (65)] and, according to Eq. (50), $C_{\gamma L}=\alpha^{d}_{\gamma L}$, where $\alpha^{d}_{\gamma L}$ is given by Eq. (46). Therefore, in view of Eqs. (73) and (74), the preceding discussion can be summarized

by the following important conclusion: irrespective of the dipole location, the expansion coefficients $A_{\gamma L}(n)$ and $B_{\gamma L}(n)$ within the nth shell are both proportional to either $D_{\gamma L}$ (if the radiating dipole is inside the sphere) or $\alpha^d_{\gamma L}$ (if the dipole is radiating outside the sphere). Hence

$$A_{\gamma L}(n)\mathbf{J}_{\gamma L}(k_n,\mathbf{r}) + B_{\gamma L}(n)\mathbf{H}_{\gamma L}(k_n,\mathbf{r}) = \delta_{\gamma L}(k,\mathbf{r}_d)\mathbf{G}_{\gamma L}(k_n,\mathbf{r}), \tag{75}$$

where $\mathbf{G}_{\gamma L}$ is a general vector multipole (3) with an m-independent linear combination of Bessel functions

$$g_{\gamma l}(k_n r) = a_{\gamma l} j_l(k_n r) + b_{\gamma l} h^{(1)}_l(k_n r), \tag{76}$$

the respective $k = \omega\sqrt{\varepsilon_d \mu_d}/c$ and $k_n = \omega\sqrt{\varepsilon_n \mu_n}/c$ are the wave vector in the dipole and in the nth shell, and

$$\delta_{\gamma L} = \begin{cases} D_{\gamma L}, & \text{dipole inside the sphere,} \\ \alpha^d_{\gamma L}, & \text{dipole outside the sphere.} \end{cases} \tag{77}$$

For a dipole *inside* the sphere, the $a_{\gamma l}$ and $b_{\gamma l}$ coefficients are obtained from the analogue of Eq. (74), which is obtained by substituting on the left-hand side the $a_{\gamma l}$ and $b_{\gamma l}$ in place of $A_{\gamma L}(n)$ and $B_{\gamma L}(n)$ and by replacing on the right-hand side of Eq. (74) $D_{\gamma L}$ by *unity*, i.e.,

$$a_{\gamma l} = \mathscr{M}_{12;\gamma l}(n), \quad b_{\gamma l} = \mathscr{M}_{22;\gamma l}(n). \tag{78}$$

For dipole *outside* the sphere, the $a_{\gamma l}$ and $b_{\gamma l}$ coefficients are obtained from the analogue of Eq. (73), which is obtained by substituting on the right-hand side of Eq. (73) the *nonzero* dipole field expansion coefficients $C_{\gamma L}$ by unity and $D_{\gamma L}$ by $\mathscr{T}_{21;\gamma l}(N+1)/\mathscr{T}_{11;\gamma l}(N+1)$ (the two last replacement are equivalent to replacing $\alpha^d_{\gamma L}$ by unity), i.e.,

$$\begin{aligned} a_{\gamma l} &= \mathscr{M}_{11;\gamma l}(n) + \mathscr{M}_{12;\gamma l}(n)\mathscr{T}_{21;\gamma l}(N+1)/\mathscr{T}_{11;\gamma l}(N+1), \\ b_{\gamma l} &= \mathscr{M}_{21;\gamma l}(n) + \mathscr{M}_{22;\gamma l}(n)\mathscr{T}_{21;\gamma l}(N+1)/\mathscr{T}_{11;\gamma l}(N+1). \end{aligned} \tag{79}$$

Note different arguments of $\mathscr{M}$ and $\mathscr{T}$ here. The coefficients $a_{\gamma l}$ and $b_{\gamma l}$ should be confused neither with the Mie coefficients, nor, in the case of $a_{\gamma l}$, with the dipole expansion coefficient $a^d_{\gamma L}$ as given by Eq. (44). The dipole expansion coefficient is distinguished by the superscript d and by an explicit dependence on the magnetic angular number m. It should be reminded that, similarly to the case of the dipole field expansion coefficient $D_{\gamma L}$ [see Eq. (67)], the linear combinations $g_{\gamma l}$ of Bessel functions for the electric and magnetic polarizations are *different*. Therefore, the first line of Eq. (5) does not apply to $\mathbf{G}_{\gamma L}$.

Regarding the right-hand side of Eq. (75), the dependence on the material constants of the medium at the dipole location $\mathbf{r}_d$ is contained in $\delta_{\gamma L}$, whereas the dependence on the material constants on the material constants of the shell medium is explicitly introduced via k_n in the argument of $g_{\gamma l}(k_n r)$. The dependence of the entire sphere geometry and its material properties contained in $a_{\gamma l}$, $b_{\gamma l}$, and $\delta_{\gamma L}$ is not shown explicitly. We would like to emphasize that the $a_{\gamma l}$ and $b_{\gamma l}$ coefficients defined here do depend neither on the magnetic number m nor the dipole location $\mathbf{r}_d$. Therefore, the

linear combination $g_{\gamma l}$ of Bessel functions, defined by Eq. (76), does only depend on the orbital angular number l. The only dependence on the magnetic number m on the right-hand side of Eq. (75) is introduced via $\delta_{\gamma L}$ and the transverse and longitudinal vector spherical harmonics in the general multipole $\mathbf{G}_{\gamma L}$. Factorization of the linear combinations $A_{\gamma L}(n)\mathbf{J}_{\gamma L}(k_n,\mathbf{r}) + B_{\gamma L}(n)\mathbf{H}_{\gamma L}(k_n,\mathbf{r})$ for each γ and L into the product of two terms, one independent of the dipole location and the other independent of $\mathbf{r}$ within the nth shell, as provided by Eq. (75), will have important consequences for speeding up numerical calculations.

4.2.2. The case $n < n_d < N + 1$

In this case the dipole shell is between the surrounding of sphere medium and the nth shell under consideration, yet $n_d \neq N + 1$. Therefore, one can no longer use the transfer matrix $\mathscr{M}(n)$ to transfer electromagnetic fields between the $N + 1$th and nth shells, as we did in preceding subsections. However, using $\mathscr{T}(n)$, one can transfer electromagnetic fields between the sphere core and the nth shell,

$$A_{\gamma L}(n) = \mathscr{T}_{11;\gamma l}(n)A_{\gamma L}(1), \quad B_{\gamma L}(n) = \mathscr{T}_{21;\gamma l}(n)A_{\gamma L}(1). \tag{80}$$

Thus, the linear combinations $A_{\gamma L}(n)\mathbf{J}_{\gamma L}(k_n,\mathbf{r}) + B_{\gamma L}(n)\mathbf{H}_{\gamma L}(k_n,\mathbf{r})$ for each γ and L again factorize in the form (75), where now

$$\delta_{\gamma L}(\mathbf{r}_d) = A_{\gamma L}(1), \quad g_{\gamma l}(k_n r) = \mathscr{T}_{11;\gamma l}(n) j_l(k_n r) + \mathscr{T}_{21;\gamma l}(n) h_l^{(1)}(k_n r), \tag{81}$$

i.e.,

$$a_{\gamma l} = \mathscr{T}_{11;\gamma l}(n), \quad b_{\gamma l} = \mathscr{T}_{21;\gamma l}(n). \tag{82}$$

It only remains to determine the coefficient $A_{\gamma L}(1)$. However, this can be easily accomplished by substituting expression (60) for $D_{\gamma L}$ into Eq. (58). After a simple algebra one finds

$$A_{\gamma L}(1) = \frac{\mathscr{M}_{12;\gamma l}(n_d)a^d_{\gamma L} + \mathscr{M}_{22;\gamma l}(n_d)\alpha^d_{\gamma L}}{\mathscr{M}_{22;\gamma l}(n_d)\mathscr{T}_{11;\gamma l}(n_d) - \mathscr{M}_{12;\gamma l}(n_d)\mathscr{T}_{21;\gamma l}(n_d)}. \tag{83}$$

Upon substituting the expressions (44) and (46) for the dipole field expansion coefficients $a^d_{\gamma L}$ and $\alpha^d_{\gamma L}$ into Eq. (83), one finds

$$A_{\gamma L}(1) = 4\pi \mathrm{i}(k^3/\varepsilon)\,\mathbf{p}\cdot\mathbf{V}^*_{\gamma L}(k,\mathbf{r}_d), \tag{84}$$

where $\mathbf{V}_{\gamma L}(k,\mathbf{r}_d)$ is a general vector multipole (3) with an m-independent linear combination of Bessel functions

$$v_{\gamma l}(kr_d) = \frac{\mathscr{M}_{12;\gamma l}(n_d) j_l(kr_d) + \mathscr{M}_{22;\gamma l}(n_d) h_l^{(1)}(kr_d)}{\mathscr{M}_{22;\gamma l}(n_d)\mathscr{T}_{11;\gamma l}(n_d) - \mathscr{M}_{12;\gamma l}(n_d)\mathscr{T}_{21;\gamma l}(n_d)}. \tag{85}$$

As a consequence of Eqs. (44) and (46), the complex conjugation in Eq. (84) only applies to the vector spherical harmonics and not to the spherical Bessel functions. The last two formulas can readily be obtained by a slight modification of arguments presented in Section 4.1.4.

4.2.3. The case of an interior dipole shell $n_d = n$

Let us now consider the case when the dipole is within the shell under consideration, which is different from the ambient. Then $C_{\gamma L} \equiv 0$ and the expansion coefficients $A_{\gamma L}(n)$ and $B_{\gamma L}(n)$ can most easily be obtained from the matrix equation (54), wherein the respective expressions (60) and (63) for the dipole within a generic shell and within the sphere core are substituted for $D_{\gamma L}$.

$$A_{\gamma L}(n) = \mathscr{M}_{12;\gamma l}(n) D_{\gamma L}, \quad B_{\gamma L}(n) = \mathscr{M}_{22;\gamma l}(n) D_{\gamma L} - a^d_{\gamma L}, \tag{86}$$

It should be emphasized that if the dipole shell is the very first shell, an interior boundary condition is applied, which limits the $A_{\gamma L}(1)$ and $B_{\gamma L}(1)$ coefficients according to either Eq. (37) or Eq. (42) (see Section 3.1 for more details). In any case, note that the interior boundary condition $B_{\gamma L}(1) \equiv 0$ is automatically satisfied if the expression (63) for $D_{\gamma L}$ is substituted in the second of Eq. (86). For the dipole source within a generic shell one finds upon substituting the formula (60) for $D_{\gamma L}$ in Eq. (86),

$$B_{\gamma L}(n) = \frac{\mathscr{M}_{12;\gamma l}\mathscr{T}_{21;\gamma l} a^d_{\gamma L} + \mathscr{M}_{22;\gamma l}\mathscr{T}_{21;\gamma l}\alpha^d_{\gamma L}}{\mathscr{M}_{22;\gamma l}\mathscr{T}_{11;\gamma l} - \mathscr{M}_{12;\gamma l}\mathscr{T}_{21;\gamma l}}. \tag{87}$$

Hence, similarly to $D_{\gamma L}$, the $B_{\gamma L}$ coefficient is also an m-independent linear combination of the dipole field expansion coefficients $a^d_{\gamma L}$ and $\alpha^d_{\gamma L}$. However, unlike the preceding two cases, for $n_d = n > 1$ the linear combinations $A_{\gamma L}(n)\mathbf{J}_{\gamma L}(k_n, \mathbf{r}) + B_{\gamma L}(n)\mathbf{H}_{\gamma L}(k_n, \mathbf{r})$ do not factorize in the product of the form given by Eq. (75).

4.3. Modifications for a perfectly conducting core

According to Section 3.1, the change from the regularity boundary condition (29) to the perfectly conducting boundary conditions (36) at the sphere core amounts to a mere replacement of the initial vector for a forward recurrence from (37) to (42), accompanied by the relabeling $n \to n - 1$ of shells. The reason for the relabeling is that the sphere core is formally excluded from the formalism, since no field penetrates the perfectly conducting sphere core boundary. For dipole within (after relabeling) the very first shell, the $A_{\gamma L}(1)$ coefficient in Eq. (42) is replaced according to Eq. (51) by $A_{\gamma L}(1) + \alpha^d_{\gamma L}$. For dipole within the second and higher shell, one can verify that the results of the preceding subsections remain valid, provided that, for respective polarizations, one replaces the vector (37) on the right-hand side of Eqs. (53), (55), (56), (64), and (80) by the vectors given by Eq. (42).

5. Time-averaged dipole radiated power

In Sections 3 and 4.2, electromagnetic fields inside and outside the multilayered sphere in the presence of a radiating electric dipole have been determined. In this section, we use this knowledge to calculate the time-averaged total radiated power, P,

and the angular distribution of the radiated power, $\mathrm{d}P/\mathrm{d}\Omega$. The total radiated power of a dipole is found by integrating the radial component of the time-averaged Poynting vector over the surface of a sphere with large radius r [13],

$$P(r) = r^2 \oint \langle \mathbf{S} \rangle \cdot \mathbf{r}_0 \, \mathrm{d}\Omega, \tag{88}$$

and then letting the integration sphere radius $r \to \infty$. In the free space, the time-averaged power radiated per unit solid angle by the oscillating electric-dipole moment $\mathbf{p}$ is

$$\frac{\mathrm{d}P^0}{\mathrm{d}\Omega} = \frac{c}{8\pi} r^2 \mathrm{Re}\left[\mathbf{r}_0 \cdot (\mathbf{E} \times \mathbf{B}^*)\right] = \frac{c}{8\pi} k^4 |\mathbf{r}_0 \times (\mathbf{r}_0 \times \mathbf{p})|^2. \tag{89}$$

The state of polarization of the radiation is given by the vector inside the absolute value signs. If the components of $\mathbf{p}$ all have the same phase, the angular distribution is a typical dipole pattern,

$$\frac{\mathrm{d}P^0}{\mathrm{d}\Omega} = \frac{c}{8\pi} k^4 |\mathbf{p}|^2 \sin^2\theta, \tag{90}$$

where the angle θ is measured from the direction of $\mathbf{p}$. The time-averaged total radiated power of a free dipole is then [13,49]

$$P^0 = \frac{c}{8\pi} \sqrt{\frac{\varepsilon_h}{\mu_h}} r^2 \oint |\mathbf{E}|^2 \, \mathrm{d}\Omega = \frac{c k_h^4 p^2}{3\varepsilon_h^2} \sqrt{\frac{\varepsilon_h}{\mu_h}} = \frac{c k_h^4 p^2}{3\varepsilon_h n_h}. \tag{91}$$

The presence of a multilayered sphere modifies the radiated field. The expansion coefficients $C_{\gamma L}$ and $D_{\gamma L}$ outside the multilayered sphere were unambiguously determined in terms of the dipole expansion coefficients $a_{\gamma L}^d$ and $\alpha_{\gamma L}^d$ by solving the Maxwell equations in the presence of the scatterer by imposing two boundary conditions, one [Eq. (29)] at the sphere center and the second [either (49) or (50)] at the outer boundary of the multilayered sphere. If the dipole is *within* the multilayered sphere, then, according to Eq. (49), $C_{\gamma L} \equiv 0$ since there is no incident field on the sphere. On the other hand, $C_{\gamma L} \neq 0$ if the dipole is *outside* the scatterer, since there is an incident field on the sphere due to the radiating dipole [Eq. (50)]. Note in passing that the incident dipole field on the sphere is only present for $r < r_d$. Indeed, in view of the dipole field expansions (43) and (45) [see also expansions (47) and (47)], the expansion coefficients $C_{\gamma L}$ become identically zero for $r > r_d$, and the expansion coefficients $D_{\gamma L}$ change into

$$D_{\gamma L} \to D_{\gamma L} + a_{\gamma L}^d. \tag{92}$$

Therefore, irrespective if the dipole is located inside or outside the sphere, the field *outside* the multilayered sphere for $r > r_d$ can be represented by the expansion

$$\begin{aligned} \mathbf{E}(\mathbf{r}) &= \sum_L \left[D_{ML}\mathbf{H}_{ML} + D_{EL}\mathbf{H}_{EL}\right], \\ \mathbf{H}(\mathbf{r}) &= -\mathrm{i}\sqrt{\frac{\varepsilon_h}{\mu_h}} \sum_L \left[D_{ML}\mathbf{H}_{EL} + D_{EL}\mathbf{H}_{ML}\right]. \end{aligned} \tag{93}$$

5.1. Angular distribution of the radiated power

For a time-harmonic electromagnetic field, the time-average of the Poynting vector over interval large compared to the fundamental period is given by [49]

$$\langle \mathbf{S} \rangle = \frac{c}{4\pi} \langle \mathbf{E}_0 \times \mathbf{H}_0 \rangle = \frac{c}{8\pi} \mathrm{Re}[\mathbf{E}_0 \times \mathbf{H}_0^*], \tag{94}$$

where $\mathbf{E}_0$ and $\mathbf{H}_0$ are complex vector functions of position and c is the speed of light in the vacuum. The time-averaged angular distribution of the radiated power, $\mathrm{d}P/\mathrm{d}\Omega$, is calculated as the $r \to \infty$ limit of $\langle \mathbf{S} \rangle$,

$$\frac{\mathrm{d}P}{\mathrm{d}\Omega} = \frac{c}{8\pi} \lim_{r\to\infty} r^2 \left\{ \mathrm{Re}\left[\mathbf{E}_0 \times \mathbf{H}_0^*\right] \right\} \cdot \mathbf{r}_0. \tag{95}$$

One has $(\mathbf{E}_0 \times \mathbf{H}_0^*) \cdot \mathbf{r}_0 = \mathbf{E}_0 \cdot (\mathbf{H}_0^* \times \mathbf{r}_0)$. Since $(\mathbf{H}_0^* \times \mathbf{r}_0)$ is transverse, one has $\mathbf{E}_0 \cdot (\mathbf{H}_0^* \times \mathbf{r}_0) = \mathbf{E}_{0\|} \cdot (\mathbf{H}_0^* \times \mathbf{r}_0)$. Upon using identities (9.1.23), (10.1.11), and (10.1.12) of [48] one finds in the asymptotic region of $z \to \infty$,

$$h_l^{(1)}(z) \sim \mathrm{i}^{-l} h_0^{(1)}(z) = \mathrm{i}^{-l-1} \frac{\mathrm{e}^{iz}}{z}, \tag{96}$$

and, in the asymptotic region of $r \to \infty$,

$$\frac{\mathrm{d}(rh_l)(k_h r)}{\mathrm{d}r} \sim \mathrm{i}.\mathrm{i}^{-l-1} \mathrm{e}^{\mathrm{i}k_h r}, \quad \frac{\mathrm{d}(rh_l)^*(k_h r)}{\mathrm{d}r} \sim -\mathrm{i}.\mathrm{i}^{-l-1} \mathrm{e}^{-\mathrm{i}k_h^* r}. \tag{97}$$

Therefore, for $r \gg r_s$,

$$\begin{aligned}
\mathbf{E}_{0\|}(\mathbf{r}) &\sim \sum_L \mathrm{i}^{-l-1} [D_{ML} \mathbf{Y}_L^{(m)} + \mathrm{i} D_{EL} \mathbf{Y}_L^{(e)}] \frac{\mathrm{e}^{\mathrm{i}k_h r}}{k_h r}, \\
\mathbf{H}_0^*(\mathbf{r}) \times \mathbf{r}_0 &= \sqrt{\frac{\varepsilon_h}{\mu_h}}^* \left\{ -\mathrm{i} \sum_L \mathrm{i}^{-l-1} [\mathrm{i} D_{ML} (\mathbf{Y}_L^{(e)} \times \mathbf{r}_0) + D_{EL} (\mathbf{Y}_L^{(m)} \times \mathbf{r}_0)] \right\}^* \frac{\mathrm{e}^{-\mathrm{i}k_h^* r}}{k_h^* r} \\
&\sim \sqrt{\frac{\varepsilon_h}{\mu_h}}^* \left\{ \sum_L \mathrm{i}^{-l-1} [D_{ML} \mathbf{Y}_L^{(m)} + \mathrm{i} D_{EL} \mathbf{Y}_L^{(e)}] \right\}^* \frac{\mathrm{e}^{-\mathrm{i}k_h^* r}}{k_h^* r} = \sqrt{\frac{\varepsilon_h}{\mu_h}}^* \mathbf{E}_{0\|}^*(\mathbf{r}).
\end{aligned} \tag{98}$$

Finally,

$$\begin{aligned}
\frac{\mathrm{d}P(r)}{\mathrm{d}\Omega} &= \frac{\mathrm{e}^{-2k_h'' r}}{8\pi |k_h|^2} c \left\{ \mathrm{Re} \sqrt{\frac{\varepsilon_h}{\mu_h}}^* \right\} |\mathbf{E}_{0\|}(\mathbf{r})|^2 \\
&= \frac{\mathrm{e}^{-2k_h'' r}}{8\pi |k_h|^2} c \left\{ \mathrm{Re} \sqrt{\frac{\varepsilon_h}{\mu_h}}^* \right\} \left| \sum_L \mathrm{i}^{-l-1} [D_{ML} \mathbf{Y}_L^{(m)} + \mathrm{i} D_{EL} \mathbf{Y}_L^{(e)}] \right|^2.
\end{aligned} \tag{99}$$

5.2. Total radiated power

The total radiated power is obtained by integrating the time-averaged angular distribution of the radiated power, $\mathrm{d}P/\mathrm{d}\Omega$, over a large concentric spherical surface in the usual way. Using integral identities (B.3), (B.8), and (B.7), and assuming that the flux is calculated at the distance $r > r_d$ *outside* the sphere, and hence that the expansion (93) can be used, one finds for $r \gg r_s$

$$\begin{aligned} P(r) &= \frac{c}{4\pi} r^2 \oint \langle \mathbf{S} \rangle \cdot \mathbf{r}_0 \, \mathrm{d}\Omega = \frac{c}{8\pi} r^2 \oint \{ \mathrm{Re}[\mathbf{E}_0 \times \mathbf{H}_0^*] \} \cdot \mathbf{r}_0 \, \mathrm{d}\Omega \\ &= \frac{\mathrm{e}^{-2k_h'' r}}{8\pi |k_h|^2} c \left\{ \mathrm{Re} \sqrt{\frac{\varepsilon_h}{\mu_h}}^* \right\} \sum_L [|D_{ML}|^2 + |D_{EL}|^2], \end{aligned} \tag{100}$$

where k_h'' is the imaginary part (if any) of the wave vector in the surrounding medium. Indeed, upon introducing the identities (B.3), (B.8), and (B.7) in the first equation in (100), one arrives at

$$\begin{aligned} P(r) &= \frac{c}{8\pi} r^2 \mathrm{Re} \left\{ \mathrm{i} \sqrt{\frac{\varepsilon_h}{\mu_h}}^* \sum_L \left[D_{ML} D_{ML'}^* \oint (\mathbf{H}_{ML} \times \mathbf{H}_{EL'}^*) \cdot \mathbf{r}_0 \, \mathrm{d}\Omega \right.\right. \\ &\qquad \left.\left. + D_{EL} D_{EL'}^* \oint (\mathbf{H}_{EL} \times \mathbf{H}_{ML'}^*) \cdot \mathbf{r}_0 \, \mathrm{d}\Omega \right] \right\} \\ &= \frac{c}{8\pi} r^2 \mathrm{Re} \left\{ \mathrm{i} \sqrt{\frac{\varepsilon_h}{\mu_h}}^* \sum_L \left[|D_{ML}|^2 h_l(k_h r) \left[\frac{(r h_l)'(k_h r)}{k_h r} \right]^* \right.\right. \\ &\qquad \left.\left. - |D_{EL}|^2 \frac{(r h_l)'(k_h r)}{k_h r} h_l^*(k_h r) \right] \right\}. \end{aligned} \tag{101}$$

In arriving at the result (100) one uses identities (96) and (97) for $r \gg r_s$. The difference in sign in front of $|D_{ML}|^2$ and $|D_{EL}|^2$ in Eq. (101) is then compensated by the following identities in the asymptotic region $r \gg r_s$,

$$h_l(k_h r) \left[\frac{(r h_l)'(k_h r)}{k_h r} \right]^* \sim -\mathrm{i} \frac{\mathrm{e}^{-2k_h'' r}}{|k_h|^2 r^2}, \quad \frac{(r h_l)'(k_h r)}{k_h r} h_l^*(k_h r) \sim \mathrm{i} \frac{\mathrm{e}^{-2k_h'' r}}{|k_h|^2 r^2}. \tag{102}$$

Note in passing that in the case of an absorbing host medium, $k_h'' > 0$, the dipole radiated power, as expected, vanishes in the limit $r \to \infty$.

5.2.1. Summation over the magnetic number

The resulting expression for the total dipole radiated power (100) can be further simplified by performing in the sum

$$\sum_{l=1}^{\infty} \sum_{m=-l}^{l} [|D_{ML}|^2 + |D_{EL}|^2] \tag{103}$$

the summation over the magnetic angular momentum number m. According to Eq. (68) established in Section 4.1.4, irrespective of the dipole position each expansion coefficient $D_{\gamma L}$ can be written as follows,

$$D_{\gamma L} = 4\pi\mathrm{i}(k^3/\varepsilon)\,\mathbf{p}\cdot\mathbf{F}^*_{\gamma L}(k,\mathbf{r}_d), \tag{104}$$

where k and ε are the wave vector and dielectric constant in the dipole medium and $\mathbf{F}_{\gamma L}$ is a general vector multipole defined by Eq. (3) with an m-independent linear combination of Bessel functions $f_{\gamma l}$ given by Eq. (69).

The sum rules [52,65] imply that

$$\begin{aligned}
&\sum_{m=-l}^{l}\mathbf{Y}^{(m)}_L(\mathbf{r})\otimes\mathbf{Y}^{(m)*}_L(\mathbf{r}) = \frac{2l+1}{8\pi}(\mathbf{e}_\theta\otimes\mathbf{e}_\theta+\mathbf{e}_\phi\otimes\mathbf{e}_\phi),\\
&\sum_{m=-l}^{l}\mathbf{Y}^{(e)}_L(\mathbf{r})\otimes\mathbf{Y}^{(e)*}_L(\mathbf{r}) = \frac{2l+1}{8\pi}(\mathbf{e}_\theta\otimes\mathbf{e}_\theta+\mathbf{e}_\phi\otimes\mathbf{e}_\phi),\\
&\sum_{m=-l}^{l}\mathbf{Y}^{(o)}_L(\mathbf{r})\otimes\mathbf{Y}^{(o)*}_L(\mathbf{r}) = \frac{2l+1}{4\pi}\mathbf{e}_r\otimes\mathbf{e}_r,\\
&\sum_{m=-l}^{l}\mathbf{Y}^{(m)}_L(\mathbf{r})\otimes\mathbf{Y}^{(e)*}_L(\mathbf{r}) = \sum_{m=-l}^{l}\mathbf{Y}^{(m)}_L(\mathbf{r})\otimes\mathbf{Y}^{(o)*}_L(\mathbf{r}) = \sum_{m=-l}^{l}\mathbf{Y}^{(e)}_L(\mathbf{r})\otimes\mathbf{Y}^{(o)*}_L(\mathbf{r})\equiv 0,
\end{aligned} \tag{105}$$

where $\mathbf{e}_r$, $\mathbf{e}_\theta$, and $\mathbf{e}_\phi$ are the orthonormal unit vectors of the spherical coordinate system and $\otimes$ denotes the tensor product of vectors (dyadic) in $\mathbb{R}^3$. Therefore, for a general multipole (3),

$$\begin{aligned}
\sum_{m=-l}^{l}|\mathbf{p}\cdot\mathbf{F}_{ML}(k,\mathbf{r})|^2 &= \frac{2l+1}{8\pi}|f_{Ml}(kr)|^2(|\mathbf{p}_\theta|^2+|\mathbf{p}_\phi|^2),\\
\sum_{m=-l}^{l}|\mathbf{p}\cdot\mathbf{F}_{EL}(k,\mathbf{r})|^2 &= \frac{2l+1}{4\pi}\,l(l+1)\frac{|f_{El}(kr)|^2}{|k|^2r^2}|\mathbf{p}_r|^2\\
&\quad+\frac{2l+1}{8\pi}\frac{|(rf_{El})'(kr)|^2}{|k|^2r^2}(|\mathbf{p}_\theta|^2+|\mathbf{p}_\phi|^2).
\end{aligned} \tag{106}$$

Consequently, upon combining Eqs. (68) and (106) the sum over m in Eq. (103) is easily performed,

$$\begin{aligned}
\sum_L[|D_{ML}|^2+|D_{EL}|^2] &= 4\pi(|k|^6/|\varepsilon|^2)l(l+1)(2l+1)\frac{|f_{El}(kr)|^2}{|k|^2r^2}|\mathbf{p}_r|^2+2\pi(|k|^6/|\varepsilon|^2)\\
&\quad\times(2l+1)\left[|f_{Ml}(kr)|^2+\frac{|(rf_{El})'(kr)|^2}{|k|^2r^2}\right](|\mathbf{p}_\theta|^2+|\mathbf{p}_\phi|^2).
\end{aligned} \tag{107}$$

Upon substituting the results into Eq. (100),

$$P(r) = \frac{c|k|^4|n|^2}{2|\varepsilon|^2|n_h|^2}\left\{\mathrm{Re}\sqrt{\frac{\varepsilon_h}{\mu_h}}^{*}\right\}\mathrm{e}^{-2k_h''r} \times \sum_l (2l+1)\left\{ l(l+1)\,\frac{|f_{El}(kr)|^2}{|k|^2r^2}p_r^2 + \left[|f_{Ml}(kr)|^2 + \frac{|(rf_{El})'(kr)|^2}{|k|^2r^2}\right]\frac{p_\theta^2+p_\phi^2}{2}\right\}, \tag{108}$$

where $f_{\gamma l}$ is given by Eq. (69) and the dipole position was temporarily denoted by $\mathbf{r}$. In arriving at Eq. (108) we have used that $|k_h|^2 = |k|^2|n_h|^2/|n|^2$. We remind here that k, ε, and n are the wave vector, dielectric constant, and refractive index in the dipole medium, whereas k_h, ε_h, and n_h are the corresponding quantities in the surrounding sphere medium (ambient).

6. Energy dissipation in the case of an absorbing shell

The formula for the energy flux density (in the Gaussian units), $\mathbf{S} = c(\mathbf{E}\times\mathbf{H})/4\pi$, remains valid in variable electromagnetic fields, even if dispersion is present. The rate of change of the energy in unit volume of the body is $\nabla\cdot\mathbf{S}$. In the case when the absorption is negligible (transparency window), i.e., the imaginary parts of ε and μ are small compared to their respective real parts, the energy can be defined after averaging over the characteristic period of electromagnetic field. As a result, one obtains the so-called Brillouin expression,

$$U = \frac{1}{8\pi}\left[\mathbf{E}\cdot\mathbf{E}^*\frac{\mathrm{d}[\omega\varepsilon(\omega)]}{\mathrm{d}\omega} + \mathbf{H}\cdot\mathbf{H}^*\frac{\mathrm{d}[\omega\mu(\omega)]}{\mathrm{d}\omega}\right]. \tag{109}$$

By *averaging* with respect to time and assuming that the amplitude of a monochromatic electromagnetic field is a constant, one can find the *steady* (averaged) inflow of energy Q per unit time and unit volume from the external sources which maintain the field,

$$Q = \frac{ck_0}{8\pi}(\varepsilon''|\mathbf{E}|^2 + \mu''|\mathbf{H}|^2), \tag{110}$$

where k_0 is the vacuum wave vector and $\varepsilon''(\mu'')$ is the imaginary part of the dielectric function (magnetic permeability) at the observation point. However, as is shown in Appendix C, the formula (110) for Ohmic losses remains valid even in the regions of high absorption near resonance frequencies of the permittivity and permeability when the Brillouin expression (109) is no longer valid.

In this section, the total Ohmic loss, P^{nrad}, is calculated according to formula

$$P^{\mathrm{nrad}} = \int_a Q(\mathbf{r})\,\mathrm{d}\mathbf{r}, \tag{111}$$

where Q is given by Eq. (110) and the volume integral extends over all the absorbing regions. For simplicity, we will assume that $\mu''\equiv 0$, i.e., the Ohmic losses will be entirely determined by an integral of the squared amplitude of the electric intensity. The case of both ε'' and μ'' being nonzero follows then straightforwardly. In order to avoid confusion between the dipole shell, where the dipole is radiating, and an absorbing shell, from now on k_a and ε_a will stand for the respective wave vector and the dielectric constant in the absorbing medium, whereas k and ε will denote

the corresponding quantities in the dipole shell. The respective dipole and absorbing shells will bear the labels n_d and n_a and it will be assumed that $n_d \neq n_a$. The latter case is the most interesting from the practical point of view. The remaining case of $n_d = n_a$ follows easily from the results of Section 4.2.3 (see also Section 9 where the frequency shift is treated) and is left as an exercise.

According to Eq. (8), the electric field at $\mathbf{r}$ within a given nth shell due to a dipole $\mathbf{p}$ at $\mathbf{r}_d$ (either inside or outside the sphere) radiating at frequency ω is given as follows,

$$\mathbf{E}(\mathbf{r}) = \sum_{\gamma L} [A_{\gamma L}(n)\mathbf{J}_{\gamma L}(k_n, \mathbf{r}) + B_{\gamma L}(n)\mathbf{H}_{\gamma L}(k_n, \mathbf{r})], \tag{112}$$

where $A_{\gamma L}(n)$ and $B_{\gamma L}(n)$ are the familiar expansion coefficients. It has been shown is Section 4.2 [see Eqs. (75), (76), (77), and (81)] that in either of the cases $n_d < n_a$, $n_d = N+1$, $n_a < n_d < N+1$,

$$A_{\gamma L}(n_a)\mathbf{J}_{\gamma L}(k_a, \mathbf{r}) + B_{\gamma L}(n_a)\mathbf{H}_{\gamma L}(k_a, \mathbf{r}) = \delta_{\gamma L}(k, \mathbf{r}_d)\mathbf{G}_{\gamma L}(k_a, \mathbf{r}).$$

Here the vector multipole $\mathbf{G}_{\gamma L}(k_n,\mathbf{r})$, which is independent of dipole position, is characterized by an m-independent linear combination of the Bessel functions $g_{\gamma l}$ defined by Eqs. (76) and (81), whereas $\delta_{\gamma L}(k,\mathbf{r}_d)$, which does depend on the dipole position and dipole medium properties, is defined by Eqs. (77) and (81). Upon substituting the respective expressions (46) and (68) for the dipole field expansion coefficient $\alpha^d_{\gamma L}$ and $D_{\gamma L}$ into Eq. (77), and upon using the formula (84) for $A_{\gamma L}(1)$, one finds

$$\delta_{\gamma L}(k, \mathbf{r}_d) = 4\pi \mathrm{i}(k^3/\varepsilon)\, \mathbf{p} \cdot \mathbf{d}^*_{\gamma L}(k, \mathbf{r}_d), \tag{113}$$

$$\mathbf{d}_{\gamma L} = \begin{cases} \mathbf{F}^*_{\gamma L}, & \text{dipole inside the sphere and } n_d < n_a, \\ \mathbf{H}^*_{\gamma L}, & \text{dipole outside the sphere}, \\ \mathbf{V}^*_{\gamma L}, & \text{dipole inside the sphere and } n_a < n_d < N+1. \end{cases} \tag{114}$$

(Note that the complex conjugation in Eqs. (113) and (114) only applies to the vector spherical harmonics and not to the spherical Bessel functions.)

Let us now turn to the calculation of the integral on the right-hand side of Eq. (111). Upon combining relations (113), (76), and (81) with integration identities (B.10) and (B.11), one obtains

$$\begin{aligned} \int_a |\mathbf{E}|^2 \,\mathrm{d}\mathbf{r} &= \int_a r^2 \mathrm{d}r \oint |\mathbf{E}(\mathbf{r})|^2 \,\mathrm{d}\Omega \\ &= \frac{16\pi^2|k|^6}{|\varepsilon|^2} \sum_{l=1}^{\infty} \left\{ \left[\int_a r^2 |a_{Ml} j_l(k_a r) + b_{Ml} h_l(k_a r)|^2 \,\mathrm{d}r \right] \left(\sum_{m=-l}^{l} |\mathbf{p} \cdot \mathbf{d}_{ML}|^2 \right) \right. \\ &\quad + \frac{l(l+1)}{|k_a|^2} \left[\int_a |a_{El} j_l(k_a r) + b_{El} h_l(k_a r)|^2 \,\mathrm{d}r \right] \left(\sum_{m=-l}^{l} |\mathbf{p} \cdot \mathbf{d}_{EL}|^2 \right) \\ &\quad \left. + \frac{1}{|k_a|^2} \left[\int_a |a_{El} (r j_l)'(k_a r) + b_{El} (r h_l)'(k_a r)|^2 \,\mathrm{d}r \right] \left(\sum_{m=-l}^{l} |\mathbf{p} \cdot \mathbf{d}_{EL}|^2 \right) \right\} \\ &= \frac{16\pi^2|k|^6}{|\varepsilon|^2} \sum_{l=1}^{\infty} \left[I_{Ml} \left(\sum_{m=-l}^{l} |\mathbf{p} \cdot \mathbf{d}_{ML}|^2 \right) + \left(I^{(1)}_{El} + I^{(2)}_{El} \right) \left(\sum_{m=-l}^{l} |\mathbf{p} \cdot \mathbf{d}_{EL}|^2 \right) \right]. \end{aligned} \tag{115}$$

Here $\int_a$ denotes the radial integration over the sphere shell with a nonzero imaginary part of the dielectric constant and

$$\begin{aligned} I_{Ml} &= \int_a |a_{Ml} j_l(k_a r) + b_{Ml} h_l(k_a r)|^2 r^2 \,\mathrm{d}r, \\ I^{(1)}_{El} &= \frac{l(l+1)}{|k_a|^2} \int_a |a_{El} j_l(k_a r) + b_{El} h_l(k_a r)|^2 \,\mathrm{d}r, \\ I^{(2)}_{El} &= \frac{1}{|k_a|^2} \int_a |a_{El} (r j_l)'(k_a r) + b_{El} (r h_l)'(k_a r)|^2 \,\mathrm{d}r. \end{aligned} \tag{116}$$

Note that in virtue of the factorization (75), the respective integrals defined by Eq. (116) do not depend on the dipole location, as long as the dipole remains to be located within a given shell. Therefore, when dipole position is varied within a given shell, it is sufficient to calculate the integrals (116) only once, what greatly facilitates and speeds up numerical calculation.

6.1. Summation over the magnetic number

As in the calculation of the total radiative power in Sections 5.2 and 5.2.1, the expression on the r.h.s. of Eq. (115) can be considerably simplified by performing the sum over the magnetic number m. Indeed, using expressions (106), which are valid for any multipole of the form as that on the r.h.s. of Eq. (3),

$$\begin{aligned} \sum_{m=-l}^{l} |\mathbf{p}\cdot\mathbf{d}_{ML}(\mathbf{k},\mathbf{r})|^2 &= \frac{2l+1}{8\pi} |d_{Ml}(kr)|^2 (|\mathbf{p}_\theta|^2 + |\mathbf{p}_\phi|^2), \\ \sum_{m=-l}^{l} |\mathbf{p}\cdot\mathbf{d}_{EL}(\mathbf{k},\mathbf{r})|^2 &= \frac{2l+1}{4\pi} l(l+1) \frac{|d_{El}(kr)|^2}{|k|^2 r^2} |\mathbf{p}_r|^2 \\ &\quad + \frac{2l+1}{8\pi} \frac{|(r d_{El})'(kr)|^2}{|k|^2 r^2} (|\mathbf{p}_\theta|^2 + |\mathbf{p}_\phi|^2), \end{aligned} \tag{117}$$

where throughout this subsection $\mathbf{r}$ denotes the dipole position. Upon substituting expressions (117) back into Eq. (115),

$$\begin{aligned} \int |\mathbf{E}|^2 \,\mathrm{d}\mathbf{r} = \frac{4\pi|k|^6}{|\varepsilon|^2} \sum_l (2l+1) \Bigg\{ & l(l+1) I_{El} \frac{|d_{El}(kr)|^2}{|k|^2 r^2} p_r^2 \\ & + \left[I_{Ml} |d_{Ml}(kr)|^2 + I_{El} \frac{|(r d_{El})'(kr)|^2}{|k|^2 r^2} \right] \frac{p_\theta^2 + p_\phi^2}{2} \Bigg\}, \end{aligned} \tag{118}$$

where we have introduced $I_{El} \equiv I^{(1)}_{El} + I^{(2)}_{El}$. According to our hypothesis, the imaginary part of the magnetic permeability is zero, $\mu'' \equiv 0$. Therefore, by combining Eqs. (110), (111), and (118), the time-averaged Ohmic loss P^{nrad} of an oscillating dipole is

$$\begin{aligned} P^{\mathrm{nrad}} = P^{\mathrm{nrad}}_{\perp} + P^{\mathrm{nrad}}_{\parallel} = \frac{c|k|^6 |k_0|}{2|\varepsilon|^2} \varepsilon''_a \sum_l (2l+1) \Bigg\{ & l(l+1) I_{El} \frac{|d_{El}(kr)|^2}{|k|^2 r^2} p_r^2 \\ & + \left[I_{Ml} |d_{Ml}(kr)|^2 + I_{El} \frac{|(r d_{El})'(kr)|^2}{|k|^2 r^2} \right] \frac{p_\theta^2 + p_\phi^2}{2} \Bigg\}. \end{aligned} \tag{119}$$

According to Eq. (114), the linear combinations of Bessel functions

$$d_{\gamma l} = \begin{cases} f_{\gamma l}, & \text{dipole inside the sphere and } n_d < n_a, \\ h_l^{(1)}, & \text{dipole outside the sphere}, \\ v_{\gamma l}, & \text{dipole inside the sphere and } n_a < n_d < N+1, \end{cases} \tag{120}$$

where $f_{\gamma l}$ [see Eqs. (67)–(69)] is the same linear combinations of Bessel functions as in the case of the total radiated power treated in Sections 5.2 and 5.2.1. The linear combination of Bessel functions $v_{\gamma l}$ has been determined by Eq. (85). Note in passing that all the integrals in (116) have dimension of $1/k^3$. Therefore, as expected, the Ohmic loss P^{nrad} has the same dimension as the dipole total radiated power [see, for instance, Eq. (91)].

7. Inelastic scattering

The goal of this section is to provide the description of the intensity and angular distribution of an inelastically scattered light. All the necessary formulas have been laid down in Sections 4 and 5. Therefore, it turns out sufficient here to only provide recipes of how to combine and use the formulas of the preceding sections.

By the very definition of inelastic scattering of a monochromatic light, the scattered light has a *shifted* frequency compared to the incident light. There are several mechanisms of inelastic scattering (e.g., Compton scattering). In the following, the focus will be on the so-called combination or Raman scattering, which has its origin in excitations and deexcitations of different vibrational levels of molecules [1,4]. In the Raman scattering, shifted requencies do not depend on the scattering angle and both the red- and blue-shifted frequencies may appear. The red- and blue-shifted frequencies are conventionally called the Stokes and anti-Stokes lines, respectively. The angular distribution and polarization of the emitted fluorescent and Raman radiation is different from the elastically scattered right and from the corresponding distributions for the inelastic scattering by free molecules. The measurements of this inelastically scattered radiation may provide useful information regarding the size, shape, and refractive index of the particle. In general, the angular distribution involves more terms in the series expansion. These additional terms will contain information about the sphere radius, which is of interest to cell biology [7,9,10] and atmospheric physics [6,8]. For example, atmospheric aerosols may fluoresce [8] and this might be used to provide a means for their chemical identification and to measure their content in the atmosphere. Also Raman and fluorescent backscattering can be used for remote sensing of molecular species in the atmosphere [6,8]. The angular distribution of the radiated power, $\mathrm{d}P/\mathrm{d}\Omega$, as given by Eq. (99), when used in conjunction with the Lorentz–Mie scattering, provides an information on the distribution of the inelastically scattering molecules within the particle [1].

In the following, it will be assumed that the timescale on which the incident light is applied is significantly longer than the molecular vibrational transitions. Therefore, a conventional model of the inelastic scattering will be adopted [4,5], according to

which (a) the incident light is assumed to be applied continuously and (b) the bandwidth of the applied light is sufficiently narrow so that there is no overlap with a shifted frequency of inelastically scattered light. A conventional model of the inelastic scattering [4,5] comprises two steps. In the first step, a molecule or atom located at a particular position is excited by absorption of a photon at an incident frequency ω_0. The excited molecule electric-dipole moment is expressed as [4,5]

$$\mathbf{p}(\omega_{\mathrm{R}}) = \alpha_R \mathbf{E}_{\mathrm{loc}}(\mathbf{r}, \omega_0), \tag{121}$$

where $\omega_{\mathrm{R}} \neq \omega_0$ is a *shifted* Raman frequency and α_{R} is the molecular Raman polarizability. The primary, or the local field, $\mathbf{E}_{\mathrm{loc}}$ is the total electric field at the molecule position, which is given by the sum of the incident and scattered fields, $\mathbf{E}_{\mathrm{loc}} = \mathbf{E}_{\mathrm{i}} + \mathbf{E}_{\mathrm{s}}$. The field $\mathbf{E}_{\mathrm{loc}}$ can be determined anywhere inside and outside a multicoated sphere using the results of Section 3. The molecular Raman polarizability α_{R} is a phenomenological parameter, which is proportional to the probability that the active molecule is raised to an excited state. The latter is in turn assumed to be proportional to the number density of active molecules at a given location [82], provided that the density of the active molecules is not too high. It is well known experimentally that fluorescence intensity as a function of the duration of (constant) irradiation by a monochromatic light steadily decreases with time, i.e., the so-called photobleaching occurs [32,82]. The latter case can be modeled by a time (and the incident light intensity) dependent Raman polarizability α_{R}.

The second step is the emission of radiation at a *shifted* Raman frequency ω_{R} by the active molecules, which is entirely characterized by the field of the induced molecular dipole $\mathbf{p}$ given by Eq. (121). Using expansions (43), (45), (47), and (48) for the induced molecular dipole $\mathbf{p}$, the total Raman field, $\mathbf{E}_{\mathrm{R}}(\mathbf{r}, \omega_{\mathrm{R}})$ can be determined anywhere outside and inside a multicoated sphere using the results of Sections 4.1 and 4.2. For instance, the Raman signal $\mathbf{E}_{\mathrm{R}}(\mathbf{r}, \omega_{\mathrm{R}})$ *outside* the sphere at the observer coordinate $\mathbf{r}$ is given by expansion (48). The latter is sometimes schematically written in the form [4,5]

$$\mathbf{E}_{\mathrm{R}}(\mathbf{r}, \omega_{\mathrm{R}}) = \mathbf{E}_d(\mathbf{r}, \omega_{\mathrm{R}}) + \mathbf{E}_s(\mathbf{r}, \omega_{\mathrm{R}}), \tag{122}$$

where $\mathbf{E}_d$ is the field of an oscillating molecular dipole $\mathbf{p}$ as given by Eq. (43), and $\mathbf{E}_s$ is the dipole field after experiencing scattering due to the presence of boundaries [given by the expansion coefficients $A_{\gamma L}$ and $B_{\gamma L}$ in the expansion (48)]. $\mathbf{E}_{\mathrm{R}}(\mathbf{r}, \omega_{\mathrm{R}})$ contains a complete information about the amplitude, phase, and polarization of the inelastically scattered field at any location, be it outside, inside, or at the surface of a multicoated sphere. Since the induced molecular dipole $\mathbf{p}(\omega_{\mathrm{R}})$ according to Eq. (121) provides a link between the applied and inelastically scattered fields, the conventional model of the inelastic scattering [4,5] amounts to a simple superposition of the results of Section 3 with those of Section 4.1 and 4.2. Obviously, in the case of a remote sensing only the results of Section 4 are relevant. Angular distribution of the time-averaged radiated power and the time-averaged total radiated power are then straightforwardly determined using results of Section 5.

If a comparison is to be made between theory and experiment, the following two facts have to be taken into account. First, for an *incoherent* emission from a distri-

bution of sources within the particle it turns out necessary to sum the time-averaged power over the molecular dipoles distribution within the particle. For a *coherent* emission, the electric field at the point of observation has to be added *prior* to the time-averaged power calculation. Second, for randomly oriented dipole sources an average has to be performed over different dipole orientations. It is worthwhile to emphasize that the transversely radiated power $P_{\parallel}$ enters with a factor 2 in an orientational average, since there are possible two different transverse dipole orientations. Hence, the orientational average at a given radial distance r from the sphere center is

$$\bar{P} = (2P_{\parallel} + P_{\perp})/3. \tag{123}$$

The same also applies to the orientational average of the angular distribution of the radiated power.

Note in passing that the conventional model of the inelastic scattering [4,5] can easily be extended to also cover the case when there is an overlap between the band-width of the applied light and the shifted frequency ω of the inelastically scattered light. One has only need to (i) take into account that the $C_{\gamma L}$ coefficient becomes nonzero and (ii) amend the formulas of Section 4 appropriately. In the case of the so-called *stimulated* Raman scattering [58,59], one needs to determine the morphology-dependent resonances. According to Eq. (32), the resonances of a multicoated sphere within our formalism are determined as zeroes of $\mathscr{T}_{11;\gamma l}(N+1)$. The angle-averaged internal electric field intensities can then be calculated using the results of Section 3.

8. Changes in the spontaneous emission—normalized transition rates

The decay rate of an excited molecule inside or outside a multilayered sphere is calculated here from the viewpoint of electromagnetic theory. In the latter case, the decay rate of the emitting dipole is obtained by considering the two mechanisms through which energy is dissipated. One is the time-averaged total radiated power or the radiative loss, P^{rad}, which has been calculated from the Poynting vector in Section 5.2, and the other is the nonradiative loss due to the Ohmic losses inside the sphere absorptive shell, P^{nrad}, which has been calculated in Section 6. Afterward the correspondence principle (1) is applied which enables one to relate the two mechanisms through which energy is dissipated to corresponding radiative, W^{rad}, and nonradiative, W^{nrad}, decay rates. It is reminded that, as in Chew et al. [1,2,13,14] treatment, any coherence between elementary emitters is neglected and only *coherence properties of the radiation field* are taken into account.

8.1. Normalized radiative decay rates

According to the correspondence principle (1), the quantum theoretical expression for the power radiated by the spontaneous emission from an excited state in an electric (a magnetic) dipole transition is obtained from the classical expression

for the power radiated by an electric (a magnetic) dipole, by replacement of the dipole moment by the corresponding transition matrix element. In order to characterize the change in the spontaneous emission due to the presence of a scatterer, one usually determines the ratio of the power radiated by a dipole in the presence of the scatterer to the power radiated by the dipole in a free-space homogeneous medium. The free-space homogeneous medium is either characterized by the optical constants of the ambient surrounding the scatterer, or the free-space homogeneous medium optical constants can be taken to be those of a scatterer shell wherefrom the dipole is radiating. Obviously, the latter normalization has only sense if the shell medium is nonabsorbing. In the case of an absorbing shell medium, only the normalization of the dipole decay rates with respect to the dipole decay rates in the nonabsorbing host medium is an option. For the sake of notation, throughout this section the wave vector, dielectric constant, and refractive index of a given interior shell will be denoted by k, ε, and n, whereas in the ambient the usual notation k_h, ε_h, and n_h will be maintained.

8.1.1. Dipole outside the scatterer

In the case of a dipole radiating at the position **r** outside the sphere, the respective sets $\{k, \varepsilon, n\}$ and $\{k_h, \varepsilon_h, n_h\}$ coincide. Upon combining Eqs. (91) and (108) for $k_h'' = 0$, defining $P^{\mathrm{rad}} = P(r)$, and using correspondence principle (1), one finds for the dipole oscillating in the respective radial and tangential directions the following change in the dipole radiative decay rates (normalized to the decay rates in a free space filled in with the surrounding sphere host medium),

$$\begin{aligned}\frac{W_{\perp}^{\mathrm{rad}}}{W_{\perp}^{0}} &= \frac{P_{\perp}^{\mathrm{rad}}}{P_{\perp}^{0}} = \frac{3}{2}\,\mathrm{e}^{-2k_h'' r}\sum_{l} l(l+1)(2l+1)\frac{|f_{El}(kr)|^2}{|k|^2 r^2},\\ \frac{W_{\parallel}^{\mathrm{rad}}}{W_{\parallel}^{0}} &= \frac{P_{\parallel}^{\mathrm{rad}}}{P_{\parallel}^{0}} = \frac{3}{4}\sum_{l}(2l+1)\left[|f_{Ml}(kr)|^2 + \frac{|(rf_{El})'(kr)|^2}{|k|^2 r^2}\right].\end{aligned} \tag{124}$$

According to Eqs. (66), (69), and (72) one has

$$f_{\gamma l}(kr) = j_{\gamma l}(kr) + [\mathscr{T}_{21;\gamma l}/\mathscr{T}_{11;\gamma l}]h_{\gamma l}(kr). \tag{125}$$

In the special case of a homogeneous sphere, the ratio $\mathscr{T}_{21;\gamma l}/\mathscr{T}_{11;\gamma l}$ is nothing but the corresponding Mie coefficient (see Eqs. (32)–(34) and compare with Eqs. (4a) and (4b) of Chew [13]). Hence, in Eq. (5) of [13], $f_{Ml}(kr) = j_n(y_2) + a_n h_n^{(1)}(y_2)$ and $f_{El}(kr) = j_n(y_2) + b_n h_n^{(1)}(y_2)$. Therefore, our results for the dipole radiative decay rates are identical to those obtained by Chew [13].

8.1.2. Dipole inside the scatterer

Let us first consider radiative dipole decay rates normalized to the decay rates in a free-space having the optical constants of the ambient surrounding the scatterer. Upon combining Eqs. (91) and (108), one finds for the dipole at the position **r** inside the spherical scatterer oscillating in the respective radial and tangential directions the following change in the radiative dipole decay rates:

$$\frac{W_{\perp}^{\mathrm{rad}}}{W_{\perp}^{0}}=\frac{P_{\perp}^{\mathrm{rad}}}{P_{\perp}^{0}}=\frac{3}{2}\frac{|n|^{3}\varepsilon_{h}}{|\varepsilon|n_{h}^{3}}\sum_{l}l(l+1)(2l+1)\frac{|f_{El}(kr)|^{2}}{|k|^{2}r^{2}},$$
$$\frac{W_{\parallel}^{\mathrm{rad}}}{W_{\parallel}^{0}}=\frac{P_{\parallel}^{\mathrm{rad}}}{P_{\parallel}^{0}}=\frac{3}{4}\frac{|n|^{3}\varepsilon_{h}}{\varepsilon n_{h}^{3}}\sum_{l}(2l+1)\left[|f_{Ml}(kr)|^{2}+\frac{|(rf_{El})'(kr)|^{2}}{|k|^{2}r^{2}}\right], \tag{126}$$

where we have used that

$$\frac{|n|^{3}}{|\varepsilon|n_{h}^{2}}\sqrt{\frac{\varepsilon_{h}}{\mu_{h}}}=\frac{|n|^{3}\varepsilon_{h}}{|\varepsilon|n_{h}^{3}}. \tag{127}$$

We remind here that the linear combinations $f_{\gamma l}$ of the spherical Bessel functions are determined by Eqs. (69)–(71). For instance, the latter equation implies that, in the case of dipole within the sphere core,

$$f_{\gamma l}(kr)=j_{l}(kr)/\mathscr{M}_{22;\gamma l}(1). \tag{128}$$

For completeness, when the decay rates are normalized to the decay rates in a free-space having the optical constants of the sphere shell wherefrom the dipole is radiating,

$$\frac{W_{\perp}^{\mathrm{rad}}}{W_{\perp}^{0}}=\frac{P_{\perp}^{\mathrm{rad}}}{P_{\perp}^{0}}=\frac{3}{2}(|n|/n_{h})^{6}(\varepsilon_{h}/|\varepsilon|)^{2}\sum_{l}l(l+1)(2l+1)\frac{|f_{El}(kr)|^{2}}{|k|^{2}r^{2}},$$
$$\frac{W_{\parallel}^{\mathrm{rad}}}{W_{\parallel}^{0}}=\frac{P_{\parallel}^{\mathrm{rad}}}{P_{\parallel}^{0}}=\frac{3}{4}(|n|/n_{h})^{6}(\varepsilon_{h}/|\varepsilon|)^{2}\sum_{l}(2l+1)\left[|f_{Ml}(kr)|^{2}+\frac{|(rf_{El})'(kr)|^{2}}{|k|^{2}r^{2}}\right]. \tag{129}$$

Note that in a nonmagnetic medium with $\mu=\mu_{h}$ one has $\varepsilon_{h}/\varepsilon=n_{h}^{2}/n^{2}$, and hence

$$\frac{|n|^{3}\varepsilon_{h}}{|\varepsilon|n_{h}^{3}}=|n|/n_{h},\quad (|n|/n_{h})^{6}(\varepsilon_{h}/|\varepsilon|)^{2}=|\varepsilon|/\varepsilon_{h}. \tag{130}$$

Therefore, the respective normalized radiative decay rates, i.e., those normalized with respect to the free-space dipole radiative rates in a given sphere shell medium and in the ambient, respectively, differ by the factor $|n|/n_{h}$ [14].

The equivalence of our results for the dipole radiative decay rates in the case of a homogeneous sphere with those obtained by Chew [13,14] is discussed in Appendix E. It is worthwhile to remember that in the case of a homogeneous sphere one finds the normalized decay rates in the Rayleigh limit for $kr\ll 1$ independent of polarization and the location of dipole within the particle and given by the expression $W^{\mathrm{rad}}/W^{0}=9/(2+\varepsilon)^{2}$ [14].

8.2. Normalized nonradiative decay rates

As in the case of radiative decay rates, we have here two possibilities in calculating normalized nonradiative decay rates. One can divide the resulting Ohmic loss, P^{nrad}, which has been calculated in Section 6.1, either by the free-space time-averaged total

radiated power, P^0, in the same medium as where the dipole inside the sphere is radiating, or by the free-space time-averaged total radiated power in the surrounding sphere medium. We remind here that k, ε, and n are the wave vector, dielectric constant, and refractive index at the dipole position, whereas k_h, ε_h, and n_h are the corresponding quantities in the embedding (ambient) medium. Note that for the vacuum wave vector k_0 one has

$$k_0 = |k_h|/|n_h| = |k|/|n|. \tag{131}$$

Hence, one finds for the dipole oscillating in the respective radial and tangential directions at the position $\mathbf{r}$ inside or outside the spherical scatterer the following nonradiative decay rates. Those normalized with respect to the free-space radiative decay rates in the same medium as where the dipole is radiating are

$$\begin{aligned}
\frac{W_\perp^{\mathrm{nrad}}}{W_\perp^0} &= \frac{P_\perp^{\mathrm{nrad}}}{P_\perp^0} = \frac{3}{2}\frac{|k|^3}{|\varepsilon|}\varepsilon_a'' \sum_l l(l+1)(2l+1) I_{El} \frac{|d_{El}(kr)|^2}{|k|^2 r^2}, \\
\frac{W_\parallel^{\mathrm{nrad}}}{W_\parallel^0} &= \frac{P_\parallel^{\mathrm{nrad}}}{P_\parallel^0} = \frac{3}{4}\frac{|k|^3}{|\varepsilon|}\varepsilon_a'' \sum_l (2l+1)\left[I_{Ml}|d_{Ml}(kr)|^2 + I_{El}\frac{|(rd_{El})'(kr)|^2}{|k|^2 r^2}\right],
\end{aligned} \tag{132}$$

where $I_{\gamma l}$ have been determined as integrals over absorbing shell in Section 6 [see Eqs. (116) combined with $I_{El} \equiv I_{El}^{(1)} + I_{El}^{(2)}$] and the linear combination of Bessel functions $d_{\gamma l}$ is given by Eq. (120). In arriving to the result, we have, using relations (131), substituted $|k|^2|k_0|n = |k|^3$.

The nonradiative decay rates W^{nrad} normalized with respect to the free-space radiative decay rates in the ambient are

$$\begin{aligned}
\frac{W_\perp^{\mathrm{nrad}}}{W_\perp^0} &= \frac{P_\perp^{\mathrm{nrad}}}{P_\perp^0} = \frac{3}{2}\frac{|k|^3|n|^3}{n_h^3}\frac{\varepsilon_h}{|\varepsilon|^2}\varepsilon_a'' \sum_l l(l+1)(2l+1) I_{El} \frac{|d_{El}(kr)|^2}{|k|^2 r^2}, \\
\frac{W_\parallel^{\mathrm{nrad}}}{W_\parallel^0} &= \frac{P_\parallel^{\mathrm{nrad}}}{P_\parallel^0} = \frac{3}{4}\frac{|k|^3|n|^3}{n_h^3}\frac{\varepsilon_h}{|\varepsilon|^2}\varepsilon_a'' \sum_l (2l+1)\left[I_{Ml}|d_{Ml}(kr)|^2 + I_{El}\frac{|(rd_{El})'(kr)|^2}{|k|^2 r^2}\right].
\end{aligned} \tag{133}$$

The prefactor can be simplified in a nonmagnetic case when $\mu = \mu_h$, in which case $\varepsilon_h/|\varepsilon| = n_h^2/|n|^2$, and hence

$$\frac{|n|^3}{n_h^3}\frac{\varepsilon_h}{|\varepsilon|^2} = \frac{|n|}{n_h}\frac{1}{|\varepsilon|}. \tag{134}$$

Hence, as in the case of radiative decay rates, the respective nonradiative decay rates normalized with respect to the dipole radiative rates in a given shell medium and in the ambient, respectively, differ by the factor $|n|/n_h$.

Note that Eq. (120) implies for dipole *inside* the sphere $d_{\gamma l} = f_{\gamma l}$, where $f_{\gamma l}$ determines the radiative decay rates (see previous section). Therefore, the nonradiative rates can be viewed in that case as the radiative rates modulated by coefficients $I_{\gamma l}$. The latter depend on the entire sphere geometry and material constants of all shell.

9. Green's function and frequency shift

When a radiating atom or molecule interacts with the electromagnetic fields perturbed by the presence of a multilayered spherical cavity both the decay rate and the transition frequency are modified [38]. In the regime of validity of the Wigner–Weisskopf approximation (weak coupling, or linear-response, region), decay is exponential and the whole process is characterized by two numbers: the spontaneous emission rate and the radiative (Lamb) shift of the transition frequency, and both processes are linked via a Hilbert transform (see Eqs. (2.18) and (2.19) of [38]). So far, only changes in the electric-dipole radiative decay rates have been considered, which can easier be detected experimentally. Indeed, the decay rate is calculated in the first order of perturbation theory. On the other hand, the normalized change in the transition frequency, $(\omega - \omega_0)/\omega_0$ (also called the frequency or energy-level shift) induced by the presence of a multilayered spherical cavity is a second order perturbation theory result [39] and hence more challenging to observe experimentally. Nevertheless, it has been demonstrated by Mabuchi and Kimble [66] that the optical forces associated with evanescent fields of optical whispering gallery modes and cavity-induced frequency level shifts may be used to confine atoms in stable orbits around a dielectric microsphere. In this section, as in the discussion of the radiative decay rates, any coherence between elementary emitters is neglected and only *coherence properties of the radiation field* are taken into account.

In the case of spontaneous decay rates, entirely classical treatment in the spirit of Chew [13,14] and Ruppin [12] has been used. In the case of the frequency shift, the classical and quantum-mechanical result obtained within the domain of applicability of the linear-response theory, or in the weak coupling regime [38,39], are again equivalent [67]. The basic assumption here is, of course, that the transition frequency is not appreciably changed by the presence of a (multilayered) sphere. In the case of a homogeneous sphere, the quantum-mechanical linear-response formalism of Agarwal [38] and of Wylie and Sipe [39] yields the normalized transition rates as [13,47,67]

$$\frac{W}{W^0} = 1 + \frac{3\varepsilon_n}{2p^2k_n^3}\,\mathrm{Im}\,[\mathbf{p}\cdot\mathbf{G}(\mathbf{r}_d,\mathbf{r}_d,\omega_0)\cdot\mathbf{p}] = 1 + \mathrm{Im}\,\frac{3\varepsilon_n}{2p^2k_n^3}\,\mathbf{p}\cdot\mathbf{E}_s(\mathbf{r}_d,\omega_0), \tag{135}$$

where $k_n = \omega_0\sqrt{\varepsilon_n}/c$ is the emission wave vector in the sphere absence and $\mathbf{G}(\mathbf{r},\mathbf{r}_d,\omega)$ denotes the *scattering* Greens function normalized such that the electric field $\mathbf{E}_s(\mathbf{r},\omega)$ of the scattered radiation at $\mathbf{r}$ due to a dipole $\mathbf{p}$ radiating at frequency ω at $\mathbf{r}_d$ is given by

$$\mathbf{E}_s(\mathbf{r},\omega) = \mathbf{G}(\mathbf{r},\mathbf{r}_d,\omega)\cdot\mathbf{p}. \tag{136}$$

According to the expansions (47) and (48), the scattered electric field $\mathbf{E}_s(\mathbf{r},\omega)$ within the dipole shell is the part of the total electromagnetic field given by the expansion coefficients $A_{\gamma L}$ and $B_{\gamma L}$. The field $\mathbf{E}_s(\mathbf{r},\omega)$ accounts for the effect of the boundary upon the dipolar field and is what Chew's et al. called secondary field [1,4]. Obviously, in the absence of any boundaries $\mathbf{E}_s(\mathbf{r},\omega)\equiv 0$ and, as expected, there is no change in the transition rates.

Whereas change in the decay rate induced by the presence of a a (multilayered) sphere is determined by the *imaginary* part of $\mathbf{G}(\mathbf{r},\mathbf{r},\omega)$, which is in turn proportional

to the local density of states [68], the effective shift in the frequency separation of two levels is given in terms of the *real* part of $\mathbf{G}(\mathbf{r},\mathbf{r},\omega)$ (see [47], Appendix C of [38], and [67]),

$$\frac{\omega-\omega_0}{W^0}=-\frac{3\varepsilon_n}{4p^2k_n^3}\,\mathrm{Re}\,[\mathbf{p}\cdot\mathbf{G}(\mathbf{r}_d,\mathbf{r}_d,\omega_0)\cdot\mathbf{p}]=-\mathrm{Re}\,\frac{3\varepsilon_n}{4p^2k_n^3}\,\mathbf{p}\cdot\mathbf{E}_s(\mathbf{r}_d,\omega_0). \tag{137}$$

Equivalence of the classical and quantum-mechanical approaches in the spherical geometry has been verified by Chew [13], who has shown that decay rates calculated by Eq. (135) coincide with those obtained classically (see also Appendix E). Note in passing that in order to determine the induced change in both decay rate and frequency shift, the scattering Greens function is only needed at coinciding arguments. The *scattering* Greens function can easily be obtained using results of Section 4.1 and 4.2.

9.1. Dipole outside the sphere

Let us first consider the special case when the dipole is radiating *outside* the sphere in the ambient, in which case results of Section 4.1 apply. Then, the outgoing field is given by $\sum_{\gamma L}D_{\gamma L}\mathbf{H}_{\gamma L}$, where, depending whether the observation point $\mathbf{r}$ satisfies $r<r_d$ or $r>r_d$, $D_{\gamma L}$ is given by Eqs. (65) and (66), respectively. However, for $r>r_d$, the field directly radiated by the dipole without suffering any scattering also contributes to the outgoing field. Upon subtracting the dipole radiated part, which has been given by Eq. (43), one finds that, irrespective of the observation point location, the scattered field

$$\mathbf{E}_s(\mathbf{r})=\mathbf{E}(\mathbf{r})-\mathbf{E}_d(\mathbf{r})=\sum_{\gamma L}\left[\mathscr{T}_{21;\gamma l}(N+1)/\mathscr{T}_{11;\gamma l}(N+1)\right]\alpha^d_{\gamma L}\mathbf{H}_{\gamma L}(k_h,\mathbf{r}). \tag{138}$$

Using the explicit form of $\alpha^d_{\gamma L}$ as given by Eq. (46),

$$\mathbf{E}_s(\mathbf{r})=4\pi\mathrm{i}(k_h^3/\varepsilon_h)\sum_{\gamma L}[\mathscr{T}_{21;\gamma l}(N+1)/\mathscr{T}_{11;\gamma l}(N+1)][\mathbf{p}\cdot\mathbf{H}^*_{\gamma L}(k_h,\mathbf{r}_d)]\mathbf{H}_{\gamma L}(k_h,\mathbf{r}). \tag{139}$$

Therefore, for $r,\ r_d\geqslant r_s$,

$$\mathbf{G}(\mathbf{r},\mathbf{r}_d,\omega)=4\pi\mathrm{i}(k_h^3/\varepsilon_h)\sum_{\gamma L}[\mathscr{T}_{21;\gamma l}(N+1)/\mathscr{T}_{11;\gamma l}(N+1)]\mathbf{H}_{\gamma L}(k_h,\mathbf{r})\otimes\mathbf{H}^*_{\gamma L}(k_h,\mathbf{r}_d), \tag{140}$$

where $\otimes$ denotes the tensor product of vectors (dyadic) in $\mathbb{R}^3$. It is reminded here that the complex conjugation only applies to the vector spherical harmonics and not to the spherical Bessel functions. In order to compare our results with Chew's Eqs. (6′) and (7′) of [13], let us temporarily define

$$a_l=\mathscr{T}_{21;Ml}(N+1)/\mathscr{T}_{11;Ml}(N+1),\quad b_l=\mathscr{T}_{21;El}(N+1)/\mathscr{T}_{11;El}(N+1). \tag{141}$$

For $\mathbf{r}=\mathbf{r}_d$, the sum over magnetic angular number m can be explicitly performed upon using the sum rules (105), and one then arrives at

$$\mathbf{G}_{\parallel}(\mathbf{r},\mathbf{r},\omega) = \mathrm{i}(k_h^3/\varepsilon_h)\sum_l (l+\tfrac{1}{2})\left\{a_l[h_l^{(1)}(k_h r)]^2 + b_l\frac{[(rh_l^{(1)})'(k_h r)]^2}{k_h^2 r^2}\right\} \times (\mathbf{e}_\theta\otimes\mathbf{e}_\theta + \mathbf{e}_\phi\otimes\mathbf{e}_\phi),$$
$$\mathbf{G}_{\perp}(\mathbf{r},\mathbf{r},\omega) = \mathrm{i}(k_h^3/\varepsilon_h)\sum_l l(l+1)(2l+1)b_l\frac{[h_l^{(1)}(k_h r)]^2}{k_h^2 r^2}\mathbf{e}_r\otimes\mathbf{e}_r, \tag{142}$$

from which Chew's Eqs. (6) and (7) of Ref. [13] easily follow.

9.2. Dipole inside the sphere

Let us now proceed with the case when the dipole is radiating *inside* the sphere and let us assume that both $\mathbf{r}$ and $\mathbf{r}_d$ are within the nth interior dipole shell. Upon using Eq. (86), in combination with Eq. (68) and Eq. (87), for each γ and L one has

$$A_{\gamma L}(n)\mathbf{J}_{\gamma L}(k_n,\mathbf{r}) + B_{\gamma L}(n)\mathbf{H}_{\gamma L}(k_n,\mathbf{r}) \equiv 4\pi\mathrm{i}(k_n^3/\varepsilon_n)\mathbf{p}\cdot[\mathbf{Z}_{\gamma L}^{(1)*}(k_n,\mathbf{r}_d)\otimes\mathbf{J}_{\gamma L}(k_n,\mathbf{r}) + \mathbf{Z}_{\gamma L}^{(2)*}(k_n,\mathbf{r}_d)\otimes\mathbf{H}_{\gamma L}(k_n,\mathbf{r})], \tag{143}$$

where

$$\mathbf{Z}_{\gamma L}^{(1)*}(k_n,\mathbf{r}_d) = \mathscr{M}_{12;\gamma l}\mathbf{F}_{\gamma L}^{*}(k_n,\mathbf{r}_d),$$
$$\mathbf{Z}_{\gamma L}^{(2)*}(k_n,\mathbf{r}_d) = \frac{\mathscr{M}_{12;\gamma l}\mathscr{T}_{21;\gamma l}\mathbf{J}_{\gamma L}^{*}(k_n,\mathbf{r}_d) + \mathscr{M}_{22;\gamma l}\mathscr{T}_{21;\gamma l}\mathbf{H}_{\gamma L}^{*}(k_n,\mathbf{r}_d)}{\mathscr{M}_{22;\gamma l}\mathscr{T}_{11;\gamma l} - \mathscr{M}_{12;\gamma l}\mathscr{T}_{21;\gamma l}}. \tag{144}$$

Note that, in contrast to Chew's [13] homogeneous sphere case, $B_{\gamma l}\neq 0$, unless the dipole shell is the sphere core, in which case the regularity boundary condition (29) is applied.

According to Eqs. (47) and (48), the scattered field $\mathbf{E}_s$ within the dipole shell is that characterized by the multipole expansion with the $A_{\gamma L}$ and $B_{\gamma L}$ coefficients. Therefore, for $\mathbf{r}$ and $\mathbf{r}_d$ both within the nth interior shell,

$$\mathbf{G}(\mathbf{r},\mathbf{r}_d,\omega) = 4\pi\mathrm{i}(k_h^3/\varepsilon_h)\sum_{\gamma L}[\mathbf{J}_{\gamma L}(k_n,\mathbf{r})\otimes\mathbf{Z}_{\gamma L}^{(1)*}(k_n,\mathbf{r}_d) + \mathbf{H}_{\gamma L}(k_n,\mathbf{r})\otimes\mathbf{Z}_{\gamma L}^{(2)*}(k_n,\mathbf{r}_d)]. \tag{145}$$

For $\mathbf{r}=\mathbf{r}_d$, the sum over magnetic angular number m can be explicitly performed upon using the sum rules (105), and one then arrives at

$$\mathbf{G}_{\parallel}(\mathbf{r},\mathbf{r},\omega) = \mathrm{i}(k_n^3/\varepsilon_n)\sum_l (l+\tfrac{1}{2})\left[z_{Ml}^{(1)}(k_n r)j_{Ml}(k_n r) + z_{Ml}^{(2)}(k_n r)h_{Ml}(k_n r) + \frac{(rz_{El}^{(1)})'(k_n r)(rj_{El})'(k_n r) + (rz_{El}^{(2)})'(k_n r)(rh_{El})'(k_n r)}{k_n^2 r^2}\right](\mathbf{e}_\theta\otimes\mathbf{e}_\theta + \mathbf{e}_\phi\otimes\mathbf{e}_\phi),$$
$$\mathbf{G}_{\perp}(\mathbf{r},\mathbf{r},\omega) = \mathrm{i}(k_n^3/\varepsilon_n)\sum_l l(l+1)(2l+1)\frac{z_{El}^{(1)}(k_n r)j_{El}(k_n r) + z_{El}^{(2)}(k_n r)h_{El}(k_n r)}{k_n^2 r^2}\mathbf{e}_r\otimes\mathbf{e}_r, \tag{146}$$

where, for the sake of clarity, $h_l = h_l^{(1)}$ here. The frequency shift can then be determined by substituting the respective formulas (142) and (146) in Eq. (137).

10. Numerical results

The performance and convergence properties of our numerical implementation has been first tested for the calculation of the radiative and nonradiative decay rates in the homogeneous sphere case. In particular, Figs. 2 and 3 of [13] and Fig. 1 of [14]

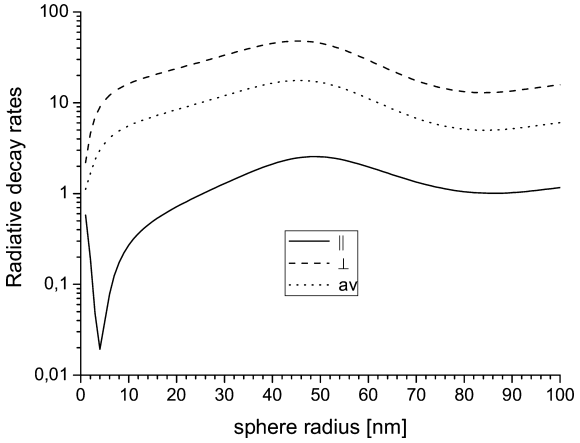

Fig. 2. Radiative decay rates normalized to the free-space decay rates in water (assuming refractive index $n_w = 1.33$) as a function of the sphere radius for a dipole radiating at wavelength of 595 nm located at a distance of 1 nm from the surface of a homogeneous gold nanosphere embedded in water. The average value plotted by dotted line is the orientational average over dipole orientations at a given radial distance r from the sphere center determined from the averaged radiated power $\bar{P}$ according to Eq. (123).

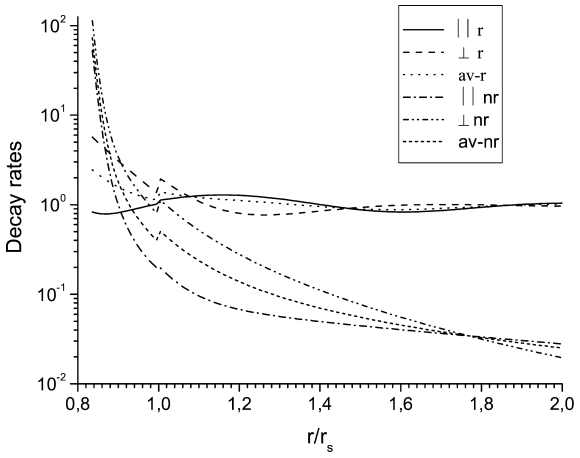

Fig. 3. Normalized radiative and nonradiative decay rates at wavelength of 595 nm as a function of dipole position in the case of $Au@SiO_2$ sphere with $r_1 = 248$ nm and $r_2 = r_s = 300$ nm embedded in water ($n_w = 1.33$).

have been reproduced. Another test was performed for the setup of a recent experiment by Dulkeith et al. [70], where the radiative and nonradiative decay rates of lissamine dye molecules, chemically attached to differently sized gold nanoparticles, were investigated in aqueous solution by means of time-resolved fluorescence experiments. Attached lissamine dye molecules were modeled as a tangentially oriented dipole located at a distance of 1 nm from the surface of a homogeneous gold nanosphere and radiating at wavelength of 595 nm. The theoretical results for decay rates as a function of the sphere radius presented in Fig. 4 of Dulkeith et al. [70] were obtained by employing the quasistatic model of Gersten and Nitzan [71] which, for a dipole outside a homogeneous sphere and in its close proximity, yields [72] (see also [43])

$$\begin{aligned}\frac{W_{\perp}^{\mathrm{rad}}}{W_{\perp}^{0}} &= \left|1+2\left(\frac{r_s}{r_s+d}\right)^3\frac{\varepsilon_s-\varepsilon_h}{\varepsilon_s+2\varepsilon_h}\right|^2,\\ \frac{W_{\parallel}^{\mathrm{rad}}}{W_{\parallel}^{0}} &= \left|1-\left(\frac{r_s}{r_s+d}\right)^3\frac{\varepsilon_s-\varepsilon_h}{\varepsilon_s+2\varepsilon_h}\right|^2,\end{aligned} \tag{147}$$

where d is the distance between the dipole (molecule) and the spherical surface. The Gersten and Nitzan model is often employed for $r_s \ll \lambda$ and $d \ll \lambda$, λ being the emission wavelength. However, in contrast to Chew results for radiative decay rates [13,14], the theory of Gersten and Nitzan [71] does not yield the correct asymptotic results for a flat surface in the limit $r_s \to \infty$ with a fixed value of d. Moreover, as emphasized by Kim et al. [72], in addition to the conditions $r_s \ll \lambda$ and $d \ll \lambda$, the value of sphere radius r_s cannot be too large for a fixed d if the Gersten and Nitzan model [71] is to be applied. Therefore, it turned out worthwhile to recalculate the

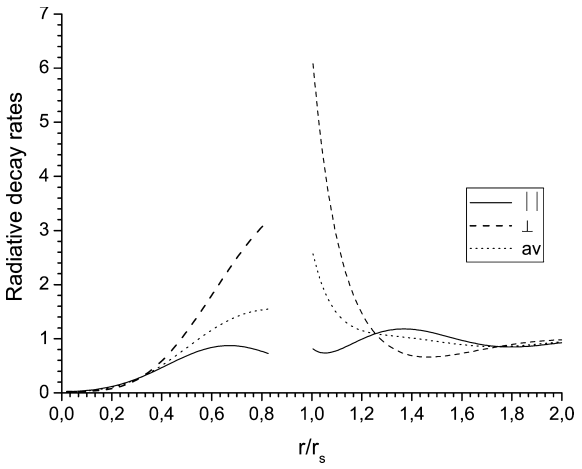

Fig. 4. Normalized radiative decay rates at wavelength of 595 nm as a function of dipole position in the case of SiO_2@Au sphere with $r_1 = 248$ nm and $r_2 = r_s = 300$ nm embedded in water ($n_w = 1.33$). The empty region for $r/r_s \in (0.82\bar{6}, 1)$ corresponds to the metallic shell.

decay rates for the same setup as in Fig. 4 of Dulkeith et al. [70] using the exact method of Chew [13,14]. The results for radiative decay rates normalized to the free-space decay rates in water (assuming refractive index $n_w = 1.33$) are shown in Fig. 2. The average value is the orientational average over dipole orientations at a given radial distance r from the sphere center determined from the averaged radiated power $\bar{P}$ according to Eq. (123). It appears that the radial decay rate is more than one magnitude larger than the tangential decay rate in the whole range of sphere radii. The tangential radiative decay rate exhibits a pronounced minimum at the distance of 4 nm from the gold nanoparticle, in accordance with experiment. It has been argued by Dulkeith et al. [70] that this is in consequence of a phase shift between the molecular and the metal dipole leading to a destructive interference effect. The local minimum of $W_{\parallel}$ at 4 nm appears to be slightly deeper than in [70], which is partially attributed to a different choice of the dielectric constant of gold, which was here chosen according to [69]. Apart from that, the overall agreement between the Gersten and Nitzan model [71] and the exact method of Chew [13,14] for sphere radii from 1 to 30 nm appears to be very good. Both the radial and tangential radiative decay rates exhibit an oscillatory behavior as a function of the sphere radius (surface curvature). The oscillatory behavior becomes only apparent for a larger range of sphere radii as that in Fig.2. Note in passing that in the quasistatic model of Gersten and Nitzan [71] a weak oscillatory behavior of radiative rates versus r_s is absent. In the calculation, neither size-dependent correction to the gold dielectric function (see Eq. (149) below and [74]), nor nonlocal effects [42,43] were taken into account (see Section 11.1 below for more details). Both these effects may effect the calculated decay rates for metal spheres with radius smaller than about 10 nm [43].

After successfully passing the test for the homogeneous sphere case, our method has been tested for coated spheres. Since a detailed comparison of theory and experiment regarding gold-coated silica beads will be studied elsewhere [32], only a few typical cases are presented here. Fig. 3 displays the radiative and nonradiative decay

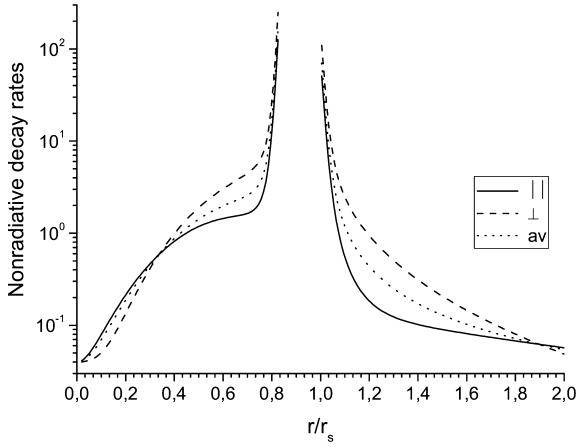

Fig. 5. Normalized nonradiative decay rates at wavelength of 595 nm as a function of dipole position in the case of SiO_2@Au sphere with $r_1 = 248$ nm and $r_2 = r_s = 300$ nm embedded in water ($n_w = 1.33$).

rates as a function of dipole position for a dipole radiating at wavelength of 595 nm in the case of Au@SiO_2 sphere with $r_1 = 248$ nm and $r_2 = r_s = 300$ nm embedded in water ($n_w = 1.33$). The respective Figs. 4 and 5 show the radiative and nonradiative decay rates as a function of dipole position in the case of SiO_2@Au sphere with $r_1 = 248$ nm and $r_2 = r_s = 300$ nm. The respective radiative and nonradiative decay rates as a function of dipole position in the case of SiO_2@Au@SiO_2 sphere with $r_1 = 200$ nm, $r_2 = 248$ nm, and $r_3 = r_s = 300$ nm are shown in Figs. 6 and 7. In all

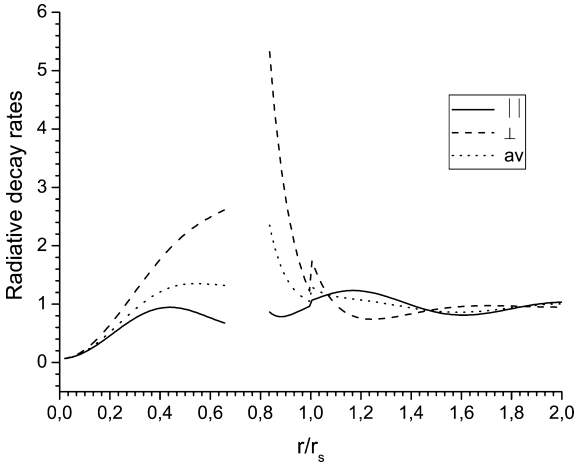

Fig. 6. Normalized radiative decay rates at wavelength of 595 nm as a function of dipole position in the case of SiO_2@Au@SiO_2 sphere with $r_1 = 200$ nm, $r_2 = 248$ nm, and $r_3 = r_s = 300$ nm embedded in water ($n_w = 1.33$). The empty region for $r/r_s \in (0.66\bar{6}, 0.82\bar{6})$ corresponds to the metallic shell.

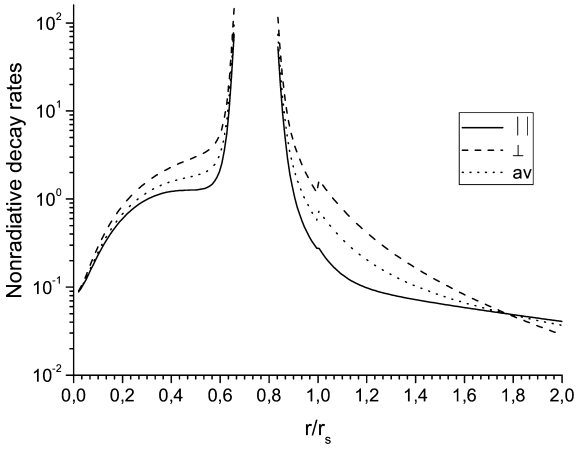

Fig. 7. Normalized nonradiative decay rates at wavelength of 595 nm as a function of dipole position in the case of SiO_2@Au@SiO_2 sphere with $r_1 = 200$ nm, $r_2 = 248$ nm, and $r_3 = r_s = 300$ nm embedded in water ($n_w = 1.33$).

figures, the decay rates are normalized with respect to the free-space radiative decay rates in the dipole medium. Empty r/r_s regions correspond to the metallic regions: first, one does not place dyes inside a metal and second, the description of decay rates in a strongly absorbing medium goes beyond the scope of theory presented here. In the calculation, the dielectric constant of SiO_2 was taken to be $n_{SiO_2} = 1.45$, dipole radiation wavelength was assumed to be 595 nm, and spheres were embedded in water ($n_w = 1.33$). Depending on the dipole position, the radiative decay rates can be either enhanced or suppressed with respect to the free-space decay rates in the same medium. It is apparent from the figures that, in the proximity of a metal shell, (i) the nonradiative decay rates are by far more dominant compared to the radiative decay rates and (ii) the radial radiative decay rate is significantly more enhanced than the tangential radiative decay rate. An oscillatory dependence of the radiative decay rates on the dipole position is also clearly visible, with the radiative decay rates approaching the free-space decay rates at $r \sim 2r_s$. Interestingly, in the case of a metal shell, the enhancement of the nonradiative decay rates is larger on the interior (with respect to the sphere center) side than on the exterior side, whereas for the radiative decay rates the reverse is true. In the most demanding case of SiO_2@Au@SiO_2 sphere (see Figs. 6 and 7), the radiative and nonradiative decay rates were calculated in a single run in approximately one second. In the latter case, calculation was performed on a standard Pentium IV PC with 200 radial position sampling points and angular-momentum cutoff was kept fixed at $l_{\max} = 60$. (There is nothing special about the choice of $l_{\max} = 60$ here, except that it guaranteed a reasonable convergence in the parameter range considered.) This high computational speed of our method renders it suitable for effective engineering of decay rates for a variety of applications.

Regarding convergence properties of the radiative and nonradiative decay rates, a diametrically different behavior is observed. As a consequence of the multipole expansion, the further is a dipole from the sphere origin, the larger cutoff value $l_{\max}$ is required to reach a comparable convergence of radiative decay rates (see Fig. 8). On the other hand, in the case of nonradiative decay rates, decisive for the convergence properties is a dipole proximity to metal boundary (see Fig. 9). In general, radiative decay rates converge faster and higher precision can be attained. Provided that summation over l is extended slightly behind the cutoff value of

$$l_c(r) \approx x + 4x^{1/3} + 2, \tag{148}$$

where $x = k_h r$, the radiative decay rates have already converged to within six digits or more. (For $r = r_s$, x reduces to the so-called size parameter and $l_c(r_s)$ becomes exactly the Wiscombe cutoff value which guarantees the convergence of single-sphere cross sections [54].) In the case of nonradiative decay rates, convergence is markedly slower. For a dipole in a very close proximity ($\lesssim 5$ nm) to metal boundary, even the angular-momentum cutoff $l_{\max}$ as large as 60 was hardly enough to ensure convergence up to two digits. A similar convergence problems in the case of nonradiative decay rates have also been encountered for the setup Fig. 4 of Dulkeith et al. [70] with the dipole-sphere separation fixed at $d = 1$ nm

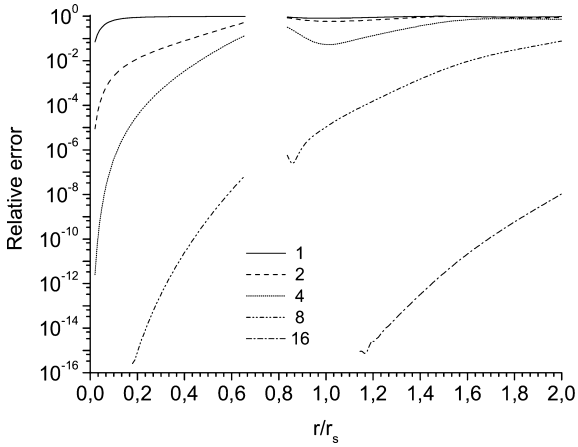

Fig. 8. Convergence of the normalized tangential radiative decay rate $W_{\perp}^{\mathrm{rad}}$ for the case of Fig. 6. Figure shows the plots of a relative error $[W_{\perp}^{\mathrm{rad}}(l) - W_{\perp}^{\mathrm{rad}}(60)]/W_{\perp}^{\mathrm{rad}}(60)$ for different values of the angular-momentum cutoff value l. Missing data in the dielectric regions signify a drop below machine accuracy. Convergence of the normalized radial radiative decay rate $W_{\parallel}^{\mathrm{rad}}$ shows a similar behavior.

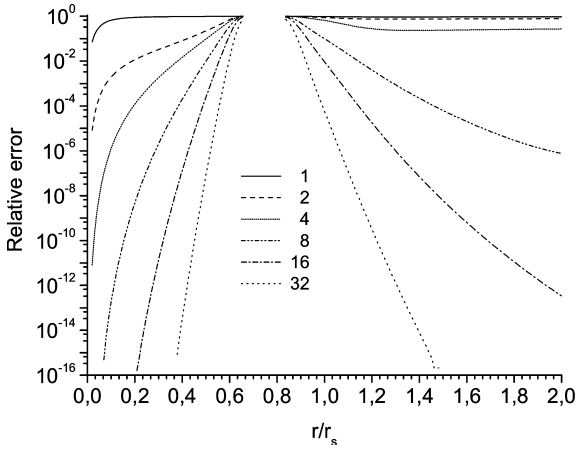

Fig. 9. Convergence of the normalized tangential nonradiative decay rate $W_{\perp}^{\mathrm{nrad}}$ for the case of Fig. 7. Figure shows the plots of a relative error $[W_{\perp}^{\mathrm{nrad}}(l) - W_{\perp}^{\mathrm{nrad}}(60)]/W_{\perp}^{\mathrm{nrad}}(60)$ for different values of the angular-momentum cutoff value l. Similarly as in the case of radiative decay rates, missing data in the dielectric regions signify a drop below machine accuracy. Convergence of the normalized radial nonradiative decay rate $W_{\parallel}^{\mathrm{nrad}}$ shows a similar behavior.

and increasing sphere radius. Provided that the sphere radius exceeded the value of $r_s \gtrsim 15\,\mathrm{nm}$, the angular-momentum cutoff $l_{\max}$ as large as 60 (i.e., more than two magnitudes larger than the Wiscombe value l_c) was still not enough to ensure con-

vergence up to two valid digits. These convergence problems with nonradiative decay rates arise due to a fact that a local theory allows for the excitation of near-field modes of an arbitrarily high angular momentum or short wavelength, although the latter is physically inhibited by the fact that the electronic wave functions extend over a spatial region of finite size. These convergence problems resulting from a close proximity of radiating dipole to metal boundaries can be overcome by taking into account a nonlocal dielectric function which introduces a cuttoff angular momentum that corrects this deficiency in a satisfactorily way [43] (see Section 11.1).

11. Recipes for an ultra-thin metallic shell and an optically active shell

In principle, one can encounter situation when the theory presented so far has to be modified, even if one limits oneself to homogeneous and isotropic media. Below two such cases are considered. First is the case of an ultra-thin metallic shell, in which nonlocal effects due to excitation of longitudinal plasmon modes may come into play [40–43]. Second, shells can be made of an optically active medium [37,44,45]. It turns out that our formal approach of Section 4 involving transfer matrices can also be applied to the case when one or several spherical shells are either ultra-thin metallic shells characterized by a nonlocal dielectric function [40–43], or shells made of an optically active medium [37,44,45]. Below recipes are provided for necessary modifications and amendments of the formalism presented until now. Note in passing that the hypothetical case of a sphere with a shell made of a negative refractive index, or "left-handed", material, which, in the simplest form of a homogeneous sphere, has been considered by Klimov [73], does not require any modification of the formalism presented in previous sections, except for filling in the relevant formulas negative permittivities and permeabilities.

11.1. Ultra-thin metallic shell and nonlocal dielectric function

Let S be the smallest length scale of a metallic region. For instance, in the case of a metal core, S equals to the core radius and, in the case of a metallic shell, S equals to the shell thickness. If theory presented in the preceding sections is to be applied for a multilayered spherical particle with a small metallic core or a thin metallic shell with $S \lesssim 20\,\mathrm{nm}$, two effects have to be considered. First, the bulk dielectric function is modified, since the electronic mean free path is shorter than in the bulk [74]. Second, nonlocal effects come into play [40–43]. The first effect does not bring any changes into our formalism and can easily be incorporated by replacing the bulk dielectric function $\varepsilon_B(\omega)$ with its size-dependent modification

$$\varepsilon(\omega) = \varepsilon_B(\omega) + \frac{\omega_p^2}{\omega^2 + \mathrm{i}\omega\tau_B^{-1}} - \frac{\omega_p^2}{\omega^2 + \mathrm{i}\omega\tau^{-1}}. \tag{149}$$

Here ω_p is the bulk plasmon frequency, τ_B is the relaxation time in the bulk metal, $\tau^{-1} = \tau_B^{-1} + v_F S^{-1}$ is the inverse relaxation time (also called damping coefficient Γ) corrected for the finite size of the particle, and v_F is the Fermi velocity. More generally,

$$\tau^{-1} = \tau_B^{-1} + A v_F S^{-1}, \tag{150}$$

where A is a parameter determined by the geometry. For simple Drude theory and isotropic scattering, $A = 1$. For a sphere of radius r_s, Kreibig and Genzel [74] used $A/S = 3/(4r_s)$.

On the other hand, *nonlocal effects*, i.e., when the Fourier transform of the dielectric function depends in addition to ω also on $\mathbf{k}$, are associated with the resonant excitation of *longitudinal* bulk plasmon modes (either propagating ones, with frequency *above* the plasma frequency ω_p, or evanescent ones, with frequency *below* the plasma frequency ω_p) [40–43]. It has already been alluded to that the nonlocal dielectric function introduces a natural cuttoff angular momentum for the excitation of near-field modes [43], and thereby a natural cuttoff for the convergence of the nonradiative decay rates. Apart from that, the nonlocal effects leave behind another important signatures. Provided that all other effects are temporarily suspended, nonlocal effects for a single sphere would manifest themselves in the blue shift of the Fröhlich local resonance at $\omega_F = \omega_p/\sqrt{3} < \omega_p$, and in the absorption fringes in the high-frequency range $\omega > \omega_p$. The blue shift, which occurs below the plasma frequency, is due to *evanescent* longitudinal plasmons [42]. On the other hand, the fringes are due to excitation of real propagating longitudinal bulk plasmons. The fringes are essentially the Tonks–Dattner resonances [75,76] of thin metallic films, which occur when

$$(\lambda_L)_n = 2d/n, \quad n = 1, 3, 5, \ldots, \tag{151}$$

where $(\lambda_L)_n$ is the normal component of the bulk longitudinal plasma wavelength and d is the film thickness. When one starts with the initial sphere radius of $\approx$1 nm, then as the sphere radius increases, the blue shift of the main resonance from its classical Fröhlich position decreases. Physically this follows from the fact that with increasing radius the slight evanescent penetration of the longitudinal modes into the sphere has smaller effect on the overall field distribution inside the sphere. Another effect caused by increasing radius is the increase in the number of secondary absorption peaks above ω_p accompanied by a decrease in their intensity. Eventually, for metal spheres larger than about 20 nm the calculated extinction curve deviates very little from the classical curve of the Mie theory [42]. With respect to the radiative rates, calculations for small ($r_s \leqslant 5$ nm) spheres reveal the following influence of nonlocal responses. For low emission frequencies ($\omega \leqslant 0.5\omega_p$), both the radial and tangential dipolar decay rates can be reduced by up to 2 orders of magnitude with respect to the local results [43]. On the other hand, for emission frequencies ($\omega \geqslant 0.5\omega_p$), the decay rates can be up to 2 orders of magnitude larger than in the local case [43].

Since only transverse modes have been considered so far [see expansions (8)–(10)], the inclusion of the nonlocal effects [40–42] requires a slight modification of our

formalism. First, the expansion (8) in the nth shell for (and only for) the electric mode of the electric field has to be amended to include longitudinal multipoles $\mathbf{J}_{\ell L}$ and $\mathbf{H}_{\ell L}$,

$$\mathbf{E}_E(\mathbf{r}) = \sum_L \left[A_{EL}(n)\mathbf{J}_{EL}(k_n,\mathbf{r}) + B_{EL}(n)\mathbf{H}_{EL}(k_n,\mathbf{r}) + K_L^-(n)\mathbf{J}_{\ell L}(k_{\ell n},\mathbf{r}) + K_L^+(n)\mathbf{H}_{\ell L}(k_{\ell n},\mathbf{r})\right]. \tag{152}$$

Second, an additional boundary condition, namely that of the continuity of the radial electric field components across an interface of two different shells (which follows the continuity of the normal component of the displacement current $\partial\mathbf{E}/\partial t$ [40]) has to be imposed [42,43]. By its very definition [53], a longitudinal multipole $\mathbf{F}_{\ell L}$ satisfies $\nabla\times\mathbf{F}_{\ell L}=0$ (and $\nabla\cdot\mathbf{F}_{\ell L}\neq 0$). Thus the expansions (8) and (9) of the magnetic mode of the electromagnetic fields are not modified by the longitudinal plasmons, since there is no magnetic field associated with the longitudinal electric field modes [42]. It turns out that Eq. (14) remain unchanged and the ratio D_{ML}/C_{ML} remains identical to the a coefficient of the classical Mie theory [see the first of Eqs. (33)]. This reflects the fact that the excitation of the magnetic modes is not affected by the longitudinal fields.

With regard to the additional boundary condition for the *electric* modes (no longer transverse), note that, in analogy to Eq. (3), a longitudinal multipole mode $\mathbf{F}_{\ell L}$, as defined by Stratton [53] (denoted there by $\mathbf{L}$), is given as follows:

$$\begin{aligned}\mathbf{F}_{\ell L} &= \frac{1}{k_\ell}\nabla[f_l(k_\ell r)Y_{lm}(\mathbf{r})] = \frac{1}{k_\ell}\left[f_l'(k_\ell r)(\mathbf{r}_0 Y_{lm}) + f_l(k_\ell r)(\nabla Y_{lm})\right]\\ &= -\frac{\mathrm{i}}{k_\ell}\left[f_l'(k_\ell r)\mathbf{Y}_L^{(o)} + \sqrt{l(l+1)}\frac{1}{r}f_l(k_\ell r)\mathbf{Y}_L^{(e)}\right],\end{aligned} \tag{153}$$

where f_l is an arbitrary linear combination of the spherical Bessel functions. The longitudinal multipole mode differs from the other modes in that it has a nonzero divergence, $\nabla\cdot\mathbf{F}_{\ell L} = -k_\ell^2 f_l$ [53]. Here k_ℓ is the longitudinal wave vector which dispersion differs from that of transverse mode. Longitudinal bulk plasmon modes obey the dispersion relation $\varepsilon_\ell(k_\ell,\omega)=0$, where $\varepsilon_\ell\ (k,\omega)$ is the nonlocal longitudinal dielectric function [40]. According to the hydrodynamic model, a model longitudinal dielectric function is

$$\varepsilon_\ell(k,\omega) = 1 - \frac{\omega_p^2}{\omega^2 - \beta k^2 + \mathrm{i}\omega\Gamma}, \tag{154}$$

where $\beta = (3/5)v_F^2$ and, as in Eq. (149), v_F is the Fermi velocity and $\Gamma = 1/\tau$ is a damping coefficient. Therefore, $k_\ell(\omega) = \sqrt{(\omega^2-\omega_p^2+\mathrm{i}\omega\Gamma)/\beta}$. In order to reflect the increasing possibility for longitudinal plasmon decay into electron hole pairs with increasing momentum, the value of Γ is sometimes approximated by $\Gamma = 1/\tau + A_\ell(k_\ell/k_F)^2$, k_F being the Fermi wave vector and $A_\ell \approx 0.05$ being a proportionality factor [42]. Note in passing that ε_ℓ reduces to the local result (Drude model) for $\beta = 0$.

Now, when the boundary conditions for the *electric* mode $\mathbf{E}_E$ given by Eq. (152) are imposed at the interface of two different shells, the longitudinal modes enter boundary condition of the continuity of both the transverse and normal components

of $\mathbf{E}_E$. Indeed, according to Eq. (153), any $\mathbf{F}_{\ell L}$ comprises both radial (proportional to $\mathbf{Y}_L^{(o)}$) and transverse (proportional to $\mathbf{Y}_L^{(e)}$) components. Therefore, a simultaneous excitation of the electric and the longitudinal modes occurs. Consequently, Eqs. (23) change in the presence of longitudinal plasmons and the resulting b ($=D_{EL}/C_{EL}$) coefficients become different from the corresponding Mie coefficients given by the second of Eq. (33). In the case that the nonlocal medium is medium **2**, the amended Eq. (23) become

$$\begin{aligned}
&\sqrt{\frac{\varepsilon_1}{\mu_1}}[u_l(k_1r_1)A_{EL}(1)+w_l(k_1r_1)B_{EL}(1)]=\sqrt{\frac{\varepsilon_2}{\mu_2}}[u_l(k_2r_1)A_{EL}(2)+w_l(k_2r_1)B_{EL}(2)],\\
&\frac{1}{k_1}[u_l'(k_1r_1)A_{EL}(1)+w_l'(k_1r_1)B_{EL}(1)]=\\
&\quad\frac{1}{k_2}[u_l'(k_2r_1)A_{EL}(2)+w_l'(k_2r_1)B_{EL}(2)]-\mathrm{i}\frac{\sqrt{l(l+1)}}{k_\ell}[j_l(k_\ell r_1)K_L^-(2)+h_l(k_\ell r_1)K_L^+(2)],\\
&\frac{\sqrt{l(l+1)}}{k_1r_1}[j_l(k_1r_1)A_{EL}(1)+h_l(k_1r_1)B_{EL}(1)]=\\
&\quad\frac{\sqrt{l(l+1)}}{k_2r_1}[j_l(k_2r_1)A_{EL}(2)+h_l(k_2r_1)B_{EL}(2)]-\frac{\mathrm{i}}{k_\ell}[j_l'(k_\ell r_1)K_L^-(2)+h_l'(k_\ell r_1)K_L^+(2)].
\end{aligned}\tag{155}$$

Let us first consider the case of the nonlocal shell different from the sphere core. Supposing that the neighboring shells are ordinary (without any longitudinal plasmon) shells, one has in total 8 sets of expansion coefficients, namely $A_{EL}(j)$, $B_{EL}(j)$, where $j=n-1,\,n,\,n+1,$ and $K_L^{\pm}(n)$. These coefficients enter 6 equations (three on each side of the nonlocal shell). For a comparison, in the case of an ordinary shell, treated in Section 3 and 4, we had in total 6 sets of expansion coefficients, namely $A_{EL}(j)$, $B_{EL}(j)$ for $j=n-1,\,n,\,n+1$, which entered 4 equations (two on each side of the ordinary shell). In both cases, the number of different sets of expansion coefficients is larger by two than the number of corresponding equations. The two unknown sets of expansion coefficients are eventually specified by two boundary conditions. One is, for instance, either the regularity condition at the origin [i.e., $B_{\gamma L}(1)\equiv 0$; see Eq. (29)], or the perfectly conducting boundary conditions (36) at the sphere core. The second boundary condition can be either that of Eqs. (49) and (50), or, in the case of an elastic scattering, the requirement that the $A_{\gamma L}(N+1)$ coefficients be equal to the expansion coefficients of an incident electromagnetic field in spherical coordinates. Hence, provided that the respective coefficients $A_{EL}(n-1)$ and $B_{EL}(n-1)$ are known, the coefficients $A_{EL}(n+1)$ and $B_{EL}(n+1)$ can be (for instance, using Gauss elimination method) unambiguously determined, and vice versa.

If the nonlocal shell is the sphere core, then, within the core, the interior (regularity) boundary condition (29) halves the number of sets of expansion coefficients to $A_{EL}(1)$ and $K_L^-(1)$. One then has in total 4 sets of expansion coefficients: in addition to $A_{EL}(1)$ and $K_L^-(1)$ also $A_{EL}(2)$ and $B_{EL}(2)$, which enter 3 matching equations at the core boundary. For a comparison, in the case of an ordinary core, treated in Section 3 and 4, one had in total 3 sets of expansion coefficients [$A_{EL}(1)$, $A_{EL}(2)$, and $B_{EL}(2)$], which entered 2 matching equations at the core boundary. Again, in both cases the number of

different sets of expansion coefficients is larger by one than the number of corresponding equations. The unknown set of expansion coefficients is then determined by imposing the second, exterior, boundary condition. Consequently, irrespective of the nonlocal shell position, one can define the corresponding forward and backward transfer matrices and proceed in the same manner as we did in earlier Sections 3 and 4.

11.2. Optically active shells

It turns out that our formal approach involving transfer matrices, as developed in Sections 3 and 4, can also be applied to the case when one or several spherical shells are made of an optically active medium [37,44,45]. The latter stands here for an isotropic chiral medium which is known to rotate the electric field of a linearly polarized light. In the case of an optically active medium, homogeneous plane waves can be propagated only when circularly polarized. Otherwise the major axis of an elliptically polarized plane wave changes direction (optical rotation) and the ratio of minor to major axes increases. As it will be shown in a while, such a medium is characterized by different wave vectors for circularly polarized light of opposite handedness. In Bohren convention [37,44,45], an electromagnetic wave is called right-handed (left-handed) if the vibration ellipse, imagined to be viewed looking toward the source, is traced out clockwise (counterclockwise). Since circularly polarized plane waves of opposite handedness experience different refractive indices, an optically active medium is sometimes also referred to as a circularly birefringent medium.

For an isotropic optically active medium, the usual constitutive equations in the isotropic medium $\mathbf{D} = \varepsilon\mathbf{E}$ and $\mathbf{B} = \mu\mathbf{H}$ change into

$$\mathbf{D} = \varepsilon\mathbf{E} + \chi_E\varepsilon\boldsymbol{\nabla}\times\mathbf{E}, \quad \mathbf{B} = \mu\mathbf{H} + \chi_H\mu\boldsymbol{\nabla}\times\mathbf{H}, \tag{156}$$

where the coefficients χ_E and χ_H are scalars [44,45]. The amended constitutive equations, which are also known as the Drude–Born–Fedorov relations, are consistent with the Lorentz reciprocity relations. Note that the presence of the cross product in the constitutive equations explicitly violates mirror-symmetry, which is an essential feature of an optically active medium. The change in the constitutive relations brings about the change in the stationary Maxwell's equations, which are no longer given by Eqs. (2). Consequently, the form of the expansions of electromagnetic fields in terms of vector multipoles within a given shell both in the absence of a dipole [see Eqs. (8)–(10)] and in the presence of a dipole [see Eqs. (47) and (48)] will change. First one performs a linear transformation of electromagnetic fields,

$$\begin{pmatrix}\mathbf{E}\\ \mathbf{H}\end{pmatrix} = \begin{pmatrix}1 & a^+\\ a^- & 1\end{pmatrix}\begin{pmatrix}\mathbf{Q}_L\\ \mathbf{Q}_R\end{pmatrix} = \mathscr{A}\begin{pmatrix}\mathbf{Q}_L\\ \mathbf{Q}_R\end{pmatrix}, \tag{157}$$

where

$$\begin{aligned} a^+ &= -\frac{\mathrm{i}}{\omega\varepsilon}[k^+(1-\chi_E\chi_H k^2)+\chi_E k^2],\\ a^- &= -\frac{\mathrm{i}}{\omega\mu}[k^-(1-\chi_E\chi_H k^2)-\chi_H k^2], \end{aligned} \tag{158}$$

$$k^+ = k\frac{[1+(\chi_E-\chi_H)^2k^2/4]^{1/2}-(\chi_E+\chi_H)k/2}{1-\chi_E\chi_Hk^2} \approx k[1-(\chi_E+\chi_H)k/2], \qquad (159)$$

$$k^- = k\frac{[1+(\chi_E-\chi_H)^2k^2/4]^{1/2}+(\chi_E+\chi_H)k/2}{1-\chi_E\chi_Hk^2} \approx k[1+(\chi_E+\chi_H)k/2], \qquad (160)$$

$k=\omega(\varepsilon\mu)^{1/2}$ being the wave vector in the isotropic homogeneous medium characterized by ε and μ. Here the fields $\mathbf{Q}_L$ and $\mathbf{Q}_R$ independently satisfy the following equations [44],

$$\nabla^2\mathbf{Q}+\kappa^2\mathbf{Q}=0, \quad \nabla\times\mathbf{Q}=\kappa\mathbf{Q}, \quad \nabla\cdot\mathbf{Q}\equiv 0. \qquad (161)$$

As notation indicates, the respective $\mathbf{Q}_L$ and $\mathbf{Q}_R$ fields are the left- and right-handed fields. In Eq. (161), $\kappa=k^-$ for $\mathbf{Q}_L$ and $\kappa=-k^+$ for $\mathbf{Q}_R$. For any real medium one can assume both $\chi_Ek,\chi_Hk\ll 1$ without any loss of generality. Then the second equation of each of the Eqs. (159) and (160) follows from the first one by retaining only the first order terms in the quantities χ_Ek,χ_Hk [44,45]. Note in passing that both the nominator and denominator in the Eqs. (159) and (160) are dimensionless, since the coefficients χ_E and χ_H, as read from the Maxwell's equations (156), have the dimension of length.

The second equation in (161) defines the transformed fields $\mathbf{Q}_L$ and $\mathbf{Q}_R$ as the so-called vector Beltrami fields. This equation restricts the expansion of electromagnetic fields in terms of vector multipoles within a given shell both in the absence and in the presence of a dipole. Indeed, the Beltrami condition (161) implies that the normalized vector multipoles $\mathbf{F}_{\gamma L}$, as defined by Eqs. (3), enter the expansions of the respective $\mathbf{Q}_L$ and $\mathbf{Q}_R$ fields only in specific combinations and for $f_{Ml}=f_{El}$. Upon using Eqs. (5), one finds the following general solution for Beltrami fields $\mathbf{Q}_L$ and $\mathbf{Q}_R$ within a given optically active shell,

$$\begin{aligned}\mathbf{Q}_L(k^-,\mathbf{r}) &= \sum_L\left\{A_L^-(n)[\mathbf{J}_{ML}(k^-,\mathbf{r})+\mathbf{J}_{EL}(k^-,\mathbf{r})]+B_L^-(n)[\mathbf{H}_{ML}(k^-,\mathbf{r})+\mathbf{H}_{EL}(k^-,\mathbf{r})]\right\},\\ \mathbf{Q}_R(k^+,\mathbf{r}) &= \sum_L\left\{A_L^+(n)[\mathbf{J}_{ML}(k^+,\mathbf{r})-\mathbf{J}_{EL}(k^+,\mathbf{r})]+B_L^+(n)[\mathbf{H}_{ML}(k^+,\mathbf{r})-\mathbf{H}_{EL}(k^+,\mathbf{r})]\right\}.\end{aligned} \qquad (162)$$

Upon substituting (162) back into Eq. (157), the corresponding expansions of the original electromagnetic fields $\mathbf{E}$ and $\mathbf{H}$ within an optically active shell are obtained.

The further treatment is then as in Sections 3 and 4. Upon imposing the continuity of tangential components of $\mathbf{E}$ and $\mathbf{H}$, equations for the expansion coefficients $A_L^\pm(n)$ and $B_L^\pm(n)$ in neighboring shells are obtained, which are then used to determine the corresponding forward and backward transfer matrices. However, there is one significant difference: each matching equation involves all for sets of coefficients, namely $A_L^-(n)$, $A_L^+(n)$, $B_L^-(n)$, and $B_L^+(n)$. Therefore, the corresponding transfer matrices become 4×4 matrices. Note that transfer matrices of Sections 3 and 4 can formally be written as 4×4 matrices too. However, in the latter case, although the 4×4 matrix form is conceivable, it is largely artificial. Indeed, when the transfer matrices are written for column vectors $(A_{ML}(n),B_{ML}(n),A_{EL}(n),B_{EL}(n))$, each

4×4 transfer matrix would be block-diagonal matrix consisting of two 2×2 blocks on the 4×4 matrix diagonal, one for the TM and second for the TE polarization. In contrast, in the present case of an isotropic chiral medium the 4×4 matrix form is unavoidable. In a sense, the transition from 2×2 to 4×4 transfer matrices in a circularly birefringent, or optically active, medium bears similarity with the planar case. In the latter case, in a nonbirefringent isotropic homogeneous medium, the 2×2 Abelés transfer matrices are used [35–37]. On the other hand, in a birefringent medium, it is necessary to employ the 4×4 Yeh's [77] transfer matrix formalism.

12. Discussion

12.1. Radiative vs nonradiative and local vs nonlocal decay rates

12.1.1. Radiative vs nonradiative decay rates

In Sections 8.1 and 8.2 the respective normalized radiative and nonradiative decay rates W^{rad} and W^{nrad} were determined by considering two mechanisms through which dipole energy is dissipated. One is the radiative loss, P^{rad}, which is calculated from the Poynting vector, and the other is the nonradiative loss, P^{nrad}, which is calculated from the Ohmic losses inside the sphere absorptive shell. However, it is rare to observe the said two decay rates in their pure form. Before any comparison is made between the calculated normalized decay rates W^{rad} and W^{nrad} and experiment, one has to take into consideration that many other nonradiative mechanisms, such as, for instance, multiphoton relaxation, coupling to defects, direct electron-transfer processes, concentration quenching, and lasing all contribute to the nonradiative decay rate W^{nrad} [19,20,46,47,70,78,79]. Since there are many contributions to W^{nrad}, let us denote the nonradiative decay rates due to the Ohmic losses by $W_{\Omega}^{\mathrm{nrad}}$. Therefore, the sum $W^{\mathrm{rad}}+W_{\Omega}^{\mathrm{nrad}}$, of the two contributions considered above does only provide the lower bound for the total decay rate W^{tot}.

It turns out that even in a purely dielectric case, in the absence of any Ohmic losses, the nonradiative decay W^{nrad} can be higher than the radiative decay W^{rad} [80,81]. Hence the ratio $W^{\mathrm{rad}}/W^{\mathrm{tot}}$, known as the *fluorescence quantum yield*, or simply *quantum efficiency*, is then smaller than 0.5. When dye concentrations increase above a certain threshold value, the quantum efficiencies of most organic dyes are substantially reduced even further with respect to a zero-concentration limit value. In liquid solutions, the threshold value is $\sim10^{-4}$ M, whereas in a solid, for instance, in the case of fluorescein (FITC) dyed colloidal silica spheres, the threshold value is ~1 mM [82]. These effects are caused by an increased energy transfer between the dye molecules as their concentration increases. (Nevertheless, pyrene-doped PMMA spheres with pyrene concentrations up to 10^{-2} M do not exhibit any concentration dependence [83].) Note in passing that the interactions between neighboring radiating molecules may lower their excited state energy leading to a red shift in the emission frequency [82]. Usually, as in the case of erbium doped silica glass, for a low quencher and elementary emitters concentration the nonradiative decay rate increases *linearly* with concentration. The total decay rate can then be written as

$$W^{\mathrm{tot}} = W^{\mathrm{rad}} + W^{\mathrm{i}} + 8\pi C_{Er-Q}[Er][Q], \tag{163}$$

where C_{Er-Q} is a coupling constant, $[Er]$ and $[Q]$ are the Er and quencher concentration, respectively, and W^{i} is the nonradiative decay rate in the quencher zero concentration limit [46], which is also called the *internal* nonradiative decay rate. It should be emphasized that, for a dipole outside the sphere, the radiative decay rate W^{rad} is proportional to the intensity of the time-resolved fluorescence spectra at $t = 0$ [70]. Therefore, in the latter case, W^{rad} and W^{nrad} can easily be disentangled experimentally [70].

12.1.2. Local vs nonlocal decay rates

It should be emphasized that the nonradiative mechanisms different from the Ohmic losses, such as local field corrections [47,84], do only depend on the immediate neighborhood of a radiating dipole. Therefore, one can include all such mechanisms of nonradiative decay rates under the *local* nonradiative decay rate, W^{loc}. On the other hand, the nonradiative decay rate due to Ohmic losses and the radiative decay rate can be viewed as a *nonlocal decay rate*, $W^{\mathrm{nloc}} \equiv W^{\mathrm{rad}} + W^{\mathrm{nrad}}_{\Omega}$. The reason behind this nomenclature is that the latter two rates depend on the geometry and material composition of the entire sphere and surrounding medium, and not only on the immediate proximity of the radiating dipole. The total decay rate is then written as

$$W^{\mathrm{tot}} = W^{\mathrm{loc}} + W^{\mathrm{nloc}}. \tag{164}$$

As a rule, both the nonradiative decay rate due to Ohmic losses and the radiative decay rate change if the optical properties of a shell being far away from the radiating dipole (for instance, surrounding medium) change [46,80,81]. In the case of a homogeneous dielectric sphere, the local and nonlocal decay rates have been disentangled by measuring the total decay rate using the same sphere in different environments [80]. For instance, the sphere can be embedded in a refractive index matched liquid [80]. Its radiative decay rates then becomes that of a dipole in a homogeneous dielectric slab [81,85]. Other possible environments include air or liquids with different refractive indices [80]. The difference of the respective total decay rates measured in different sphere environments then corresponds to the difference of the nonlocal decay rates [80]. The latter is obviously also true for a multicoated sphere. The local and nonlocal decay rates can then be separated by fit of Eq. (164) to the measured data [46,80]. Only after the *local* nonradiative decay rate W^{loc} is determined, a comparison of measured data and theory presented here can be performed.

12.2. Quantum vs classical treatment of transition rates

12.2.1. Weak vs strong coupling regime

The domain of validity of any classical result for the decay rates is limited by several factors. One of them is the validity of the linear-response theory, or the Wigner–Weisskopf approximation, which justifies the use of the correspondence principle (1) (see also Appendix D). In the regime of validity of the Wigner–Weisskopf approximation, decay is exponential and the whole process is characterized by two numbers:

the spontaneous emission rate and the radiative (Lamb) shift of the transition frequency. The basic assumption for the validity of the linear-response theory [and correspondence principle (1)] is, of course, that neither the transition matrix element nor the transition frequency are appreciably changed by the presence of the interface. Both the rate and the shift depend, in this case, only on the density of modes in a photon reservoir. The condition of the validity of the linear-response theory is usually translated into the requirement of a *smooth* variation of the decay rate with frequency. The smoothness condition is considered satisfied if the excitation or emission frequency is far away from a multilayered sphere resonance. In the case that the frequency coincides with a multilayered sphere resonance, the enhancement factors of the nonlocal decay rates are due to the complex zeros of the denominator of the $D_{\gamma L}$ coefficient near the real ω axis, at $\omega = \omega_n = \alpha_n + \mathrm{i}\Gamma_n$ with Γ_n small. The imaginary part Γ_n is approximately equal to the width (the reciprocal of the lifetime) of the corresponding multipole resonances. The smoothness condition in the resonance case, as discussed by Chew [13,14], is that $\Gamma_t \ll \Gamma_n$, or $W^{\mathrm{rad}}/\delta\omega \ll 1$, where Γ_t (reciprocal of the excited state lifetime τ) is the imaginary part of the transition frequency ω_t, and $\delta\omega$ is the width of the emission line. Experimentally, the lifetimes of atomic transition vary over many decades, with $\Gamma_t = 1/\tau$ in the range 10^6–10^8 being common. For $\Gamma_t \gg \Gamma_n$, an oscillatory exchange of energy between the atomic and photonic degrees of freedom takes place, described in the literature as vacuum Rabi splitting [86]. If the Wigner–Weisskopf linear-response approach breaks down, one may also observe a qualitative change of the spectrum from a single Lorentzian peak into a two-peaked structure as a clear indication of the onset of a *nonexponential* decay [86].

Strong interaction between a two-level atom and the whispering-gallery modes of a dielectric microsphere requires a full quantum mechanical treatment. The latter have been provided by several authors [87,88]. However, the knowledge of a classical solution is an indispensable first step in full quantum electrodynamic treatment of the spontaneous and stimulated emission involving spherical cavities [87,88]. Therefore, even in the strongly interacting case, in the regime of cavity quantum electrodynamics, our classical solution does not loose its value and can be used to extend results obtained by Lenstra et al. [87] and Klimov et al. [88] for the case of a homogeneous spherical cavity to the case of a multicoated spherical cavity.

12.2.2. Coherent emitters

Another condition involves the density of radiating atoms or molecules. In the preceding section it has been alluded to that the density of elementary emitters has an effect on the *nonradiative* decay rates [see, for instance, Eq. (163)]. However, the density of elementary emitters also effects the *radiative* decay rate. In the high concentration limit, in the extreme case of Dicke superradiance [89], the radiative decay rate may increases *quadratically* with the emitters concentration. More precisely, let us consider a collection of $\mathcal{N}$ identical elementary emitters confined to a region whose dimensions are small compared to a wavelength. Then for a half-full (fully) inverted population the radiative decay rate is proportional to $\mathcal{N}^2$ ($\mathcal{N}$) and the peak intensity is nearly proportional to $\mathcal{N}^2$ [89]. The Dicke results were derived for a gas of elementary emitters. Provided that emitters are brought closer together, as in J

aggregates of dyes in a solid matrix, additional phenomena occur. Study of a simple linear chain of the fully population-inverted system of emitters, in which an excitation can propagate from atom to atom through dipolar interactions, show that the radiative decay is *biexponential* and is accompanied by *red and blue shifts* of the emitted frequency [90].

According to Chew [14], the critical density, ρ_c, of radiating atoms for the onset of collective quantum effects, such as superradiance or ringings in the emitted power, is estimated to be

$$\rho_c = 8\pi^2 n/(Q\sigma\lambda). \tag{165}$$

Here Q is the mode quality factor, σ is the photon absorption cross section (for the photon absorption by a radiating atom), and λ is the (vacuum) radiating wavelength. Depending on a resonance, the critical density values range between 10^8 and 10^{18} atoms/cm^3. The former density value is when emission frequency coincide with a sphere resonance, whereas the the latter density value is for a nonresonant case. Surprisingly enough, a biexponential decay accompanied by a frequency shift is also observed in the case of the concentration quenching of the *nonradiative* decay rate [82] (see also [83]). For instance, in the case of FITC dyed colloidal silica spheres, a large red shift of 10 nm in the emission frequency was observed for dye concentrations in excess of $\sim$1 mM [82]. In the latter case, the red shift results from the lowering of the excited state energy due to the interactions between neighboring radiating molecules [82].

It should be emphasized that the coherence in the Dicke model is due to *atomic coherence*, or coherence between elementary emitters, whereas our main focus has been on the changes in the decay rates due to the *coherence properties of the radiation field*. Surprisingly enough, the coherence of a plurality of emitters has qualitatively similar effect on decay properties as does the strong interaction of a single emitter with the whispering gallery mode of a sphere.

12.3. Numerical limitation on the size parameter

Computer program built according to our recursive transfer-matrix solution is expected to produce reliable results in the purely dielectric case and for typical dielectric constants of metals in the visible and in the infrared up to the size parameter $x = k_h r_s \approx 50$. This is more than enough to perform simulations for multilayered metallo-dielectric nanospheres fabricated by colloidal techniques [23–32]. However, in atmospheric physics, aerosol science, and meteorology size parameters as large as a few thousands are required. (For instance, for a 100 μm water droplet at a visible wavelength of 0.5 μm the size parameter is about 1260.) For a such large size parameter numerical problems may arise, because our expressions (17), (22), (25), and (26) of the forward and backward transfer matrices involve a difference of the products of two Bessel functions. This may lead to a distortion of significant digits if the product values are large and of the same order. The latter predominantly occurs for complex arguments with large imaginary parts. This is a well-known problem in the Mie scattering community [54,55,57] and several ways have been proposed to circumvent it. First and the most important step involves factorizing matrix elements so as to

replace the Riccati–Bessel functions with their logarithmic derivatives. For instance, one can factorize the matrix element $T^{+}_{Ml;11}(1)$ given by Eq. (22) as follows,

$$\begin{aligned} T^{+}_{Ml;11}(1) &= -\mathrm{i}k_2\mu_2[w_l'(k_2r_1)u_l(k_1r_1)/\mu_2 - w_l(k_2r_1)u_l'(k_1r_1)/\mu_1] \\ &= -\mathrm{i}k_2\mu_2 u_l(k_1r_1)w_l(k_2r_1)\{[w_l'(k_2r_1)/w_l(k_2r_1)]/\mu_2 \\ &\quad - [u_l'(k_1r_1)/u_l(k_1r_1)]/\mu_1\}. \end{aligned} \tag{166}$$

This trick, long used in standard Mie theory, circumvents the exponential dependence of the functions on the size parameter [54–57]. The state of the art of techniques for obtaining convergence at large size parameters is given by Yang [57].

12.4. Further extensions

The presented recursive transfer-matrix solution for a dipole radiating inside and outside a stratified sphere can be expanded is several ways. Three of them are briefly outlined here.

The first in an extension of our results to the case of more complicated particles, such as spheroids, ellipsoids, Chebyshev particles, etc. This case is not only interesting by itself [92] but such particles can also be readily manufactured experimentally. Indeed, an intense ion bombardment of a multilayered nano- or microsphere induces a plastic deformation of the sphere shape into a regular axially symmetric spheroid [91]. Wang et al. [92] have already applied the so-called extended boundary method (EBCM) of Waterman [93] to provide solution for a dipole in the presence of a homogeneous dielectric spheroid. The EBCM, often also called as the T-matrix method [51,52], has a reputation of being the most efficient numerical method in describing the scattering off axially symmetric particles [51,52]. It is interesting to note that the T-matrix formulation of electromagnetic scattering from multilayered axially symmetric scatterers has been supplied by Peterson and Ström [94]. Therefore, it appears that an efficient numerical description of the classical electromagnetics problem of a dipole in the presence of an arbitrary multilayered axially symmetric scatterer can be rather straightforwardly obtained by combining the solution for the case of a multilayered sphere presented here with the teaching of Wang et al. [92] and Peterson and Ström [94]. The subject matter of Section 3 can also be straightforwardly extended to the case of an infinitely long multilayered circular cylinder consisting of concentric cylindrical shells [95]. The case of a radiating dipole in the presence of such a multilayered cylinder can then be, in principle, obtained by combining the extension of Section 3 with the teaching of Chew et al. [96], who provided solution for the case of a homogeneous cylinder. However, in contrast to the case of a multilayered sphere, the resulting expressions are not expected to be obtainable in purely algebraic form [96]. The reason is a mismatch between the spherical multipole expansion of the dipole radiating field and the cylindrical symmetry of the multilayered cylinder.

The second is an extension of our results obtained for an electric dipole to the case of an electric quadrupole. Classically, an electric quadrupole can be viewed as a system of two identical electric dipoles of opposite orientations in close proximity, one of which is stationary and the other oscillating about the first. One can anticipate that an

application of techniques developed in Sections 3–5 to the case of radiating electric quadrupole can be useful. The classical solution can then again find an immediate application in inelastic scattering and in the description of electric quadrupole decay rates. Indeed, as shown by Klimov and Letokhov (see Secs. III and IV of [97]), equivalence of the classical and quantum-mechanical descriptions of radiative decay rates also holds for the quadrupole transitions. In a free space, electric quadrupole decay rates in the optical region are typically lower by a factor of $(a_0/\lambda)^2 \approx 10^{-6}$–$10^{-8}$ than the electric-dipole rates, a_0 and λ being the Bohr radius and radiation wavelength, respectively. Nevertheless, the quadrupole decay rates appear to exhibit much stronger sensitivity to the presence of and distance from material bodies than the electric-dipole transitions do [97]. This stronger sensitivity makes quadrupole decay rates an interesting subject for the remote sensing and spectroscopic applications.

Last but not the least, the classical electromagnetics problem of a radiating dipole (or quadrupole) in the presence of a regular array of (multilayered) scatterers [60,61] appears to be another interesting avenue of research. Regular array of scatterers, also known as photonic crystals, possess many interesting properties, most notably a photonic band gap, wherein light propagation for all polarizations and all directions of propagation is forbidden [60,61,98]. Photonic crystals promise to become a laboratory for testing fundamental processes involving interactions of radiation with matter under novel conditions [99]. Since dye labeled multilayered spheres can easily be integrated within photonic crystals [60,61,98,99], the former may serve as sensitive fluorescence probes of photonic crystal properties. It appears that a combination of techniques developed here with the multiple-scattering approach [60,61,68] will yield the most efficient method to deal with the problem of an elementary radiator in the presence of a regular array of (multilayered) scatterers.

13. Summary and conclusions

Particles found in nature, such as water insoluble aerosols in atmosphere, hydrological particles coated with biological material, micro-encapsulated material, biological cells, or a variety of colloidal particles designed experimentally to satisfy specific optical properties, are frequently not homogeneous and exhibit a layered or radially stratified structure. In order to cover these (and possibly many other) experimental situations and, at the same time, provide a larger freedom in engineering of spherical particles properties, theory of Chew et al. [5,13,14] has been extended to the case of a multilayered sphere consisting of concentric spherical shells. A complete description of the classical electromagnetic fields was achieved outside and inside a multi-structured spherical particle, both in the absence and in the presence of a radiating electric dipole. By formulating a fast and numerically stable transfer-matrix solution, electromagnetic fields were determined anywhere in the space, and the time-averaged angular distribution of the radiated power, the total radiated power, and Ohmic losses due to an absorbing shell were calculated. There is no limitation on the dipole position, nor on the number of the concentric shells, nor on the shell medium. An absorbing, optically active, and ultrathin ($\lesssim 10\,\text{nm}$) metallic shell

(core), characterized by a nonlocal dielectric function, are all allowed. The classical solution was then applied for the description of inelastic light scattering (fluorescence and Raman), the radiative and nonradiative normalized decay rates, and frequency shift. The importance of grouping various radiative and nonradiative decay mechanisms into local and nonlocal decay rates was emphasized. The issues of experimentally disentangling the local (radiative and nonradiative due to Ohmic losses) and nonlocal (remaining nonradiative) decay rates, numerical limitations on the size parameter and ways how to overcome them, and the domain of applicability of our classical description of decay rates were all addressed. Suggestions for further extensions of the theory presented here to the case of an arbitrary multilayered (axially symmetric) particle and to the classical problem of a radiating quadrupole in the presence of a multilayered particle were briefly outlined.

We believe that the solution presented in this article, in conjunction with computer program freely available at http://www.wave-scattering.com will provide a larger freedom in engineering of spherical particles properties, rendering them more suitable for a variety of applications. Many of possible applications have already been listed in Section 1, where the homogeneous sphere case has been discussed. The incomplete list includes inelastic light-scattering (fluorescence or Raman) spectroscopy [1,3,4], which had proved to be a sensitive tool for characterizing single micrometer sized particles (chemical speciation) of both inorganic and organic compounds, aerosols, and particulates [6], in LIDAR applications for remote sensing of both molecular and particulate constituents of atmosphere [6,8], for identification of biological particles in fluorescence-activated flow of cytomeres [7], to monitor specific cell functions, or in the cell identification and sorting systems [9,10], in the investigation thermal radiation from spherical microparticles [11], engineering of the radiative decay for biophysical and biomedical applications [16], imaging of buried saturated fluorescent molecules [17], and imaging of surfaces [18] in near-field optical microscopy, and in the study of the effects of light absorption and amplification on the *stimulated* transition rates of the electric-dipole emission of atoms or molecules embedded in micro- or nano-structured spheres [19–22,100], stimulated Raman scattering [58,59], and on the interplay between lasing and stimulated Raman scattering [101,102]. Note that our classical solution provides the classical modes of a multicoated sphere, and thereby it yields the indispensable first step for the full quantum electrodynamic treatment of the spontaneous and stimulated emission involving spherical multi-structured quantum cavities [84,87,88].

The ability of modifying radiative rates for atoms or molecules in the excited state is of great importance since dissipative pathways of the excited state can be controlled. Therefore, one can imagine immediate use of our solution for designing nanoprobes with enhanced quantum yield for fluorescent microscopy and with enhanced photostability for biological applications. In the latter case, if one assumes that photobleaching of a dye takes place only while the dye is in its excited states, a sufficiently large enhancement of the spontaneous emission rates can significantly lower the probability of switching into nonfluorescent dark states, thereby increasing stability against photobleaching [32,82]. Enhanced spontaneous emission rates could also provide increased sensitivity in low level fluorescence applications [78,82].

Designing of small noble metal nanoparticles with reduced quantum yield, $W^{\mathrm{rad}}/W^{\mathrm{tot}}$, at the particle close proximity (cca 1 nm) may have crucial implications for the particles use as acceptors in biophysical Förster resonant energy transfer experiments in vitro as well as in vivo [70].

Acknowledgment

To my family for supporting this my free-time activity.

Appendix A. Transverse and longitudinal vector spherical harmonics

Because of $\nabla\times\mathbf{r}=0$, one has $(\mathbf{r}\times\nabla)\mathrm{Y}_L=-\nabla\times(\mathbf{r}\mathrm{Y}_L)$. Therefore, one can also write

$$\mathbf{Y}_L^{(m)}=\frac{\mathrm{i}}{\sqrt{l(l+1)}}\nabla\times(\mathbf{r}Y_L)=\frac{\mathrm{i}}{\sqrt{l(l+1)}}\nabla\times(r\mathbf{Y}_L^{(o)}). \tag{A.1}$$

The vector spherical harmonics $\mathbf{Y}_L^{(m)}$, $\mathbf{Y}_L^{(e)}$, and $\mathbf{Y}_L^{(o)}$ are mutually orthogonal to one another in the ordinary vector sense (with respect to the ordinary scalar product of vectors in $\mathbb{R}^3$). One also finds

$$\begin{aligned}&\mathbf{r}_0\times\mathbf{Y}_L^{(e)}=-\mathbf{Y}_L^{(m)},\\&\mathbf{r}_0\times\mathbf{Y}_L^{(m)}=\mathbf{Y}_L^{(e)},\\&\mathbf{r}_0\times\mathbf{Y}_L^{(o)}=0.\end{aligned} \tag{A.2}$$

The first identity follows from Eq. (4), whereas the second is a direct consequence of

$$\mathbf{r}_0\times[\mathbf{r}_0\times\mathbf{X}]=[\mathbf{r}_0\cdot\mathbf{X}]\mathbf{r}_0-(\mathbf{r}_0\cdot\mathbf{r}_0)\mathbf{X}=-\mathbf{X}. \tag{A.3}$$

Here the first equation is a general vector identity, whereas the second equation is only valid for transverse vectors, $\mathbf{r}_0\cdot\mathbf{X}\equiv 0$. Using that $\partial_r\mathbf{r}_0=0$, one can show that

$$\partial_r\mathbf{Y}_L^{(e)}=\partial_r\mathbf{Y}_L^{(o)}=0. \tag{A.4}$$

In the electromagnetic scattering literature [51,52] the respective $\mathbf{Y}_L^{(m)}$, $\mathbf{Y}_L^{(e)}$, and $\mathbf{Y}_L^{(m)}$ are often disguised under a different notation,

$$\begin{aligned}&\mathbf{Y}_L^{(m)}=\mathrm{i}\gamma_L\mathbf{C}_L^{TKS}=\mathrm{i}d_L\mathbf{C}_L^{M}\mathrm{e}^{\mathrm{i}m\varphi},\\&\mathbf{Y}_L^{(e)}=\mathrm{i}\gamma_L\mathbf{B}_L^{TKS}=\mathrm{i}d_L\mathbf{B}_L^{M}\mathrm{e}^{\mathrm{i}m\varphi},\\&\mathbf{Y}_L^{(o)}=\mathrm{i}\gamma'_L\mathbf{P}_L^{TKS}=\mathrm{i}\sqrt{l(l+1)}\,d_L\mathbf{P}_L^{M}\mathrm{e}^{\mathrm{i}m\varphi}.\end{aligned} \tag{A.5}$$

Eqs. (A.5) establish a relation of the *magnetic*, *electric*, and *longitudinal* vector spherical harmonics to the vector spherical harmonics $\mathbf{C}_L^{TKS}$, $\mathbf{B}_L^{TKS}$, $\mathbf{P}_L^{TKS}$, as used by Tsang, Kong, and Shin [51], and $\mathbf{C}_L^{M}$, $\mathbf{B}_L^{M}$, and $\mathbf{P}_L^{M}$, as used by Mishchenko [52], respectively. Here the numerical constant γ_L and γ'_L of [51] and numerical constant d_L of [52], are related by

$$\gamma'_L = \sqrt{l(l+1)}\gamma_L, \quad \gamma_L = \sqrt{\frac{(l-m)!}{(l+m)!}}d_L, \quad d_L = \left[\frac{2l+1}{4\pi l(l+1)}\right]^{1/2}. \tag{A.6}$$

The *magnetic*, *electric*, and *longitudinal* vector spherical harmonics are *complete* and *orthonormal* in the sense

$$\oint_S \mathbf{Y}^{(c)}_{lm}(\mathbf{r}) \cdot \mathbf{Y}^{(c')*}_{l'm'}(\mathbf{r})\,\mathrm{d}\Omega = \delta_{ll'}\delta_{mm'}\delta_{cc'}, \tag{A.7}$$

$$\sum_{l=0}^{\infty}\sum_{m=-l}^{l}\sum_{c}\mathbf{Y}^{(c)}_{lm}(\mathbf{r})\mathbf{Y}^{(c)*}_{lm}(\mathbf{r}') = \mathbf{1}\delta_S(\mathbf{r},\mathbf{r}'), \tag{A.8}$$

where $\oint_S$ denotes integration over the unit sphere, and $\delta_S(\mathbf{r},\mathbf{r}')$ is the Dirac delta function on the unit sphere, or the solid-angle Dirac function. The latter means that for any function f defined on the unit sphere one has

$$\oint_S \delta_S(\mathbf{r},\mathbf{r}')f(\mathbf{r}')\,\mathrm{d}\Omega = f(\mathbf{r}). \tag{A.9}$$

In the case of $L = L'$, the orthogonality (A.7) follows from the fact that the vector spherical harmonics (4) are mutually orthogonal with respect to the usual scalar product of two vectors in $\mathbb{R}^3$. The orthonormality of the longitudinal spherical harmonics follows from the orthonormality of the scalar spherical harmonics. The orthonormality of the magnetic spherical harmonics can be established by using self-adjointness of $\mathbf{L}$, or simply by calculating the scalar product directly. The orthonormality of the electric spherical harmonics then easily follows from the first Eq. (4).

Appendix B. Normalized Stratton's vector multipoles

Note that [see Eq. (A.2)]

$$\mathbf{Y}^{(m)}_L \times \mathbf{r}_0 = -\mathbf{Y}^{(e)}_L, \quad \mathbf{Y}^{(e)}_L \times \mathbf{r}_0 = \mathbf{Y}^{(m)}_L. \tag{B.1}$$

Therefore, for an arbitrary vector multipole $\mathbf{F}_{\gamma L}$, given by Eq. (3),

$$\begin{aligned}\mathbf{F}_{ML}(k,\mathbf{r}) \times \mathbf{r}_0 &= -f_{Ml}(kr)\mathbf{Y}^{(e)}_L(\mathbf{r}),\\ \mathbf{F}_{EL}(k,\mathbf{r}) \times \mathbf{r}_0 &= \frac{(rf_{El})'(kr)}{kr}\,\mathbf{Y}^{(m)}_L(\mathbf{r}).\end{aligned} \tag{B.2}$$

Using the latter two identities together with the orthonormality of the vector spherical harmonics $\mathbf{Y}^{(a)}_L$ one can show that for any vector multipoles $\mathbf{F}_{\gamma L}$ and $\mathbf{G}_{\gamma' L'}$

$$\oint [(\mathbf{F}_{\gamma L} \times \mathbf{G}^*_{\gamma' L'}) \cdot \mathbf{r}_0]\,\mathrm{d}\Omega = 0, \tag{B.3}$$

unless $\gamma \neq \gamma'$ and $L = L'$. Indeed, let us first consider the case $\gamma = \gamma'$. Then, since

$$(\mathbf{F}_{\gamma L} \times \mathbf{G}^*_{\gamma' L'}) \cdot \mathbf{r}_0 = \mathbf{F}_{\gamma L} \cdot (\mathbf{G}^*_{\gamma' L'} \times \mathbf{r}_0), \tag{B.4}$$

and by applying identities (B.2) one finds that the right-hand side of the last equation is proportional to the scalar product $\mathbf{Y}_L^{(m)} \cdot \mathbf{Y}_{L'}^{(e)*}$ and hence the result is zero,

$$\oint (\mathbf{F}_{\gamma L} \times \mathbf{G}^*_{\gamma L'}) \cdot \mathbf{r}_0 \, \mathrm{d}\Omega = 0, \tag{B.5}$$

in virtue of the orthonormality of the vector spherical harmonics $\mathbf{Y}_L^{(m)}$ and $\mathbf{Y}_{L'}^{(e)}$.

In the case $\gamma \neq \gamma'$, one finds by using identities (B.2) that the right-hand side of Eq. (B.4) is proportional to the scalar product $\mathbf{Y}_L^{(a)} \cdot \mathbf{Y}_{L'}^{(a)*}$, where either $a = m$ or $a = e$. Explicitly,

$$\begin{aligned}
\left(\mathbf{F}_{ML} \times \mathbf{G}^*_{EL'}\right) \cdot \mathbf{r}_0 &= \mathbf{F}_{ML} \cdot \left(\mathbf{G}^*_{EL'} \times \mathbf{r}_0\right) \\
&= f_{Ml}(kr) \left[\frac{(r g_{El'})'(kr)}{kr}\right]^* \mathbf{Y}_L^{(m)} \cdot \mathbf{Y}_{L'}^{(m)*}, \\
\left(\mathbf{F}_{EL} \times \mathbf{G}^*_{ML'}\right) \cdot \mathbf{r}_0 &= \mathbf{F}_{EL} \cdot \left(\mathbf{G}^*_{ML'} \times \mathbf{r}_0\right) \\
&= -\frac{(r f_{El})'(kr)}{kr} \, g^*_{Ml'}(kr) \, \mathbf{Y}_L^{(e)} \cdot \mathbf{Y}_{L'}^{(e)*}.
\end{aligned} \tag{B.6}$$

Therefore,

$$\begin{aligned}
\oint \left[\left(\mathbf{F}_{ML} \times \mathbf{G}^*_{EL'}\right) \cdot \mathbf{r}_0\right] \mathrm{d}\Omega &= f_{Ml}(kr) \left[\frac{(r g_{El'})'(kr)}{kr}\right]^* \oint \mathbf{Y}_L^{(m)} \cdot \mathbf{Y}_{L'}^{(m)*} \, \mathrm{d}\Omega \\
&= f_{Ml}(kr) \left[\frac{(r g_{El})'(kr)}{kr}\right]^* \delta_{LL'},
\end{aligned} \tag{B.7}$$

$$\begin{aligned}
\oint \left[\left(\mathbf{F}_{EL} \times \mathbf{G}^*_{ML'}\right) \cdot \mathbf{r}_0\right] \mathrm{d}\Omega &= -\frac{(r f_{El})'(kr)}{kr} \, g^*_{Ml'}(kr) \oint \mathbf{Y}_L^{(e)} \cdot \mathbf{Y}_{L'}^{(e)*} \, \mathrm{d}\Omega \\
&= -\frac{(r f_{El})'(kr)}{kr} \, g^*_{Ml}(kr) \delta_{LL'}.
\end{aligned} \tag{B.8}$$

Similarly, using the orthonormality of the vector spherical harmonics $\mathbf{Y}_L^{(a)}$ one can show that for any vector multipoles $\mathbf{F}_{\gamma L}$ and $\mathbf{G}_{\gamma' L'}$ defined by Eqs. (3)

$$\oint \mathbf{F}_{\gamma L} \cdot \mathbf{G}^*_{\gamma' L'} \, \mathrm{d}\Omega = 0, \tag{B.9}$$

unless $\gamma = \gamma'$ and $L = L'$. Indeed, in the $\gamma = \gamma'$ case,

$$\oint \mathbf{F}_{ML} \cdot \mathbf{G}^*_{ML'} \, \mathrm{d}\Omega = f_{Ml}(kr) g^*_{Ml'}(kr) \oint \mathbf{Y}_L^{(m)} \cdot \mathbf{Y}_{L'}^{(m)*} \, \mathrm{d}\Omega = f_{Ml}(kr) g^*_{Ml}(kr) \, \delta_{LL'}, \tag{B.10}$$

$$\begin{aligned}
\oint \mathbf{F}_{EL} \cdot \mathbf{G}^*_{EL'} \, \mathrm{d}\Omega &= \frac{l(l+1)}{|k|^2 r^2} f_{El}(kr) g^*_{El'}(kr) \oint \mathbf{Y}_L^{(o)} \cdot \mathbf{Y}_{L'}^{(o)*} \, \mathrm{d}\Omega \\
&\quad + \frac{(r f_{El})'(kr)}{kr} \left[\frac{(r g_{El'})'(kr)}{kr}\right]^* \oint \mathbf{Y}_L^{(e)} \cdot \mathbf{Y}_{L'}^{(e)*} \, \mathrm{d}\Omega \\
&= \left\{\frac{l(l+1)}{|k|^2 r^2} f_{El}(kr) g^*_{El}(kr) + \frac{(r f_{El})'(kr)}{kr} \left[\frac{(r g_{El})'(kr)}{kr}\right]^*\right\} \delta_{LL'}.
\end{aligned} \tag{B.11}$$

Note in passing that the orthogonality relations (B.9), (B.10), and (B.11) can be straightforwardly extended also to the case of arbitrary vector multipoles,

$$\begin{aligned}\mathbf{F}_{ML}(k,\mathbf{r}) &= f_{ML}(kr)\mathbf{Y}_L^{(m)}(\mathbf{r}),\\ \mathbf{F}_{EL}(k,\mathbf{r}) &= \frac{1}{kr}\left\{\sqrt{l(l+1)}f_{EL}(kr)\mathbf{Y}_L^{(o)}(\mathbf{r}) + (rf_{EL})'(kr)\,\mathbf{Y}_L^{(e)}(\mathbf{r})\right\},\end{aligned} \tag{B.12}$$

where the linear combination of Bessel function $f_{\gamma L}$ explicitly depends on the magnetic number m (similarly for $\mathbf{G}_{\gamma L}$).

Appendix C. Dissipation in a dispersive and absorptive material

The most general form of the averaged energy density, which can also be applied to the left-handed materials, has recently been discussed by Ruppin [103] (see Eq. (11) therein). The form of the averaged energy density is valid at all frequencies and is nonnegative also in the regions of high absorption near resonance frequencies of the permittivity and permeability. In the Appendix we show that, in spite of the averaged energy density expressions being different, depending on the level of generality (see Eqs. (1), (2), (11), (15), and (16) of [103]), the expression for the electromagnetic energy dissipation, or, to be more precise, the *steady* (averaged) inflow of energy Q per unit time and unit volume from the external sources which maintain the field, remains always the same and given by Eq. (110). The latter formula is exactly the same as the expression for the time averaged energy dissipation first derived for a weekly dispersive and absorptive medium under the assumption that the imaginary parts of ε and μ are small compared to their respective real parts.

Let ε_0 and μ_0 be, as in [103], the vacuum permittivity and permeability, respectively. Starting from the equation of motion for the electric polarization (Eq. (3) of Ruppin [103]),

$$\ddot{\mathbf{P}} + \Gamma_e\dot{\mathbf{P}} + \omega_r^2\mathbf{P} = \varepsilon_0\omega_p^2\mathbf{E}, \tag{C.1}$$

where ω_r is the resonance frequency of the electric-dipole oscillators, Γ_e is the damping frequency, and ω_p is a measure of the strength of the interaction between the oscillators and the electric field, one finds for harmonic fields with a $\mathrm{e}^{-\mathrm{i}\omega t}$ time dependence

$$\mathbf{P} = -\varepsilon_0\frac{\omega_p^2}{\omega^2 - \omega_r^2 + \mathrm{i}\omega\Gamma_e}\,\mathbf{E}. \tag{C.2}$$

Since $\mathbf{P} = \chi_e\varepsilon_0\mathbf{E}$ and $\varepsilon(\omega) = 1 + \chi_e$, one has

$$\varepsilon(\omega) = 1 - \frac{\omega_p^2}{\omega^2 - \omega_r^2 + \mathrm{i}\Gamma_e\omega}. \tag{C.3}$$

Consequently,

$$\operatorname{Im}\varepsilon(\omega) = \Gamma_e\omega\frac{\omega_p^2}{(\omega^2 - \omega_r^2)^2 + \Gamma_e^2\omega^2} = \frac{\Gamma_e\omega}{\omega_p^2}\,|\varepsilon(\omega) - 1|^2. \tag{C.4}$$

Since $\dot{\mathbf{P}} = -\mathrm{i}\omega\chi_e\varepsilon_0\mathbf{E} = -\mathrm{i}\omega\varepsilon_0\left[\varepsilon(\omega) - 1\right]\mathbf{E}$, one has

$$|\dot{\mathbf{P}}|^2 = \omega^2\varepsilon_0^2|[\varepsilon(\omega) - 1]|^2|\mathbf{E}|^2. \tag{C.5}$$

Therefore, upon combining the last equation with Eq. (C.4) one obtains

$$\frac{\Gamma_e|\dot{\mathbf{P}}|^2}{\varepsilon_0\omega_p^2} = \frac{\Gamma_e\omega^2}{\omega_p^2}\,\varepsilon_0|[\varepsilon(\omega) - 1]|^2|\mathbf{E}|^2 = \omega\varepsilon_0[\mathrm{Im}\,\varepsilon(\omega)]|\mathbf{E}|^2. \tag{C.6}$$

According to Eq. (10) of Ruppin [103], the term of the left-hand side of our Eq. (C.6) describes dissipation of the electromagnetic energy density in a nonmagnetic dispersive and absorptive material. One can show that, after time averaging, this term is nothing but the dissipation rate Q as given by our Eq. (110). The missing prefactor $c/(8\pi)$ compared to our Eq. (110) results from the use of Gaussian units in our case and the SI units in the Ruppin case. In the Ruppin case [see his Eq. (7)], the Poynting vector is $\mathbf{S} = \mathbf{E}_0 \times \mathbf{H}_0$, whereas in our case it contains an additional prefactor $c/(4\pi)$. The additional factor 2 results then from time averaging [see Eq. (94)].

In the nonmagnetic dispersive and absorptive material, a general expression for electromagnetic energy density reduces to that of Loudon [104],

$$W = \frac{\varepsilon_0}{4}\left(\varepsilon' + \frac{2\omega\varepsilon''}{\Gamma_e}\right)|\mathbf{E}|^2 + \frac{\mu_0}{4}|\mathbf{H}|^2 = \frac{\varepsilon_0}{2}\left(n^2 + \frac{2\omega n\kappa}{\Gamma_e}\right)|\mathbf{E}|^2. \tag{C.7}$$

In arriving to the Loudon expression we have used that $\varepsilon = \varepsilon' + \mathrm{i}\varepsilon'' = (n + \mathrm{i}\kappa)^2 = (n^2 - \kappa^2) + 2\mathrm{i}n\kappa$ and $\mathbf{H} = [\varepsilon(\omega)\varepsilon_0/\mu_0]^{1/2}\mathbf{E}$, i.e.,

$$|\mathbf{H}|^2 = |\varepsilon(\omega)||\mathbf{E}|^2\varepsilon_0/\mu_0. \tag{C.8}$$

Appendix D. An explicit verification of the correspondence principle

In the case of a homogeneous sphere, Chew [13] showed explicitly the equivalence of the quantum-mechanical formalism of Wylie and Sipe [39], which yields the normalized transition rates in terms the imaginary part of a suitably normalized *scattering* Greens function [see Eq. (135) above] and the classical formalism, which yields the normalized transition rates in terms of the radiated power of an oscillating dipole. Chew [13] considered the case of a dipole both inside and outside homogeneous isotropic sphere. However, in the case of dipole inside the sphere it was not immediately obvious (at least to the author) how Chew's final expression for Im E_n' on page 1357 was derived. Since this is such a rare case that one can explicitly verify the correspondence of classical and quantum-mechanical formalisms, a few intermediary steps between the definition of quantity the E_n' and the final results for Im E_n' are filled in below to make Chew's derivation more amenable to general audience.

The quantity E_n', as defined in the left column on page 1357 of [13], is

$$E_n' = \left\{\varepsilon_2 h_n^{(1)}(\rho_2)[\rho_1 y_n(\rho_1)]' - \varepsilon_1 y_n(\rho_1)[\rho_2 h_n^{(1)}(\rho_2)]'\right\}/D_n, \tag{D.1}$$

where the prime denotes derivative with respect to the argument and y_n is the spherical Bessel function of the second kind [48]. Now, when the nominator and denominator of E'_n are both multiplied by D^*_n, the complex conjugate of

$$D_n = \varepsilon_1 j_n(\rho_1)\left[\rho_2 h_n^{(1)}(\rho_2)\right]' - \varepsilon_2 h_n^{(1)}(\rho_2)[\rho_1 j_n(\rho_1)]', \tag{D.2}$$

then the terms proportional to the products $\varepsilon_1\,\varepsilon_1$ and $\varepsilon_2\varepsilon_2$ cancel out in the nominator of $\operatorname{Im} E'_n$. The remaining terms then yield

$$\begin{aligned}\operatorname{Im} E'_n = \frac{\varepsilon_1\varepsilon_2}{|D_n|^2}\big\{ & j(\rho_1)[\rho_1 y(\rho_1)]'\big\{y(\rho_2)[\rho_2 j(\rho_2)]' - j(\rho_2)[\rho_2 y(\rho_2)]'\big\} \\ & + y(\rho_1)[\rho_1 j(\rho_1)]'\big\{j(\rho_2)[\rho_2 y(\rho_2)]' - y(\rho_2)[\rho_2 j(\rho_2)]'\big\}\big\}\,.\end{aligned} \tag{D.3}$$

By substituting

$$f(zg)' - g(zf)' = z(fg' - f'g) = z\{f,g\}, \tag{D.4}$$

where $\{f,g\}$ is the Wronskian, the above equation reduces to

$$\operatorname{Im} E'_n = -\frac{1}{|D_n|^2}\,\varepsilon_1\varepsilon_2\rho_1\rho_2\{j(\rho_1), y(\rho_1)\}\{j(\rho_2), y(\rho_2)\}. \tag{D.5}$$

Eventually, using the Wronskian identity [see Eq. (10.1.6) of [48] and our Eq. (19)]

$$\{j(z), y(z)\} = \frac{1}{z^2}, \tag{D.6}$$

one arrives at Chew's final result,

$$\operatorname{Im} E'_n = -\frac{\varepsilon_1\varepsilon_2}{\rho_1\rho_2|D_n|^2}\,. \tag{D.7}$$

Appendix E. Equivalence of our radiative decay rates with Chew's result for the case of a dipole inside a homogeneous sphere

In Section 10 it has been discussed that, in the case of a homogeneous sphere, our numerical results coincide with those obtained by Chew [13,14]. In particular, Figs. 2 and 3 of [13] and Fig. 1 of [14] have been reproduced. In Section 8.1.1, for the case of a dipole *outside* the sphere, equivalence of our results for the dipole radiative decay rates with those obtained by Chew [13,14] has been established analytically. Here it will be shown analytically that the same is also true for a dipole *inside* a homogeneous sphere.

In the case of a dipole *inside* a multilayered sphere, general formulas for the radiative decay rates were given in Section 8.1.2. The case of a homogeneous sphere can be viewed as a special case of the multilayered sphere case where the dipole is within the sphere core and the number of shells $N = 2$. In the case of a dipole within the sphere core, radiative decay rates were expressed in terms of the function $f_{\gamma l}(kr) = j_l(kr)/\mathscr{M}_{22;\gamma l}(1)$ given by Eq. (128). In the homogeneous sphere case the number of shells $N = 2$ and hence the ordered product $\mathscr{M}_{22;\gamma l}(1)$ of backward trans-

fer matrix reduces to the single backward matrix $T^{-}_{\gamma l}$. The latter is given by Eq. (17) for $\gamma = M$ and by Eq. (25) for $\gamma = E$. Now, in the case $\gamma = M$, one obtains from Eq. (17),

$$\mathscr{M}_{22;Ml} = T^{-}_{22;Ml} = -\frac{\mathrm{i}k_1}{\mu_2}\left[\mu_1 u_l(k_1 r_1) w_l'(k_2 r_1) - \mu_2 u_l'(k_1 r_1) w_l(k_2 r_1)\right]. \tag{E.1}$$

Similarly, in the case $\gamma = E$, Eq. (25) yields

$$\mathscr{M}_{22;El} = T^{-}_{22;El} = -\frac{\mathrm{i}k_1 n_1}{\varepsilon_1 \varepsilon_2}\sqrt{\frac{\varepsilon_2}{\mu_2}}\left[\varepsilon_1 u_l(k_1 r_1) w_l'(k_2 r_1) - \varepsilon_2 u_l'(k_1 r_1) w_l(k_2 r_1)\right]. \tag{E.2}$$

Upon substituting $u_l(kr) = r j_l(kr)$, $w_l(kr) = r h_l^{(1)}(kr)$, and noting that, in the above formulas,

$$(r g_{El})'(kr) = \frac{\mathrm{d}[r g_{El}(kr)]}{\mathrm{d}r} = \frac{\mathrm{d}[kr g_{El}(kr)]}{\mathrm{d}(kr)}, \tag{E.3}$$

where g_l stands for either j_l or $h_l^{(1)}$, one finds

$$\begin{aligned} \frac{n_1^3 \varepsilon_2}{\varepsilon_1 n_2^3}\left|\mathscr{M}_{22;Ml}\right|^{-2} &= \varepsilon_1 n_1 \sqrt{\frac{\varepsilon_2}{\mu_2}}\frac{\mu_1 \mu_2}{\varepsilon_1 \varepsilon_2}\left|k_1 r_1 D_l'\right|^{-2} = \mu_1 n_1 \sqrt{\frac{\mu_2}{\varepsilon_2}}\left|k_1 r_1 D_l'\right|^{-2}, \\ \frac{n_1^3 \varepsilon_2}{\varepsilon_1 n_2^3}\left|\mathscr{M}_{22;El}\right|^{-2} &= \varepsilon_1 n_1 \sqrt{\frac{\varepsilon_2}{\mu_2}}\left|k_1 r_1 D_l\right|^{-2}, \end{aligned} \tag{E.4}$$

where D_l and D_l' are those of Chew's as defined by his Eqs. (9a) and (9b) of [13] [D_l is reproduced here in Eq. (D.2), and D_l' follows from D_l by interchanging electric permittivities and magnetic permeabilities]. This proves that the radiative rates as calculated by our Eq. (126) coincide with those as calculated by Eqs. (10) and (11) of [13]. In arriving at the result, we have used that

$$\frac{n_1^3 \varepsilon_2}{\varepsilon_1 n_2^3}\mu_2^2 = \mu_1 n_1 \sqrt{\frac{\mu_2}{\varepsilon_2}}, \quad \frac{n_1^3 \varepsilon_2}{\varepsilon_1 n_2^3} n_1^2 \varepsilon_1^2 \varepsilon_2^2 \frac{\mu_2}{\varepsilon_2} = \varepsilon_1 n_1 \sqrt{\frac{\varepsilon_2}{\mu_2}}. \tag{E.5}$$

References

[1] H. Chew, P.J. McNulty, M. Kerker, Phys. Rev. A 13 (1976) 396–404.
[2] H. Chew, M. Kerker, D.D. Cooke, Phys. Rev. A 16 (1977) 320–323.
[3] R.E. Benner, P.W. Barber, J.F. Owen, R.K. Chang, Phys. Rev. Lett. 44 (1980) 475–478.
[4] M. Kerker, D.S. Wang, H. Chew, Appl. Opt. 19 (1980) 4159–4174.
[5] H. Chew, M. Kerker, P.J. McNulty, J. Opt. Soc. Am. 66 (1976) 440–444.
[6] G.J. Rosasco, E.S. Etz, W.A. Cassat, Appl. Spectrosc. 29 (1975) 396–404.
[7] B.H. Mayall, B.L. Gledhill (Eds.), Proceedings of the Sixth Conference on Automated Cytology, J. Histochem. Cytochem. 27 (1979) 1–64.
[8] J. Gelbwachs, M. Birnbaum, Appl. Opt. 12 (1973) 2442–2447.
[9] P.F. Mullaney, P.N. Dean, Biophys. J. 10 (1970) 764–772.
[10] X. Yataganas, B.D. Clarkson, J. Histochem. Cytochem. 22 (1974) 651–659.
[11] S. Lange, G. Schweiger, J. Opt. Soc. Am. B 11 (1994) 2444–2452.
[12] R. Ruppin, J. Chem. Phys. 76 (1982) 1681–1684.

[13] H. Chew, J. Chem. Phys. 87 (1987) 1355–1360.
[14] H. Chew, Phys. Rev. A 38 (1988) 3410–3416.
[15] R.R. Chance, A. Prock, R. Silbey, Adv. Chem. Phys. 37 (1978) 1–65.
[16] J.R. Lakowicz, Anal. Biochem. 298 (2001) 1–24.
[17] D. Pastré, P. Grossel, M. Troyon, Opt. Commun. 156 (1998) 92–100.
[18] G. Parent, D. Van Labeke, D. Barchiesi, J. Opt. Soc. Am. A 16 (1999) 896–908.
[19] A.J. Campillo, J.D. Eversole, H.-B. Lin, Phys. Rev. Lett. 67 (1991) 437–440.
[20] V.V. Datsyuk, J. Opt. Soc. Am. B 19 (2002) 142–147.
[21] H.-B. Lin, J.D. Eversole, C.D. Merrit, A.J. Campillo, Phys. Rev. A 45 (1992) 6756–6760.
[22] H. Schniepp, V. Sandoghdar, Phys. Rev. Lett. 89 (2002) 257403.
[23] L.M. Liz-Marzán, M. Giersig, P. Mulvaney, Langmuir 12 (1996) 4329–4335.
[24] T. Ung, L.M. Liz-Marzán, P. Mulvaney, Langmuir 14 (1998) 3740–3748.
[25] V.V. Hardikar, E.J. Matijević, J. Colloid Interface Sci. 221 (2000) 133–136.
[26] A. van Blaaderen, A. Vrij, Langmuir 8 (1992) 2921–2931.
[27] K.P. Velikov, A. Moroz, A. van Blaaderen, Appl. Phys. Lett. 80 (2002) 49–51.
[28] S.J. Oldenburg, R.D. Averitt, S.L. Westcott, N.J. Halas, Chem. Phys. Lett. 288 (1998) 243–247.
[29] S.J. Oldenburg, J.B. Jackson, S.L. Westcott, N.J. Halas, Appl. Phys. Lett. 75 (1999) 2897–2899.
[30] J.B. Jackson, N.J. Halas, J. Phys. Chem. B 105 (2001) 2743–2746.
[31] C. Graf, A. van Blaaderen, Langmuir 18 (2002) 524–534.
[32] C. Graf, D.J. van den Heuvel, A. Moroz, H.C. Gerritsen, A. van Blaaderen, Enhanced photostability and reduced lifetimes of dye molecules in colloidal gold shell particles, (submitted).
[33] V.V. Klimov, V.S. Letokhova, Chem. Phys. Lett. 301 (1999) 441–448.
[34] J. Enderlein, Appl. Phys. Lett. 80 (2002) 315–317.
[35] F. Abelès, Ann. Phys. 5 (1950) 596–640.
[36] F. Abelès, Ann. Phys. 5 (1950) 706–782.
[37] M. Born, E. Wolf, Principles of Optics, third ed., Pergamon Press, Oxford, 1964, Section 1.6.
[38] G.S. Agarwal, Phys. Rev. A 12 (1975) 1475–1497.
[39] J.M. Wylie, J.E. Sipe, Phys. Rev. A 30 (1984) 1185–1193.
[40] A.R. Melnyk, M.J. Harrison, Phys. Rev. B 2 (1970) 835–850.
[41] M. Anderegg, B. Feuerbacher, B. Fitton, Phys. Rev. Lett. 27 (1971) 1565–1568.
[42] R. Ruppin, Phys. Rev. B 11 (1975) 2871–2876.
[43] P.T. Leung, Phys. Rev. B 42 (1990) 7622–7625.
[44] C.F. Bohren, Chem. Phys. Lett. 29 (1974) 458–462.
[45] C.F. Bohren, J. Chem. Phys. 62 (1975) 1566–1571.
[46] M.J.A. de Dood, L.H. Slooff, A. Moroz, A. Polman, A. van Blaaderen, Appl. Phys. Lett. 79 (2001) 3585–3587.
[47] A. Rahmani, G.W. Bryant, Phys. Rev. A 65 (2002) 033817.
[48] M. Abramowitch, I.A. Stegun, Handbook of Mathematical Functions, Dover Publications, New York, 1973.
[49] J.D. Jackson, Classical Electrodynamics, Wiley, New York, 1962.
[50] R.G. Newton, Scattering theory of waves and particles, Springer, New York, 1982.
[51] L. Tsang, J.A. Kong, R.T. Shin, Theory of Microwave Remote Sensing, Wiley, New York, 1985.
[52] M.I. Mishchenko, J. Opt. Soc. Am. A 8 (1991) 871–882, errata J. Opt. Soc. Am. A 9 (1992) 497.
[53] J. Stratton, Electromagnetics Theory, McGraw-Hill, New York, 1941.
[54] W.J. Wiscombe, Appl. Opt. 19 (1980) 1505–1509.
[55] O.B. Toon, T.P. Ackerman, Appl. Opt. 2 (1981) 3657–3660.
[56] T. Kaiser, G. Schweiger, Comput. Phys. 7 (1993) 682–686.
[57] W. Yang, Appl. Opt. 42 (2003) 1710–1720.
[58] J.B. Snow, S.-X. Qian, R.K. Chang, Opt. Lett. 10 (1985) 37–39.
[59] S.C. Hill, R.E. Benner, J. Opt. Soc. Am. B 3 (1986) 1509–1514.
[60] A. Moroz, C. Sommers, J. Phys.: Condens. Matter 11 (1999) 997–1008.
[61] A. Moroz, Phys. Rev. B 66 (2002) 115109.
[62] G. Burlak, S. Koshevaya, J. Sanchez-Mondragon, V. Grimalsky, Opt. Commun. 180 (2000) 49–58.

[63] G. Burlak, S. Koshevaya, J. Sanchez-Mondragon, V. Grimalsky, Opt. Commun. 187 (2001) 91–105.
[64] K.A. Fuller, D.W. Mackowski, in: M.I. Mishchenko et al. (Eds.), Light Scattering by Nonspherical Particles: Theory Measurements and Applications, Academic Press, San Diego, 2000.
[65] J.D. Pendleton, J. Opt. Soc. Am. 18 (2001) 610–613.
[66] H. Mabuchi, H.J. Kimble, Opt. Lett. 19 (1994) 749–751.
[67] V.V. Klimov, M. Ducloy, V.S. Letokhov, J. Mod. Opt. 43 (1996) 549–563.
[68] A. Moroz, Europhys. Lett. 46 (1999) 419–424.
[69] E.D. Palik (Ed.), Handbook of Optical Constants of Solids, Academic, New York, 1985.
[70] E. Dulkeith, et al., Phys. Rev. Lett. 89 (2002) 203002.
[71] J. Gersten, A. Nitzan, J. Chem. Phys. 75 (1981) 1139–1152.
[72] Y.S. Kim, P.T. Leung, T.F. George, J. Phys. Chem. 92 (1988) 6206–6208.
[73] V.V. Klimov, Opt. Commun. 211 (2002) 183–196.
[74] U. Kreibig, L. Genzel, Surf. Sci. 156 (1985) 678–700.
[75] L. Tonks, Phys. Rev. 37 (1931) 1458–1483; Phys. Rev. 38 (1931) 1219–1223.
[76] A. Dattner, Ericsson Tech. 2 (1957) 309; Ericsson Tech. 8 (1963) 1.
[77] P. Yeh, Surf. Sci. 96 (1979) 41–53.
[78] P.B. Bisht, K. Fukuda, S. Hirayama, J. Chem. Phys. 105 (1996) 9349–9361.
[79] B.I. Ipe, K.G. Thomas, S. Barazzouk, S. Hotchandani, P.V. Kamat, J. Phys. Chem. B 106 (2002) 18–21.
[80] M.J.A. de Dood, L.H. Slooff, A. Moroz, A. Polman, A. van Blaaderen, Phys. Rev. A 64 (2001) 033807.
[81] E. Snoeks, A. Lagendijk, A. Polman, Phys. Rev. Lett. 74 (1995) 2459–2462.
[82] A. Imhof, M. Megens, J.J. Engelberts, D.T.N. de Lang, R. Sprik, W.L. Vos, J. Phys. Chem. B 103 (1999) 1408–1415.
[83] H. Fujiwara, K. Sasaki, H. Masuhara, J. Appl. Phys. 85 (1999) 2052–2056.
[84] M.S. Tomaš, Phys. Rev. A 63 (2001) 053811.
[85] H.P. Urbach, G.L.J.A. Rikken, Phys. Rev. A 57 (1998) 3913–3930.
[86] M. Lewenstein, J. Zakrzewski, T.W. Mossberg, J. Mostowski, J. Phys. B: At. Mol. Opt. Phys. 21 (1988) L9–L14.
[87] D. Lenstra, G. Kurizki, L.D. Bakalis, K. Banaszek, Phys. Rev. A 54 (1996) 2690–2697.
[88] V.V. Klimov, M. Ducloy, V.S. Letokhov, Phys. Rev. A 59 (1999) 2996–3014.
[89] R.H. Dicke, Phys. Rev. 93 (1954) 99–110.
[90] T. Tokihiro, Y. Manabe, E. Hanamura, Phys. Rev. B 47 (1993) 2019–2030.
[91] E. Snoeks, A. van Blaaderen, T. van Dillen, C.M. van Kats, K.P. Velikov, M.L. Brongersma, A. Polman, Nucl. Instr. Meth. B 178 (2001) 62–68.
[92] D.S. Wang, M. Kerker, H. Chew, Appl. Opt. 19 (1980) 2315–2328.
[93] P.C. Waterman, Phys. Rev. D 3 (1971) 825–839.
[94] B. Peterson, S. Ström, Phys. Rev. D 10 (1974) 2670–2684.
[95] V. Poborchii, T. Tada, T. Kanayama, A. Moroz, Appl. Phys. Lett. 82 (2003) 508–510.
[96] H. Chew, D.D. Cooke, M. Kerker, Appl. Opt. 19 (1980) 44–52.
[97] V.V. Klimov, V.S. Letokhov, Phys. Rev. A 54 (1996) 4408–4423.
[98] E. Yablonovitch, T.J. Gmitter, K.M. Leung, Phys. Rev. Lett. 67 (1991) 2295–2298.
[99] C.M. Soukoulis (Ed.), Proceedings of the NATO ASI School "Photonic Crystals and Localization in the 21st Century", Kluwer, Dordrecht, 2001.
[100] P. Chýlek, H.-B. Lin, J.D. Eversole, A.J. Campillo, Opt. Lett. 16 (1991) 1723–1725.
[101] H. Latifi, A. Biswas, R.L. Armstrong, R.G. Pinnick, Appl. Opt. 29 (1990) 5387–5392.
[102] A.S. Kwok, R.K. Chang, Opt. Lett. 18 (1993) 1597–1599.
[103] R. Ruppin, Phys. Lett. A 299 (2002) 309–312.
[104] R. Loudon, J. Phys. A 3 (1970) 233–245.